NASA TECHNICAL NOTE

NASA TN D-8478

NASA TN D-8478

EFFECT OF WINGLETS ON A FIRST-GENERATION JET TRANSPORT WING

III - Pressure and Spanwise Load Distributions for a Semispan Model at Mach 0.30

Lawrence C. Montoya
Dryden Flight Research Center
Edwards, Calif. 93523

and

Peter F. Jacobs and Stuart G. Flechner
Langley Research Center
Hampton, Va. 23665

NATIONAL AERONAUTICS AND SPACE ADMINISTRATION • WASHINGTON, D. C. • JUNE 1977

1. Report No.	2. Government Accession No.	3. Recipient's Catalog No.
NASA TN D-8478		

4. Title and Subtitle	5. Report Date
EFFECT OF WINGLETS ON A FIRST-GENERATION JET TRANSPORT WING. III - PRESSURE AND SPANWISE LOAD DISTRIBUTIONS FOR A SEMISPAN MODEL AT MACH 0.30	June 1977
	6. Performing Organization Code
7. Author(s) Lawrence C. Montoya (Dryden Flight Research Center), Peter F. Jacobs, and Stuart G. Flechner (Langley Research Center)	8. Performing Organization Report No. L-11370
	10. Work Unit No. 505-11-16-08
9. Performing Organization Name and Address NASA Langley Research Center Hampton, VA. 23665	11. Contract or Grant No.
	13. Type of Report and Period Covered Technical Note
12. Sponsoring Agency Name and Address National Aeronautics and Space Administration Washington, D.C. 20546	14. Sponsoring Agency Code

15. Supplementary Notes

16. Abstract

Pressure and spanwise load distributions on a first-generation jet transport semispan model at a Mach number of 0.30 are presented. The data are given for the basic wing and for configurations with an upper winglet only, upper and lower winglets, and a simple wing-tip extension. To simulate second-segment-climb lift conditions, leading- and/or trailing-edge flaps were added to some configurations.

17. Key Words (Suggested by Author(s))	18. Distribution Statement
Winglets Pressure distributions Spanwise load distributions Flaps	Unclassified - Unlimited Subject Category 02

19. Security Classif. (of this report)	20. Security Classif. (of this page)	21. No. of Pages	22. Price*
Unclassified	Unclassified	100	$5.00

* For sale by the National Technical Information Service, Springfield, Virginia 22161

EFFECT OF WINGLETS ON A FIRST-GENERATION JET TRANSPORT WING

III - PRESSURE AND SPANWISE LOAD DISTRIBUTIONS FOR A SEMISPAN MODEL AT MACH 0.30

Lawrence C. Montoya
Dryden Flight Research Center

Peter F. Jacobs and Stuart G. Flechner
Langley Research Center

SUMMARY

Pressure and spanwise load distributions on a first-generation jet transport semispan model at a Mach number of 0.30 are presented. The data were measured for the basic wing and for configurations with an upper winglet only, upper and lower winglets, and a simple wing-tip extension. To simulate second-segment-climb lift conditions, leading- and/or trailing-edge flaps were added to some configurations. Selected data are discussed to show the trends for the various configurations at high lift conditions. The results show that the upper-and-lower-winglet and tip-extension configurations have the highest wing-tip loads. At high lift conditions the lower winglet has a higher loading than the upper winglet.

INTRODUCTION

Winglets, as described in reference 1, are intended to provide reductions in drag coefficients, near cruise conditions, substantially greater than those obtained with a simple wing-tip extension, which has been designed to impose the same bending increments on the wing structure as the winglets. The National Aeronautics and Space Administration has been conducting extensive experimental investigations of winglets on jet transport wings at high subsonic Mach numbers. (See refs. 2 and 3.)

This investigation was conducted to determine the effects of winglets and a simple wing-tip extension on the longitudinal aerodynamic characteristics, surface static-pressure distributions, and cross-flow velocities behind the wing tip of a first-generation jet transport. This paper, which is one of a series, presents wing and winglet pressure coefficients and spanwise load distributions at Mach 0.30 obtained from chordwise static-pressure measurements only. Longitudinal aerodynamic characteristics and cross-flow velocities are presented in reference 4. Chordwise pressure and spanwise load distributions for the wing and winglets at high subsonic speeds are presented in reference 5. Results herein are given for the basic wing and for configurations with an upper winglet only, upper and lower winglets, and a simple wing-tip extension. To simulate the second-segment-climb lift conditions, which was the primary objective of the tests at Mach 0.30, leading- and/or trailing-edge flaps were added to some of the configurations.

Data are presented for a wind-tunnel free-stream Mach number of 0.30 at a constant dynamic pressure of 12 kPa (251 psf) and Reynolds number of 11.68×10^6 per m (3.56×10^6 per ft). The angle of attack ranged from about 4° to 12°.

SYMBOLS

Force and moment data have been reduced to coefficient form based on the exposed trapezoidal area of the basic wing. All dimensional values are given in both the International System of Units (SI) and U.S. Customary Units (ref. 6). All measurements and calculations were made in U.S. Customary Units.

Coefficients and symbols used herein are defined as follows:

b'	exposed semispan of wing with basic tip, 124.26 cm (48.92 in.)
$\Delta b'$	incremental increase in exposed wing semispan (tip extension), 0.38 of span of upper winglet, 7.62 cm (3.00 in.)
c	local chord, cm (in.)
$\bar{c}$	mean geometric chord of exposed basic wing, 39.98 cm (15.74 in.)
c_{av}	average chord of exposed basic wing, S/b', 37.41 cm (14.73 in.)
c_t	tip chord of basic wing, cm (in.)
C_L	lift coefficient, $\text{Lift}/q_\infty S$
c_n	section normal-force coefficient obtained from integration of pressure measurements
C_m	pitching-moment coefficient, $\text{Pitching moment}/q_\infty S\bar{c}$
C_p	pressure coefficient, $(p_l - p_\infty)/q_\infty$
h	span of upper winglet from chord plane of wing tip (see fig. 2(b)), cm (in.)
i	incidence of winglet measured from free-stream direction, positive with leading edge inward for upper winglet, outward for lower winglet (see fig. 2(b)), deg
M_∞	free-stream Mach number
p_l	local static pressure, Pa (psf)
p_∞	free-stream static pressure, Pa (psf)
q_∞	free-stream dynamic pressure, Pa (psf)

S	exposed trapezoidal area of basic wing, 0.4648 m^2 (5.0034 ft^2)
x	chordwise distance from leading edge, positive aft, cm (in.)
y	spanwise distance from wing-fuselage juncture, positive outboard, cm (in.)
z	vertical coordinate of airfoil, positive upward, cm (in.)
z'	distance along winglet span from chord plane of wing, cm (in.)
α	angle of attack, deg
η	exposed wing semispan station (based on basic-wing panel), y/b'

Abbreviations:

L.S.	lower surface
U.S.	upper surface

EXPERIMENTAL APPARATUS AND PROCEDURES

Test Facility

This investigation was conducted in the Langley 8-foot transonic pressure tunnel, a continuous single-return tunnel with a slotted rectangular test section. The longitudinal slots in the floor and ceiling of the test section reduce tunnel wall interference and allow relatively large models to be tested through the subsonic speed range. Controls are available to permit independent variation of Mach number, stagnation pressure, temperature, and dew point. A more detailed description of the wind tunnel is given in reference 7.

Model Description

To obtain the highest possible winglet Reynolds number and sufficient winglet size in which to install surface pressure measurement tubes, a semispan model was utilized. The 0.07-scale semispan model used in this investigation was of the KC-135A transport aircraft. Photographs of the model in the wind tunnel are shown in figure 1, and drawings of the model in figure 2.

Fuselage.- The fuselage contours closely simulate the full-scale fuselage shape, with the exception of the wheel-well area. An enlargement of this area was necessary to enclose the model mounting apparatus. The fuselage midsection covers the balance and has a slot in it through which the wing protrudes. The fuselage is not attached to the balance, but it does rotate with the wing through the angle-of-attack range.

Wing.- The basic wing of the KC-135A model has 7° dihedral and 2° of incidence at the root chord. The wing has no geometric twist. A typical outboard

airfoil section is shown in figure 3, with its coordinates presented in table I. The wing thickness ratio varies nonlinearly from 15 percent at the wing-fuselage juncture to 9 percent at the trailing-edge break and then remains constant at 9 percent to the wing tip. The trapezoidal planform of the total wing (extended to the fuselage center line) has a sweep at the quarter-chord of 35°, an aspect ratio of 7.0, and a taper ratio of 0.35. For all data analysis, the reference geometry parameters S, b', c, and c_{av} are based on the exposed trapezoidal planform of the basic wing. The model wing stiffness was designed so that the relative model bending deflection at the tip was approximately the same as that for the actual airplane at cruise conditions.

Nacelles.- Flow-through nacelles were used with an inlet diameter of 5.64 cm (2.22 in.) and exit diameter of 3.45 cm (1.36 in.). The inlet diameter was maintained back to approximately 0.66 of the nacelle length and then tapered linearly to the exit.

Flaps.- Fixed-position leading- and trailing-edge flaps were attached to the model on some of the configurations to simulate second-segment-climb characteristics. The flaps tested were designed merely to be representative and are not modeled after the actual KC-135A flaps. The leading- and trailing-edge flaps were deflected 120° and 20°, respectively. Flap details are shown in figure 4. The configurations tested with and without flaps are shown in the following table:

Flaps	Test configuration			
	Basic tip	Upper winglet	Upper and lower winglets	Tip extension
Off	X		X	
Trailing edge	X	X	X	X
Leading and trailing edge	X	X	X	

Tip extension.- The 7.62-cm (3.00-in.) wing-tip extension (see fig. 2(a)) had the same coordinates as the outboard wing section. The span was estimated so that the tip extension produced essentially the same increments in bending moment at the wing-fuselage juncture as the winglets.

Winglets.- A detailed drawing of the winglets used in this investigation is presented in figure 2(b). The winglets employed an 8-percent-thick general aviation airfoil. Winglet airfoil coordinates are presented in table II.

The upper winglet has a span equal to the wing-tip chord, a root chord equal to 65 percent of the wing-tip chord, a leading-edge sweep of 38°, a taper ratio of 0.32, and an aspect ratio of 2.33. The planform area of the upper winglet is 3.8 percent of the exposed trapezoidal planform area of the basic wing. The upper winglet is canted outboard 15° from vertical (75° dihedral) and toed

out 4° (leading edge outboard) relative to the fuselage center line. The upper winglet is untwisted and therefore has constant negative geometric incidence across its span. The "upper surface" of the upper winglet is the inboard surface.

The lower winglet has a span equal to 23 percent of the wing-tip chord, a root chord equal to 40 percent of the wing-tip chord, a leading-edge sweep of 52°, a taper ratio of 0.40, and an aspect ratio of 0.82. The planform area of the lower winglet is 0.6 percent of the exposed trapezoidal planform area of the basic wing. The lower winglet is canted outboard from vertical 36° (54° anhedral) and toed in 7° relative to the fuselage center line (trailing edge outboard for negative incidence). The lower winglet was twisted about its leading edge with 4° washout at the tip. The "upper surface" of the lower winglet is the outboard surface.

To smooth the transition from the wing to the winglets, fillets were added to the inside corners at those junctures and the outside corners were rounded.

Boundary-Layer Transition Strips

Boundary-layer transition strips were placed on both surfaces of the wing and winglets. These strips were comprised of a 0.159-cm (0.06-in.) wide band of carborundum grains sized on the basis of reference 8 and set in a plastic adhesive. The transition strip patterns for the wing and winglets are shown in figure 5.

The transition strips on the lower surface of the winglets were located rearward in an attempt to simulate full-scale Reynolds number boundary-layer conditions (ref. 9). The strips on the upper surface of the winglets were located forward to insure transition ahead of the shock wave for the various test conditions.

The fluorescent-oil-film flow-visualization technique described in reference 10 was employed to verify the presence of laminar flow ahead of the transition strip.

Test Conditions

The data presented herein are for a wind-tunnel free-stream Mach number of 0.30 at a constant dynamic pressure of 12 kPa (251 psf) and angle-of-attack range from approximately 4° to 12°. The Reynolds number was 11.68×10^6 per m (3.56×10^6 per ft). During the tests, the stagnation temperature was maintained at 322 K (120° F), and the air was dried until the dew point was sufficiently low to prevent condensation effects.

Measurements

Force and moment data were obtained using a five-component electrical strain-gage balance. Side-force measurements were not taken. An accelerometer

attached to the wing mounting block inside the fuselage was used to measure angle of attack.

Chordwise static-pressure distributions were measured at the 0.26, 0.77, 0.92, and 0.99 semispan stations of the basic wing (fig. 6(a)). In addition, they were measured at three stations on the upper winglet and at one station on the lower winglet (fig. 6(b)), for the upper-and-lower-winglet configuration only. These stations were located at 0.15, 0.50, and 0.80 of the upper-winglet span and at 0.50 of the lower-winglet span, which correspond, respectively, to the 1.01, 1.03, 1.05, and 1.01 wing semispan stations. (Note that semispan stations are defined as a fraction of the distance from the wing-fuselage juncture to the tip of the basic wing panel. As the upper and lower winglets extend beyond this distance, semispan stations can be greater than 1.0.) The wing and winglet pressures were measured with pressure-scanning valves. The range of the pressure sensors in the valves was sized for the upper or lower wing or winglet surfaces and wind-tunnel test conditions.

Wing-tip deflections were determined from photographs of a chordwise line on the edge of the wing tip and are shown in figure 7.

Corrections

The slotted wind-tunnel test section is designed to reduce wall effects on lift. Data from this investigation show that the wing spanwise load distributions for all configurations at the same conditions are nearly identical over the major portion of the span. Therefore, wall effects on wing lift can be considered systematic, and no correction is made to the data for these effects. The wing semispan and the model frontal area were sufficiently small (1.5 percent of the test-section cross-sectional area) to avoid having to correct Mach number for wind-tunnel blockage effects (ref. 11). The angle of attack of the model was corrected for flow angularity in the wind tunnel.

PRESENTATION OF RESULTS

The results of this investigation are presented in the following figures:

DISCUSSION OF RESULTS

The discussion presented herein is limited to a few selected cases. The data discussed are considered representative of the trends for the various configurations at high lift conditions. The variation of angle of attack with lift coefficient from reference 4 has been included to show the relationship between angle of attack, for the figures presented herein, and lift coefficient.

Throughout the figures of this paper, a conscious effort has been made to retain a particular symbol with each of the four configurations tested (basic wing, upper winglet, upper and lower winglets, and tip extension). This practice is intended to facilitate identification of a particular set of data. Also, for the pressure distributions (figs. 9 to 17), the configuration is indicated at the top of each page. Note that in figures 9 to 18, the vertical scale increments of the insert plots are larger than the main scale increments.

The chordwise static-pressure distributions for the basic-wing and tip-extension configurations are representative of first-generation jet transport airfoils and are not discussed.

A comparison of the upper-winglet and upper-and-lower-winglet configurations at an angle of attack of approximately 12° with flaps is presented in figure 18. With the trailing-edge flaps (fig. 18(a)), both configurations show good agreement on the inboard stations with some differences on the outboard stations. At $\eta = 0.92$, the upper-and-lower-winglet configuration has less negative pressure coefficients near the upper-surface leading edge, while at $\eta = 0.99$, the upper-and-lower-winglet configuration has more negative pressure coefficients on the upper-surface leading edge and more positive pressure coefficients on the lower surface near the leading edge. The trailing-edge pressure recovery at all the wing stations is the same for both configurations.

Comparison between the upper-winglet and upper-and-lower-winglet configurations with leading- and trailing-edge flaps (fig. 18(b)) shows good agreement on the inboard stations with differences at $\eta = 0.99$. The upper-winglet configuration has more negative pressure coefficients on the upper center region of the

wing with better trailing-edge pressure recovery. On the lower surface near the leading edge, the pressure coefficients for the upper-and-lower-winglet configuration are much more positive because of the lower winglet.

The effects of the various configurations with trailing-edge flaps on the span loads for an angle of attack of approximately 12° is shown in figure 20(e). The tip-extension and upper-and-lower-winglet configurations have the highest loading on the wing tip. The winglet span load data show the lower winglet at a higher load level than the upper winglet at these high lift conditions.

SUMMARY OF RESULTS

A wind-tunnel investigation of winglets mounted on the tip of a 0.07-scale KC-135A jet transport model wing has been conducted. Wing and winglet pressure and spanwise load distributions at a Mach number of 0.30 have been presented for the basic wing and for configurations with an upper winglet only, upper and lower winglets, and a simple wing-tip extension. To simulate second-segment-climb lift conditions, leading- and/or trailing-edge flaps were installed on the various configurations.

A comparison of the span loads of all the configurations with trailing-edge flaps at the high lift conditions (angle of attack greater than 9°) shows the upper-and-lower-winglet and tip-extension configurations to have the highest loads at the wing tip. The winglet span loads at these conditions show the lower winglet at a higher load level than the upper winglet.

Langley Research Center
National Aeronautics and Space Administration
Hampton, VA 23665
April 20, 1977

REFERENCES

1. Whitcomb, Richard T.: A Design Approach and Selected Wind-Tunnel Results at High Subsonic Speeds for Wing-Tip Mounted Winglets. NASA TN D-8260, 1976.

2. Flechner, Stuart G.; Jacobs, Peter F.; and Whitcomb, Richard T.: A High Subsonic Speed Wind-Tunnel Investigation of Winglets on a Representative Second-Generation Jet Transport Wing. NASA TN D-8264, 1976.

3. Jacobs, Peter F.; and Flechner, Stuart G.: The Effect of Winglets on the Static Aerodynamic Stability Characteristics of a Representative Second Generation Jet Transport Model. NASA TN D-8267, 1976.

4. Jacobs, Peter F.; Flechner, Stuart G.; and Montoya, Lawrence C.: Effect of Winglets on a First-Generation Jet Transport Wing. I - Longitudinal Aerodynamic Characteristics of a Semispan Model at Subsonic Speeds. NASA TN D-8473, 1977.

5. Montoya, Lawrence C.; Flechner, Stuart G.; and Jacobs, Peter F.: Effect of Winglets on a First-Generation Jet Transport Wing. II - Pressure and Spanwise Load Distributions for a Semispan Model at High Subsonic Speeds. NASA TN D-8474, 1977.

6. Mechtly, E. A.: The International System of Units - Physical Constants and Conversion Factors (Second Revision). NASA SP-7012, 1973.

7. Schaefer, William T., Jr.: Characteristics of Major Active Wind Tunnels at the Langley Research Center. NASA TM X-1130, 1965.

8. Braslow, Albert L.; and Knox, Eugene C.: Simplified Method for Determination of Critical Height of Distributed Roughness Particles for Boundary-Layer Transition at Mach Numbers From 0 to 5. NACA TN 4363, 1958.

9. Blackwell, James A., Jr.: Preliminary Study of Effects of Reynolds Number and Boundary-Layer Transition Location on Shock-Induced Separation. NASA TN D-5003, 1969.

10. Loving, Donald L.; and Katzoff, Samuel: The Fluorescent-Oil Film Method and Other Techniques for Boundary-Layer Flow Visualization. NASA MEMO 3-17-59L, 1959.

11. Brooks, Joseph D.: Some Anomalies Observed in Wind-Tunnel Tests of a Blunt Body at Transonic and Supersonic Speeds. NASA TN D-8237, 1976.

TABLE I.- COORDINATES OF TYPICAL OUTBOARD WING SECTION

[Wing section at 2° incidence]

Upper surface		Lower surface	
x/c	z/c	x/c	z/c
0	0	0	0
.0011	.0042	.0020	-.0054
.0022	.0056	.0035	-.0063
.0034	.0071	.0061	-.0073
.0058	.0090	.0092	-.0081
.0095	.0116	.0201	-.0097
.0132	.0136	.0391	-.0116
.0180	.0161	.0631	-.0139
.0234	.0186	.0950	-.0168
.0324	.0221	.1016	-.0174
.0415	.0253	.1445	-.0212
.0536	.0291	.1826	-.0245
.0716	.0338	.2235	-.0284
.0897	.0377	.2597	-.0314
.0990	.0394	.2950	-.0341
.1132	.0417	.3326	-.0366
.1408	.0454	.3726	-.0391
.1589	.0471	.4276	-.0418
.1740	.0483	.4690	-.0429
.1861	.0492	.5110	-.0433
.2011	.0501	.5560	-.0430
.2192	.0510	.5967	-.0424
.2342	.0516	.6386	-.0414
.2584	.0522	.6818	-.0406
.3432	.0522	.7243	-.0397
.3729	.0524	.7620	-.0389
.4090	.0513	.7951	-.0381
.4572	.0489	.8308	-.0377
.5054	.0454	.8662	-.0371
.5416	.0420	.9029	-.0363
.5897	.0367	.9392	-.0358
.6379	.0304	.9790	-.0348
.6862	.0226	.9999	-.0350
.7343	.0153		
.7582	.0108		
.7823	.0065		
.8040	.0027		
.8344	-.0023		
.8642	-.0076		
.8874	-.0119		
.9223	-.0180		
.9492	-.0229		
.9718	-.0269		
.9920	-.0308		
1.0001	-.0347		

TABLE II.- AIRFOIL COORDINATES FOR WINGLETS

x/c	z/c for -	
	Upper surface	Lower surface
0	0	0
.0020	.0077	-.0032
.0050	.0119	-.0041
.0125	.0179	-.0060
.0250	.0249	-.0077
.0375	.0296	-.0090
.0500	.0333	-.0100
.0750	.0389	-.0118
.1000	.0433	-.0132
.1250	.0469	-.0144
.1500	.0499	-.0154
.1750	.0525	-.0161
.2000	.0547	-.0167
.2500	.0581	-.0175
.3000	.0605	-.0176
.3500	.0621	-.0174
.4000	.0628	-.0168
.4500	.0627	-.0158
.5000	.0618	-.0144
.5500	.0599	-.0122
.5750	.0587	-.0106
.6000	.0572	-.0090
.6250	.0554	-.0071
.6500	.0533	-.0052
.6750	.0508	-.0033
.7000	.0481	-.0015
.7250	.0451	.0004
.7500	.0419	.0020
.7750	.0384	.0036
.8000	.0349	.0049
.8250	.0311	.0060
.8500	.0270	.0065
.8750	.0228	.0064
.9000	.0184	.0059
.9250	.0138	.0045
.9500	.0089	.0021
.9750	.0038	-.0013
1.0000	-.0020	-.0067

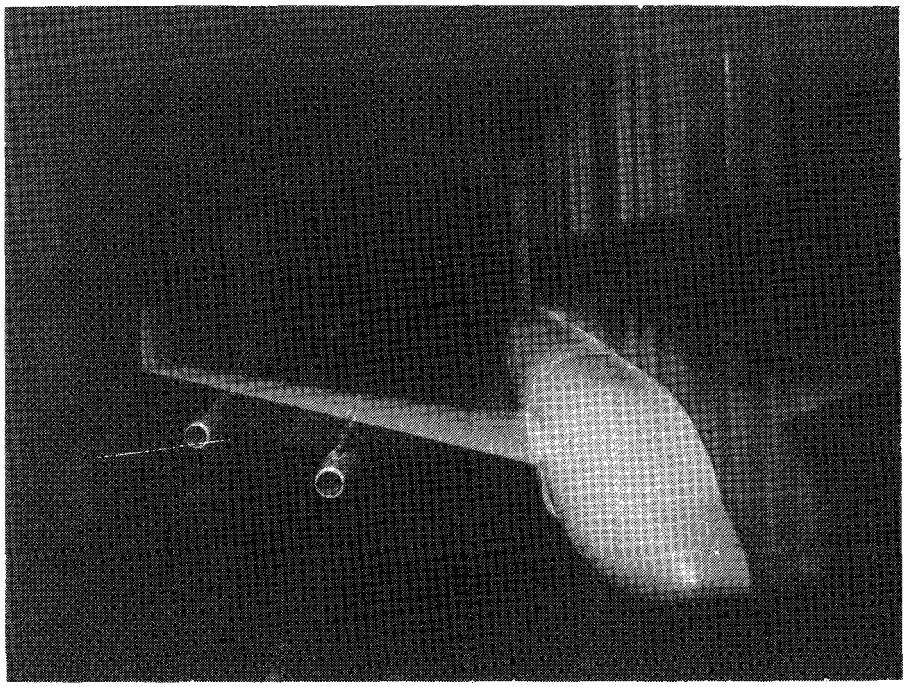

L-75-8430

(a) Complete configuration.

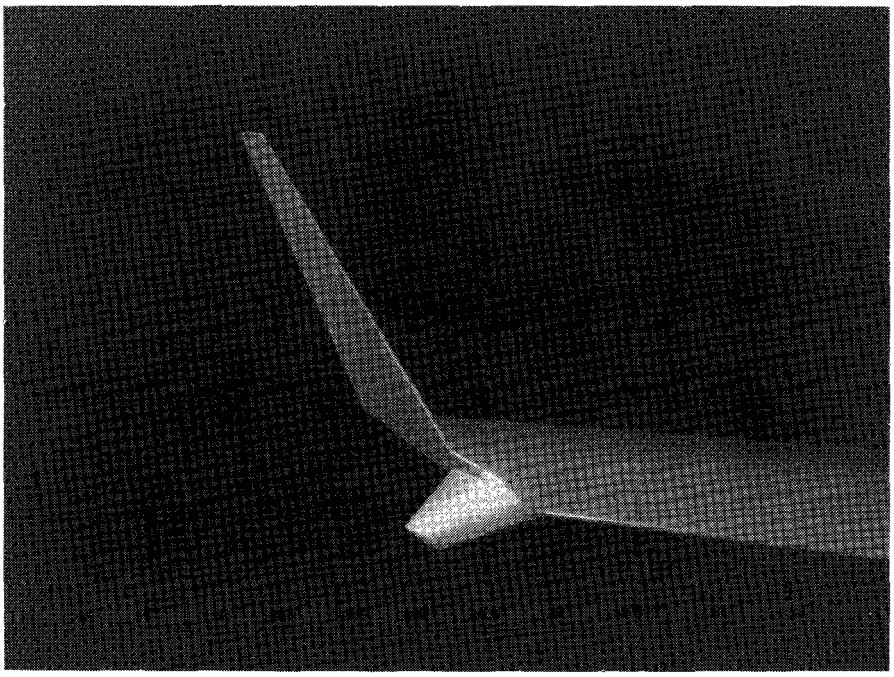

L-75-8429

(b) Winglets.

Figure 1.- Photographs of model.

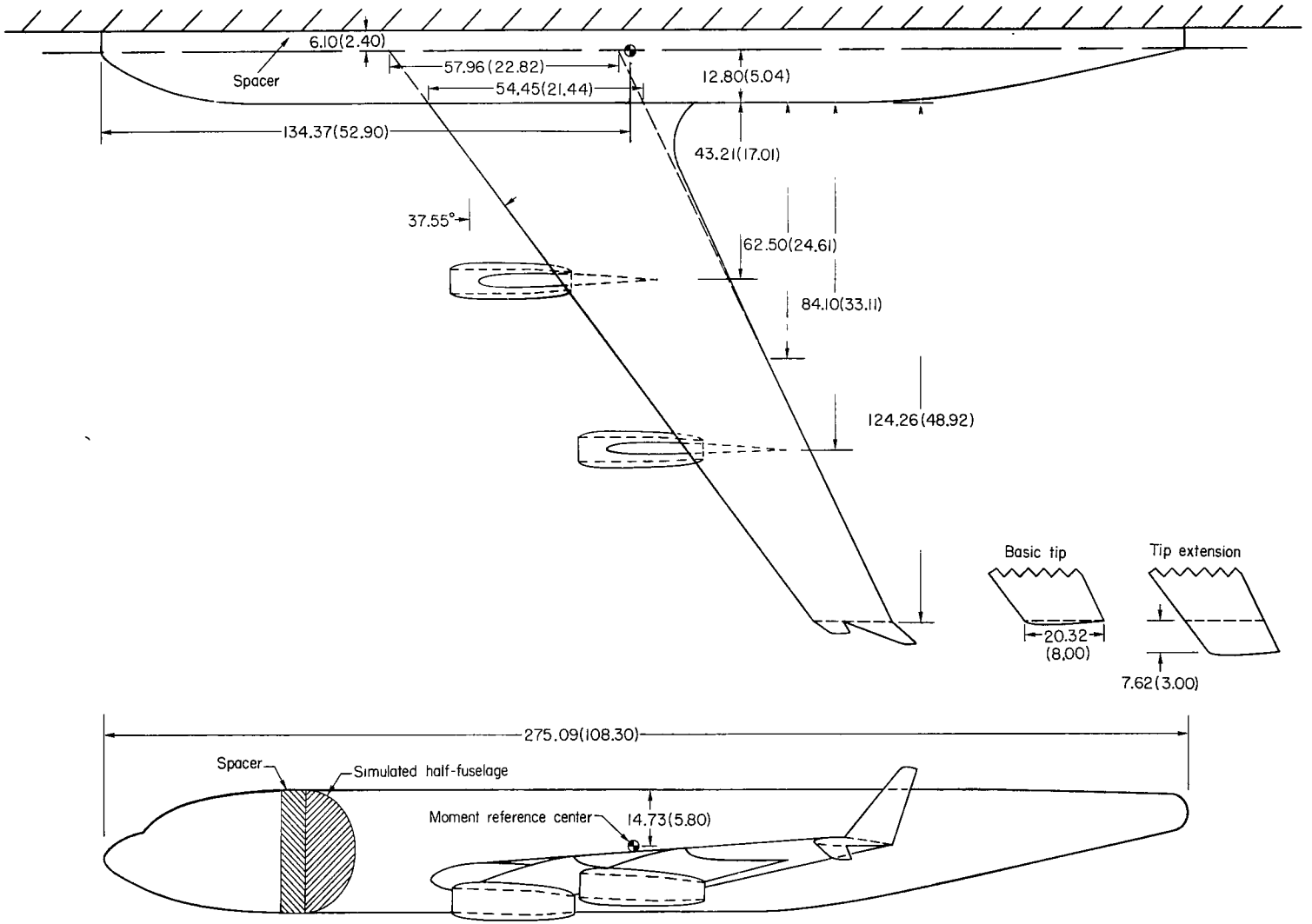

(a) General layout of model.

Figure 2.- Drawing of semispan model. Dimensions in centimeters (inches).

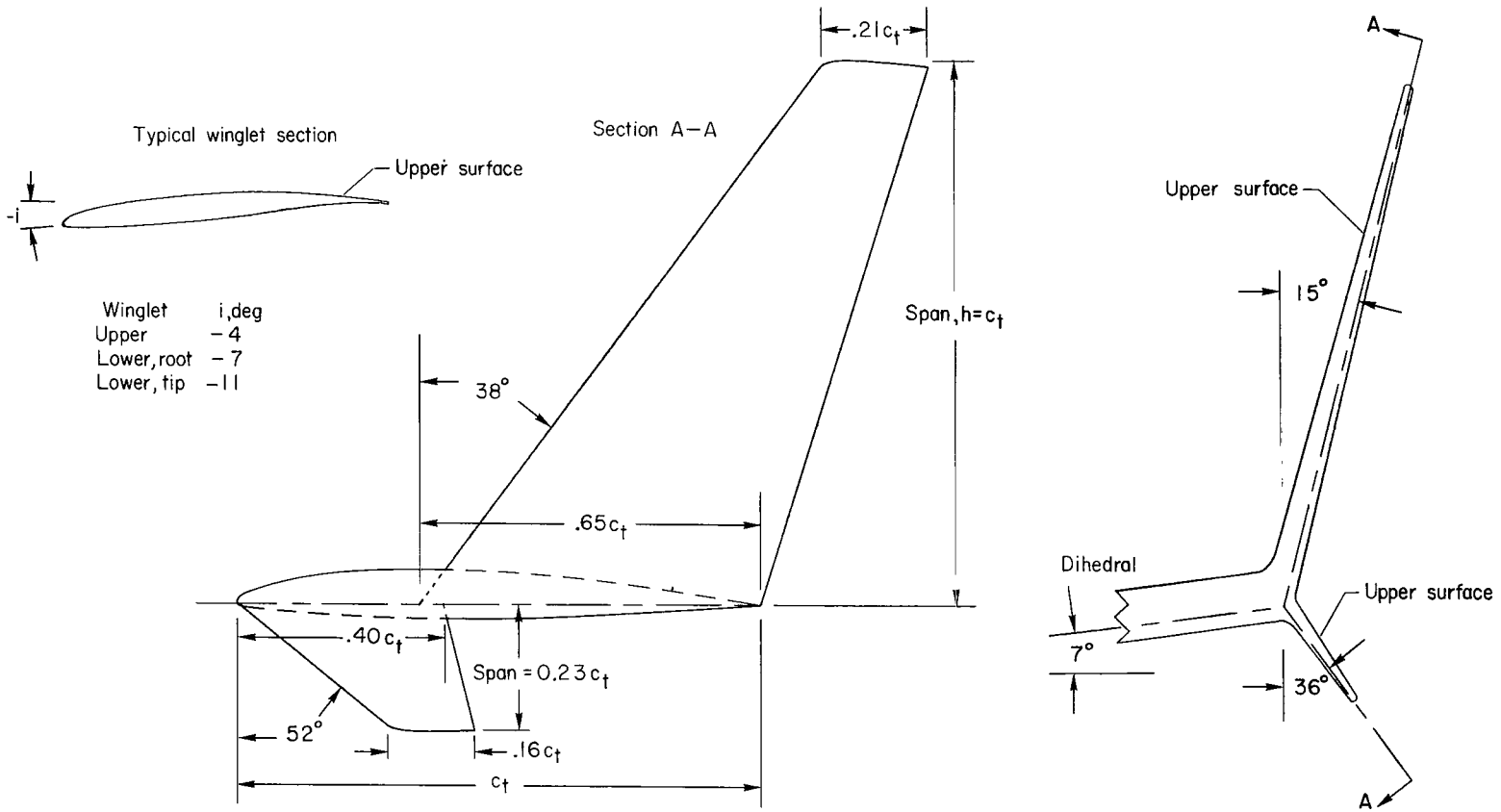

(b) Winglet details.

Figure 2.- Concluded.

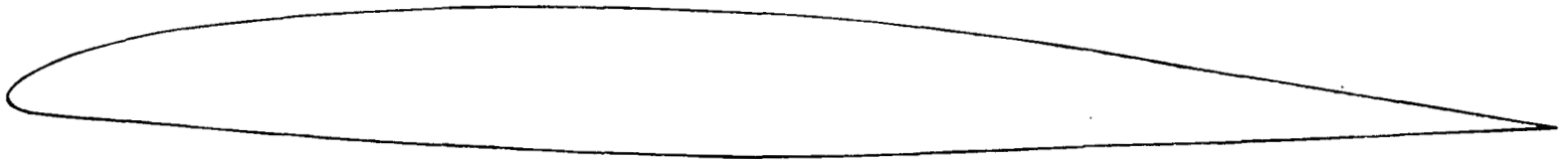

Figure 3.- Typical outboard wing airfoil section.

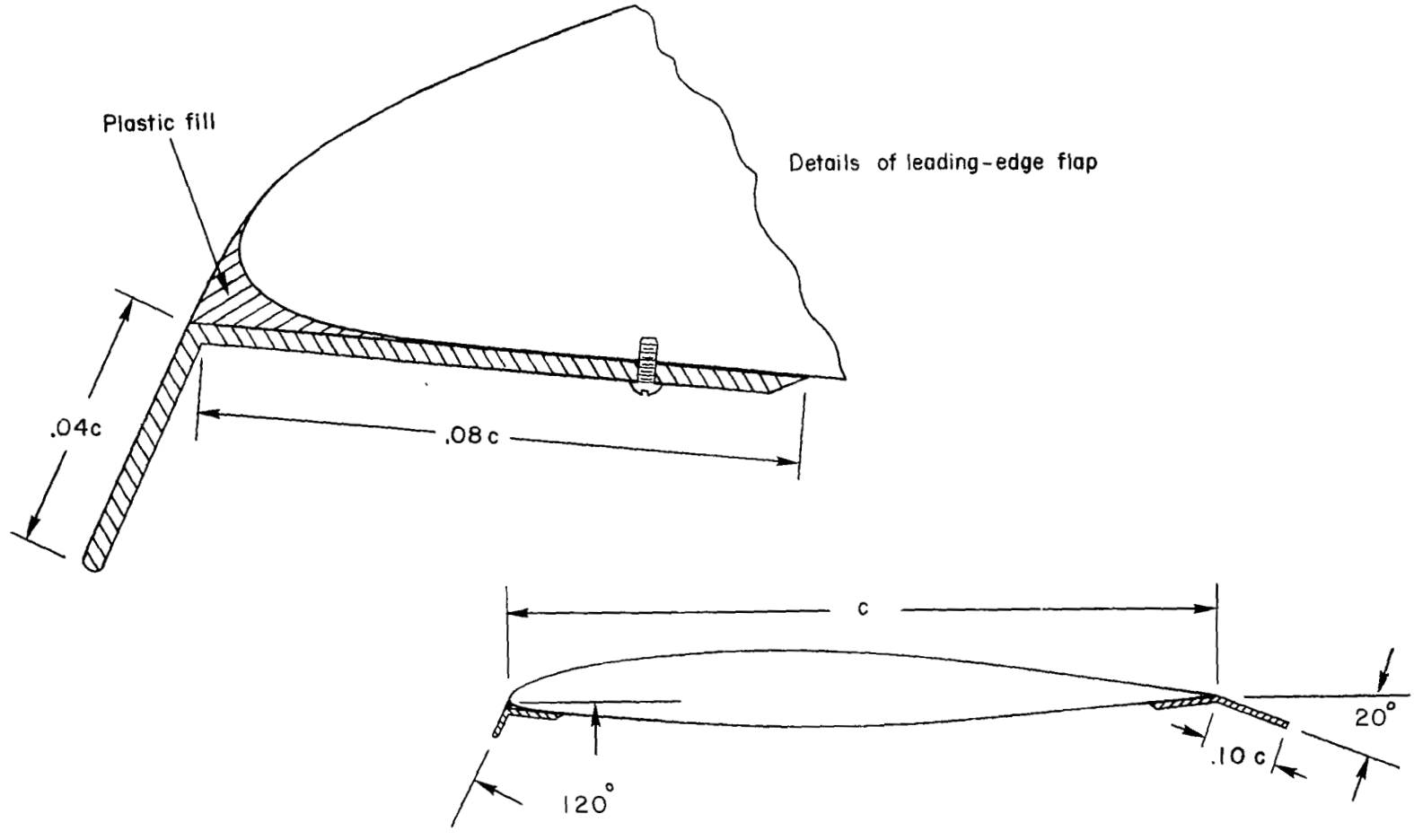

(a) Flap details.

Figure 4.- Drawings of leading- and trailing-edge flaps.

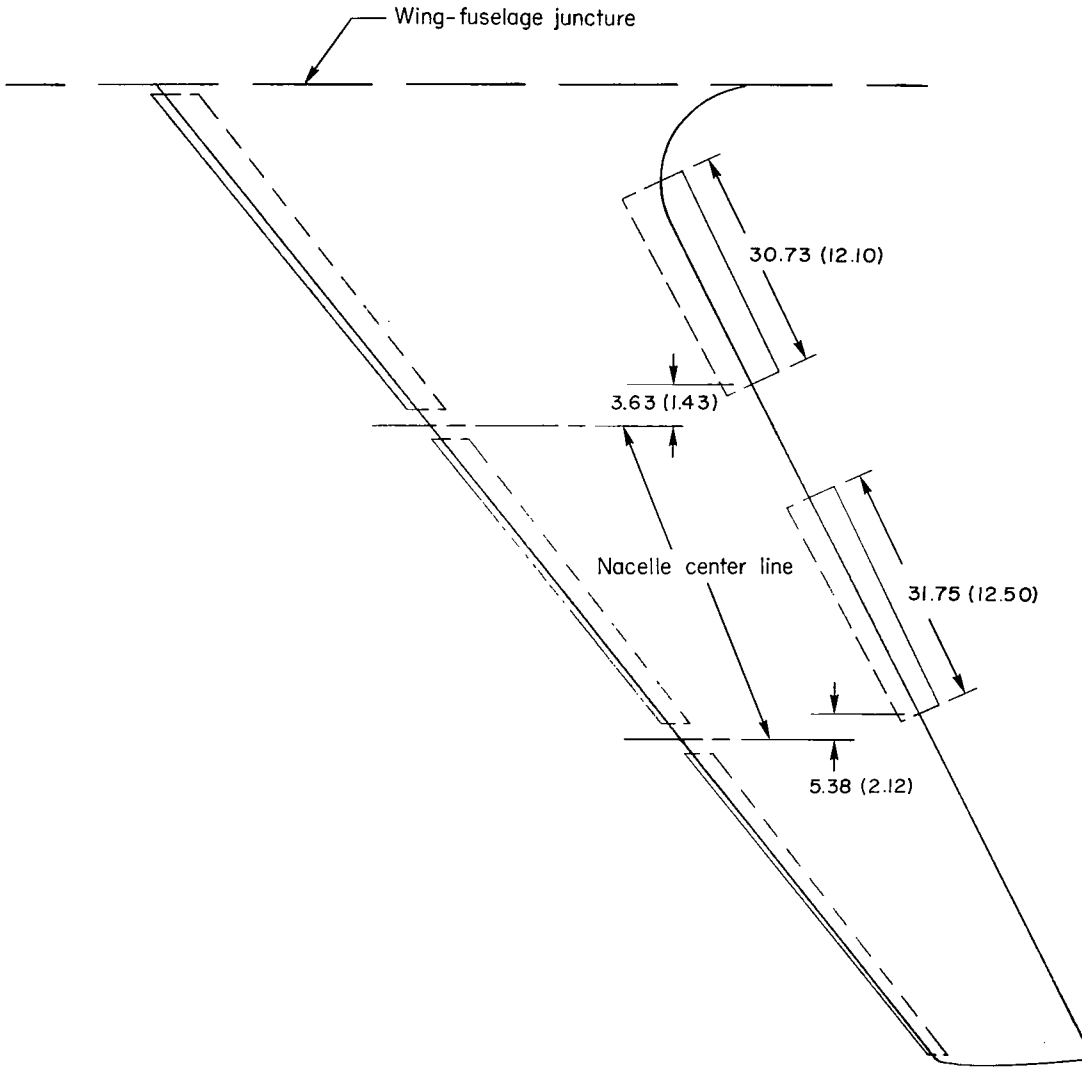

(b) Flap locations. Dimensions are in centimeters (inches).

Figure 4.- Concluded.

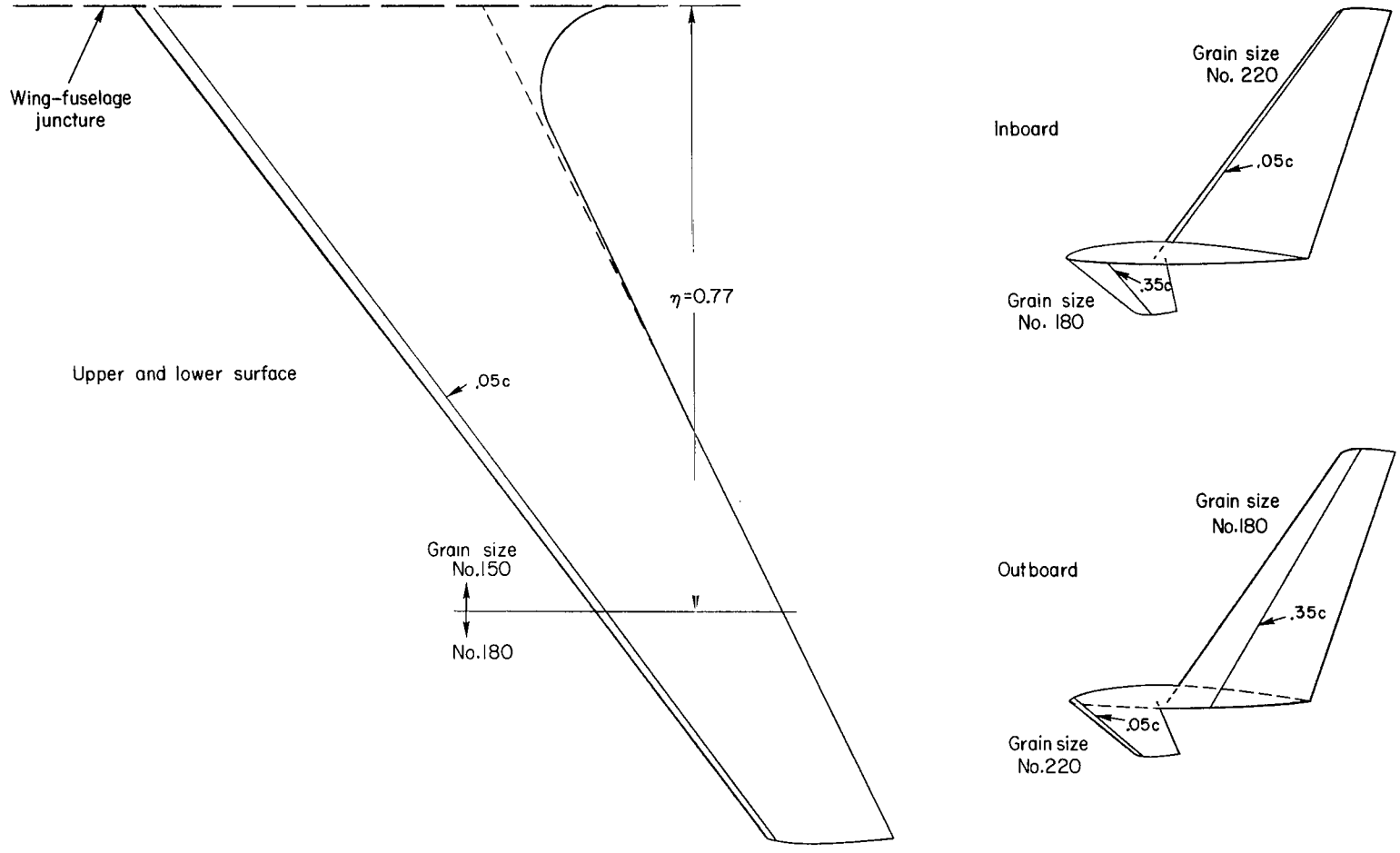

Figure 5.- Location of boundary-layer transition strips.

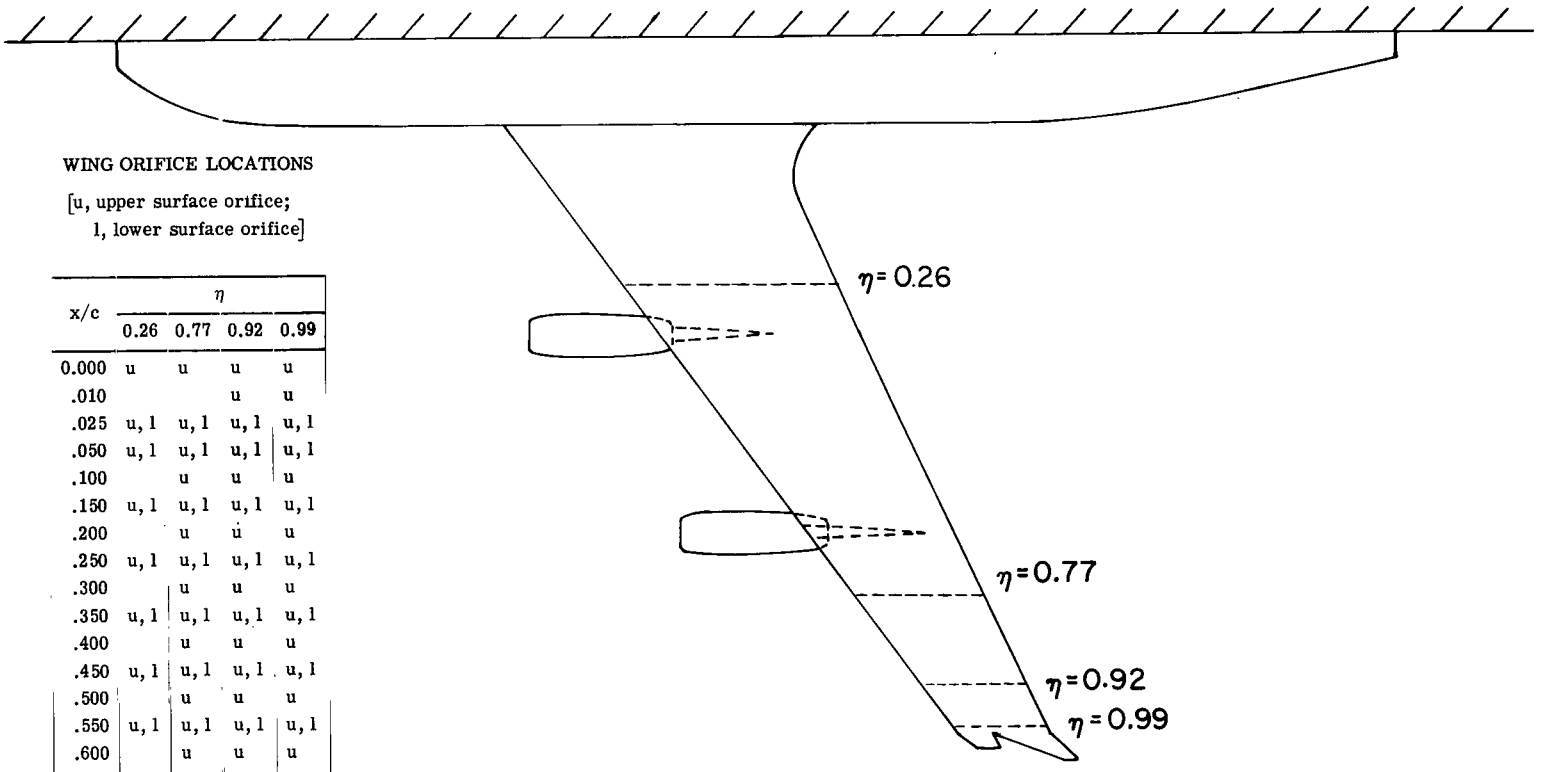

WING ORIFICE LOCATIONS

[u, upper surface orifice;
l, lower surface orifice]

x/c	η			
	0.26	0.77	0.92	0.99
0.000	u	u	u	u
.010			u	u
.025	u, l	u, l	u, l	u, l
.050	u, l	u, l	u, l	u, l
.100		u	u	u
.150	u, l	u, l	u, l	u, l
.200		u	u	u
.250	u, l	u, l	u, l	u, l
.300		u	u	u
.350	u, l	u, l	u, l	u, l
.400		u	u	u
.450	u, l	u, l	u, l	u, l
.500		u	u	u
.550	u, l	u, l	u, l	u, l
.600		u	u	u
.650	u, l	u, l	u, l	u, l
.700		u	u	u
.750	u, l	u, l	u, l	u, l
.800		u	u	
.850	u	u, l	u, l	u, l
.900		u	u	u
.950	u, l	u, l	u, l	u, l

(a) On wing.

Figure 6.- Wing and winglet static-pressure orifice locations.

WINGLET ORIFICE LOCATIONS

[u, upper surface orifice;
l, lower surface orifice]

x/c	η			
	Upper winglet			Lower winglet
	1.01	1.03	1.05	1.01
0.000	u	u	u	u
.020	u, l	u, l	u, l	u, l
.050	u, l	l	u, l	u, l
.150	u, l	u, l	u, l	u, l
.250	u, l	u, l	u, l	u, l
.350	u, l	u	u, l	u, l
.450	u, l	u, l	u, l	u, l
.550	u, l	u, l	u, l	u, l
.650	u, l	u, l	u, l	u, l
.750	u, l	u, l	u, l	u, l
.850	u, l	u, l	u, l	u, l
.950	u, l	u, l	u, l	u, l

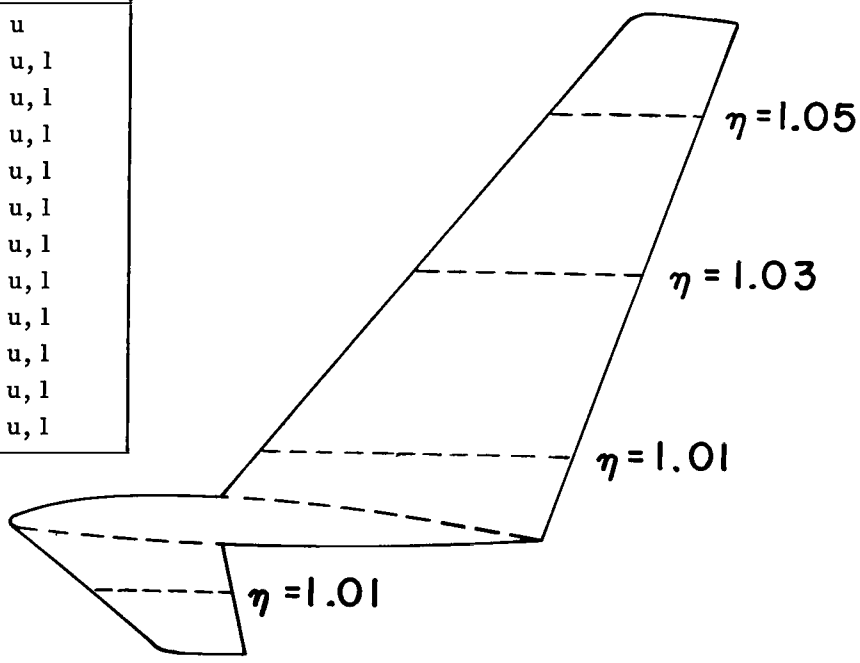

(b) On winglets.

Figure 6.- Concluded.

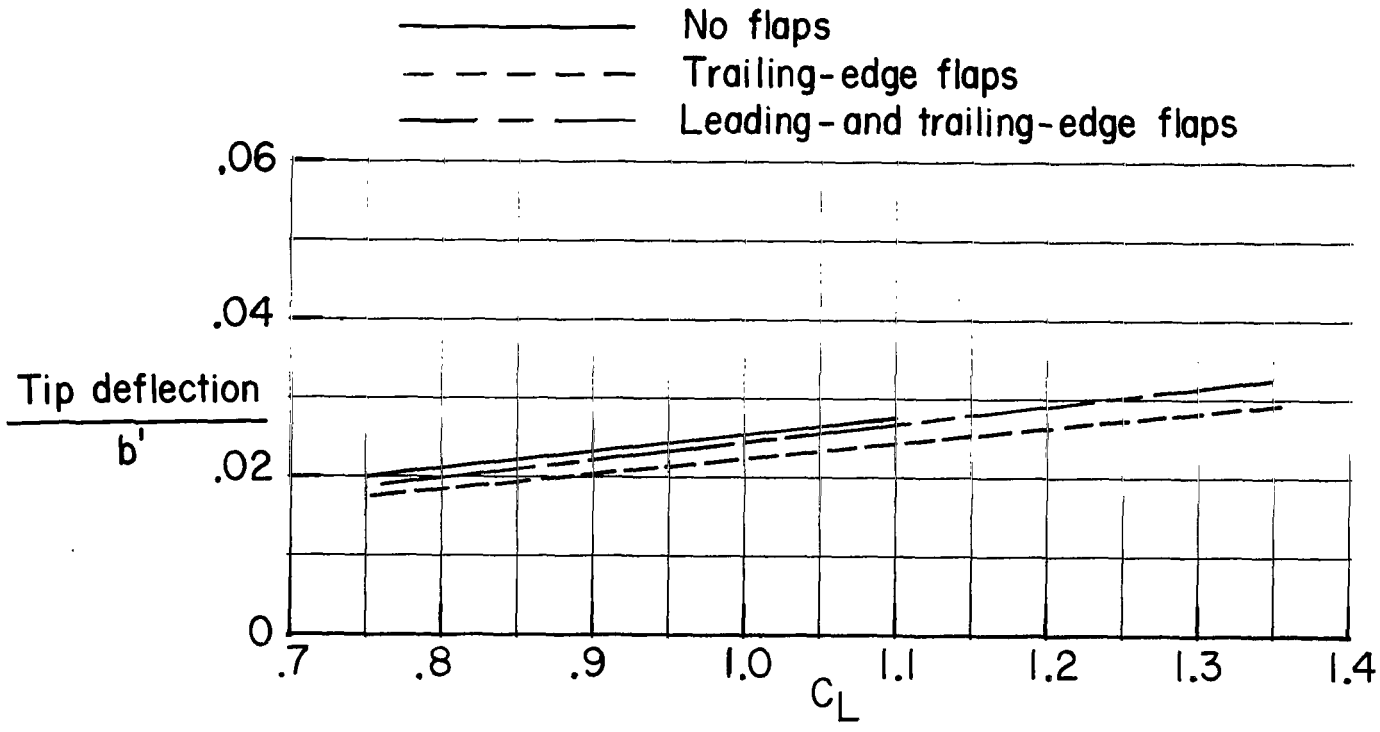

Figure 7.- Wing-tip deflection for basic-tip configuration.

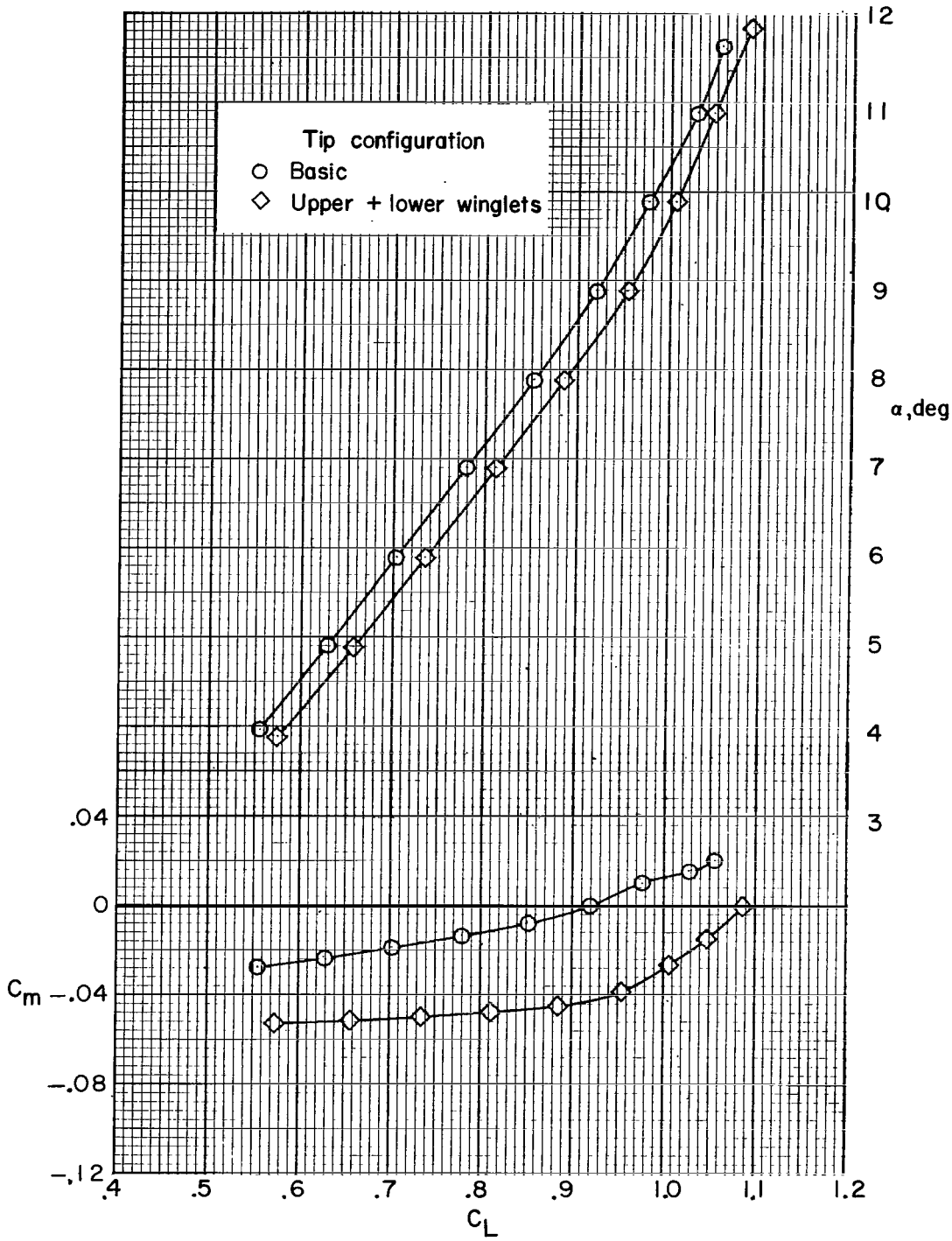

(a) No flaps.

Figure 8.- Variation of pitching-moment coefficient and angle of attack with lift coefficient. $M_\infty = 0.30$.

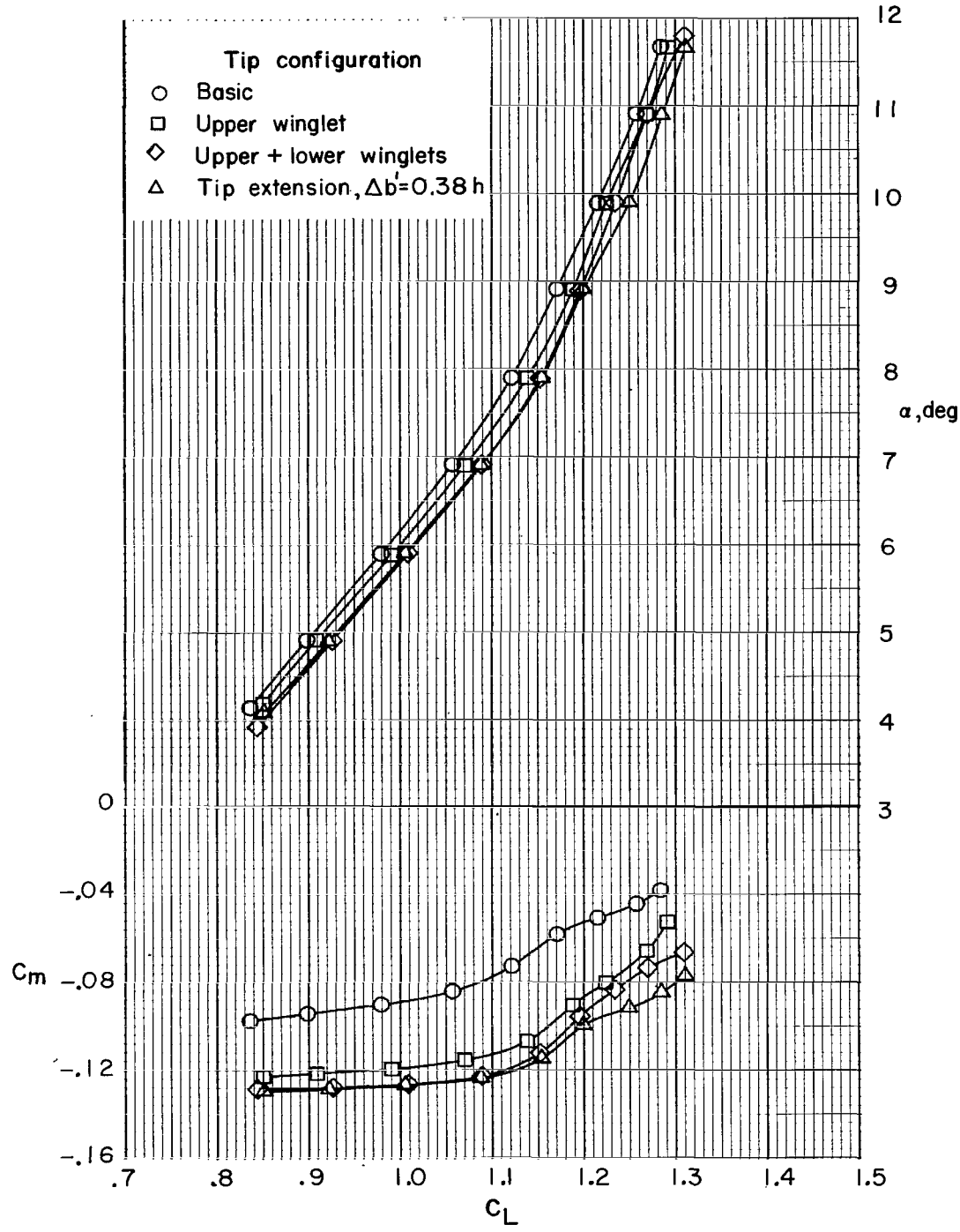

(b) Trailing-edge flaps.

Figure 8.- Continued.

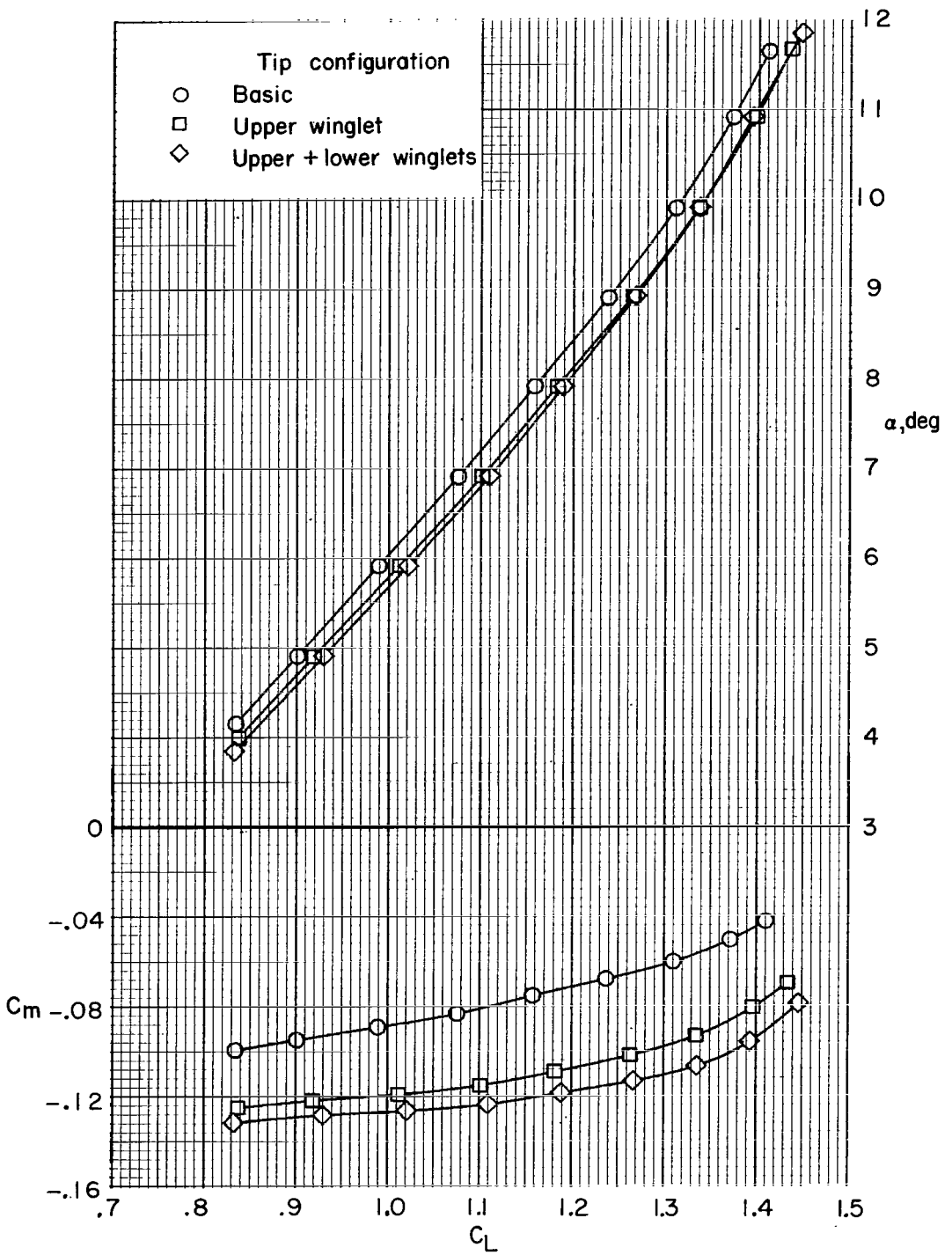

(c) Leading- and trailing-edge flaps.

Figure 8.- Concluded.

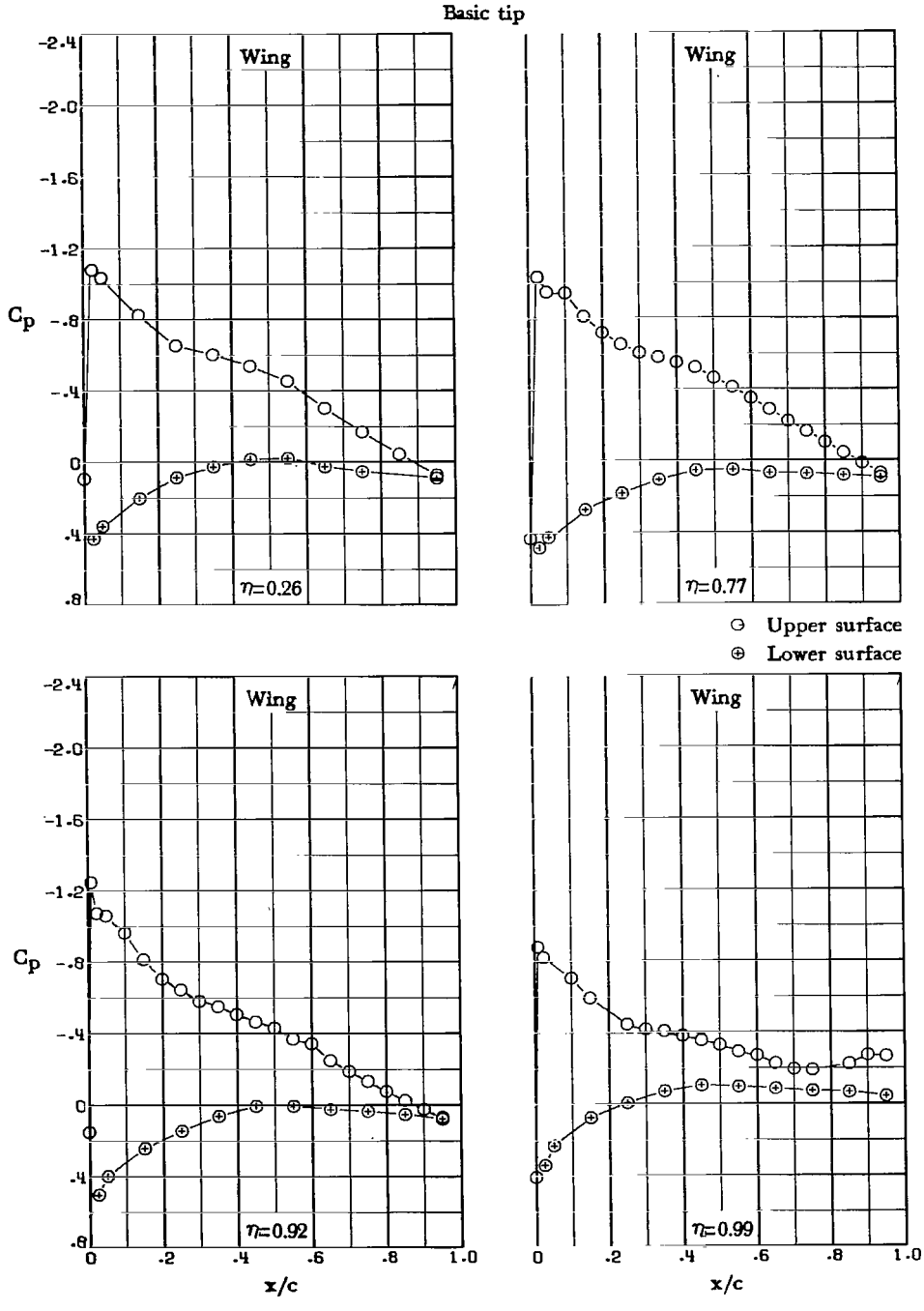

(a) $\alpha = 4.1^{\circ}$.

Figure 9.- Pressure distributions for basic-tip configuration. Note that vertical scale increment of insert plots is larger.

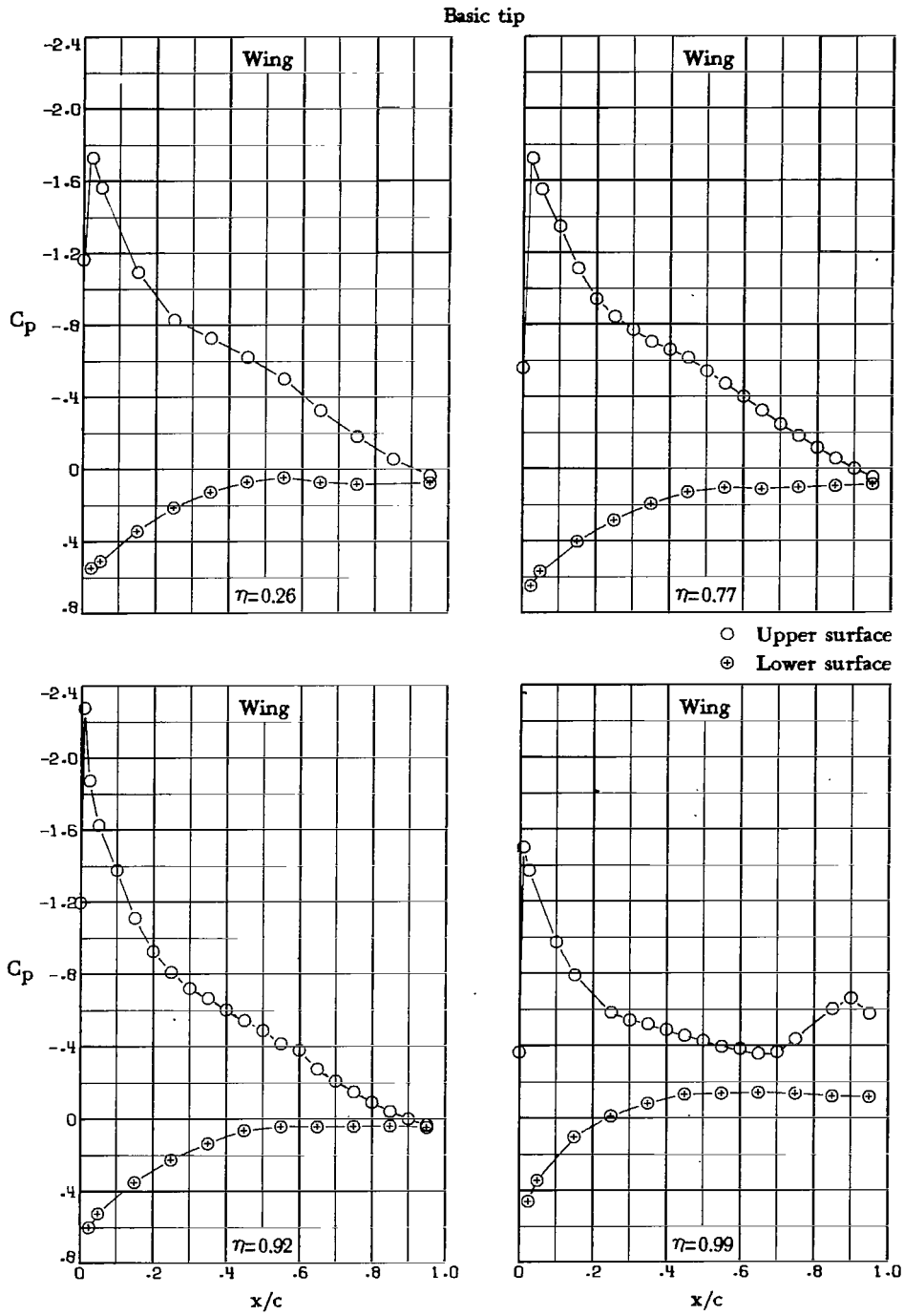

(b) $\alpha = 7.0^{\circ}$.

Figure 9.- Continued.

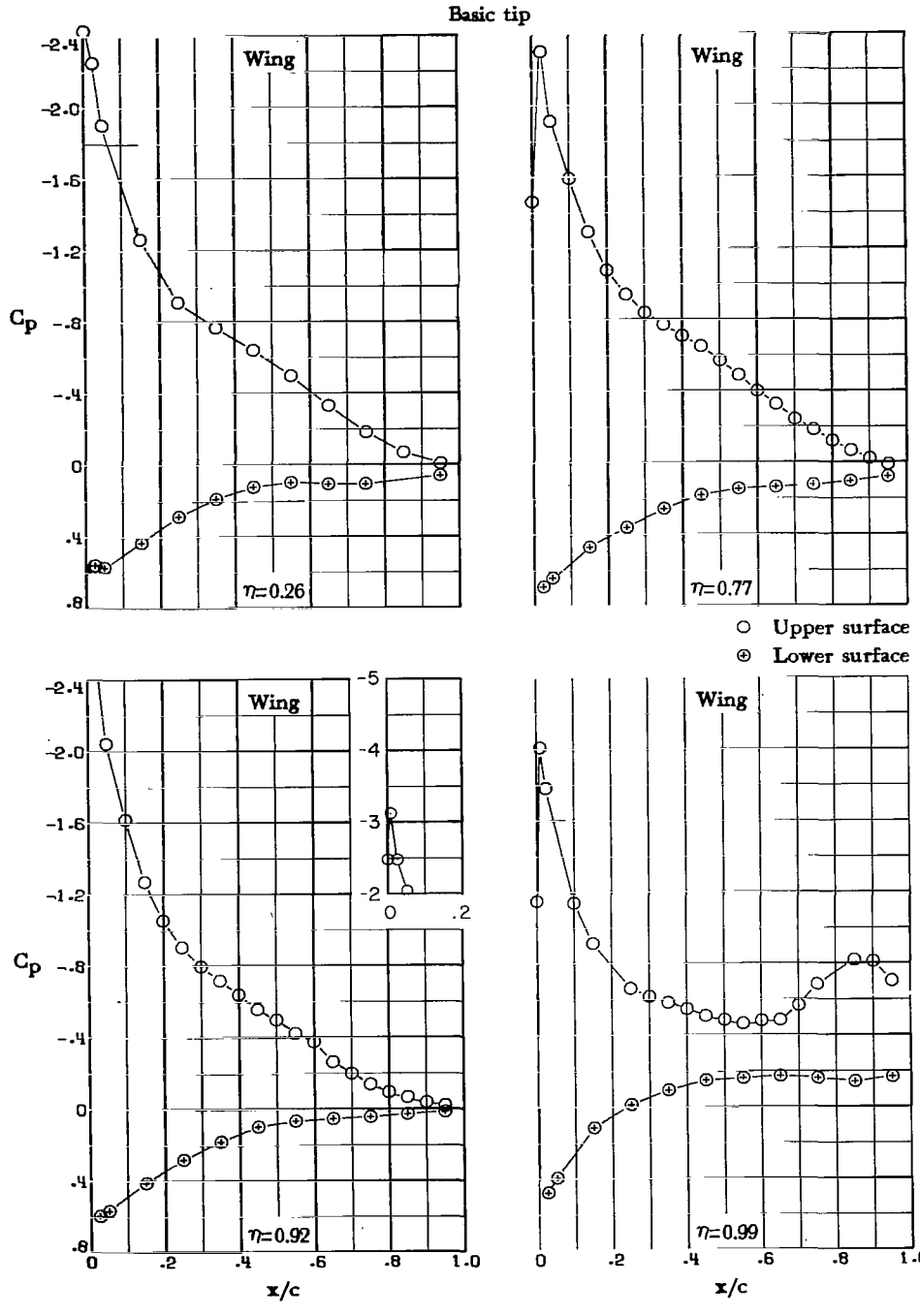

(c) $\alpha = 9.0^{\circ}$.

Figure 9.- Continued.

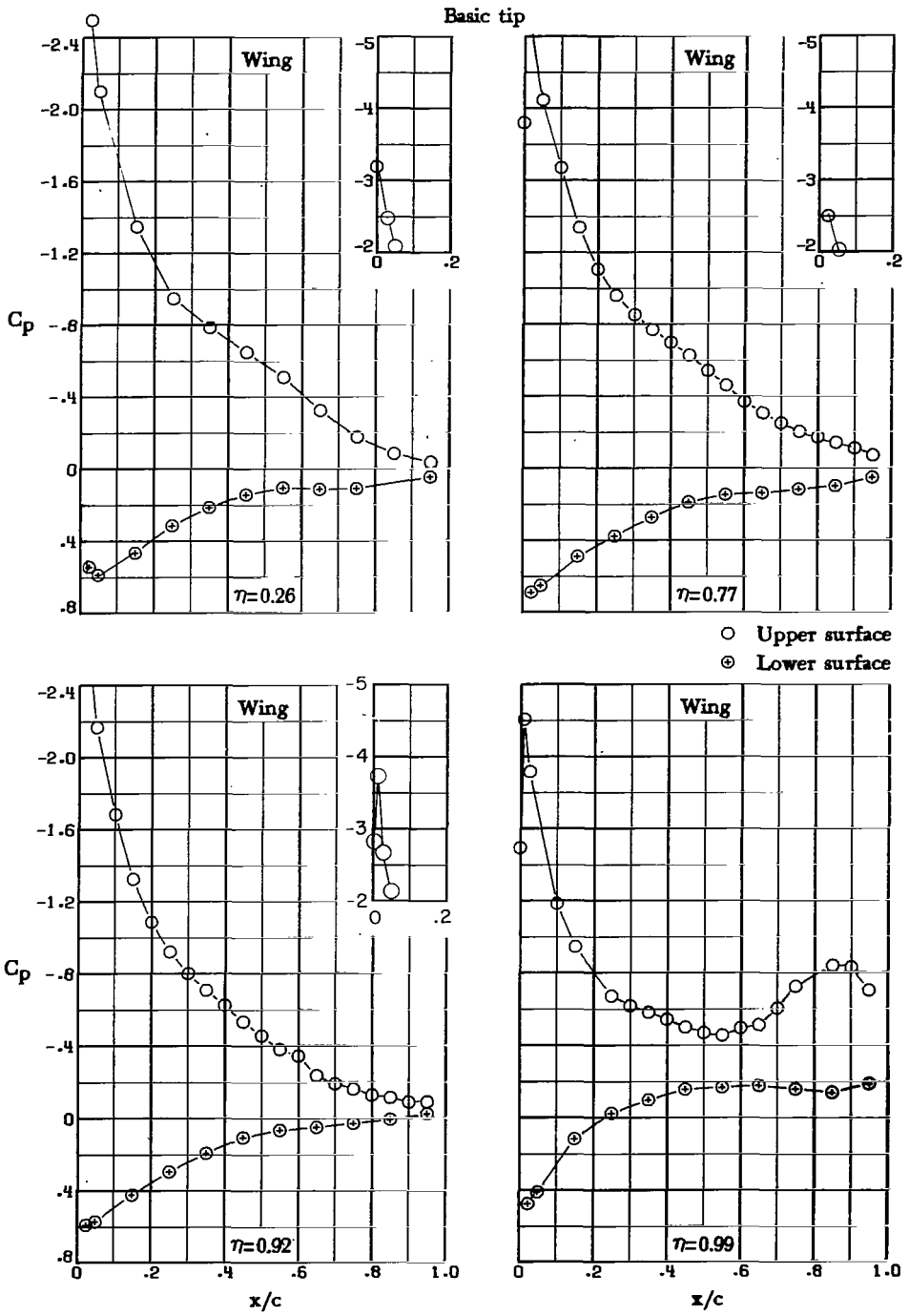

(d) $\alpha = 10.0^{o}$.

Figure 9.- Continued.

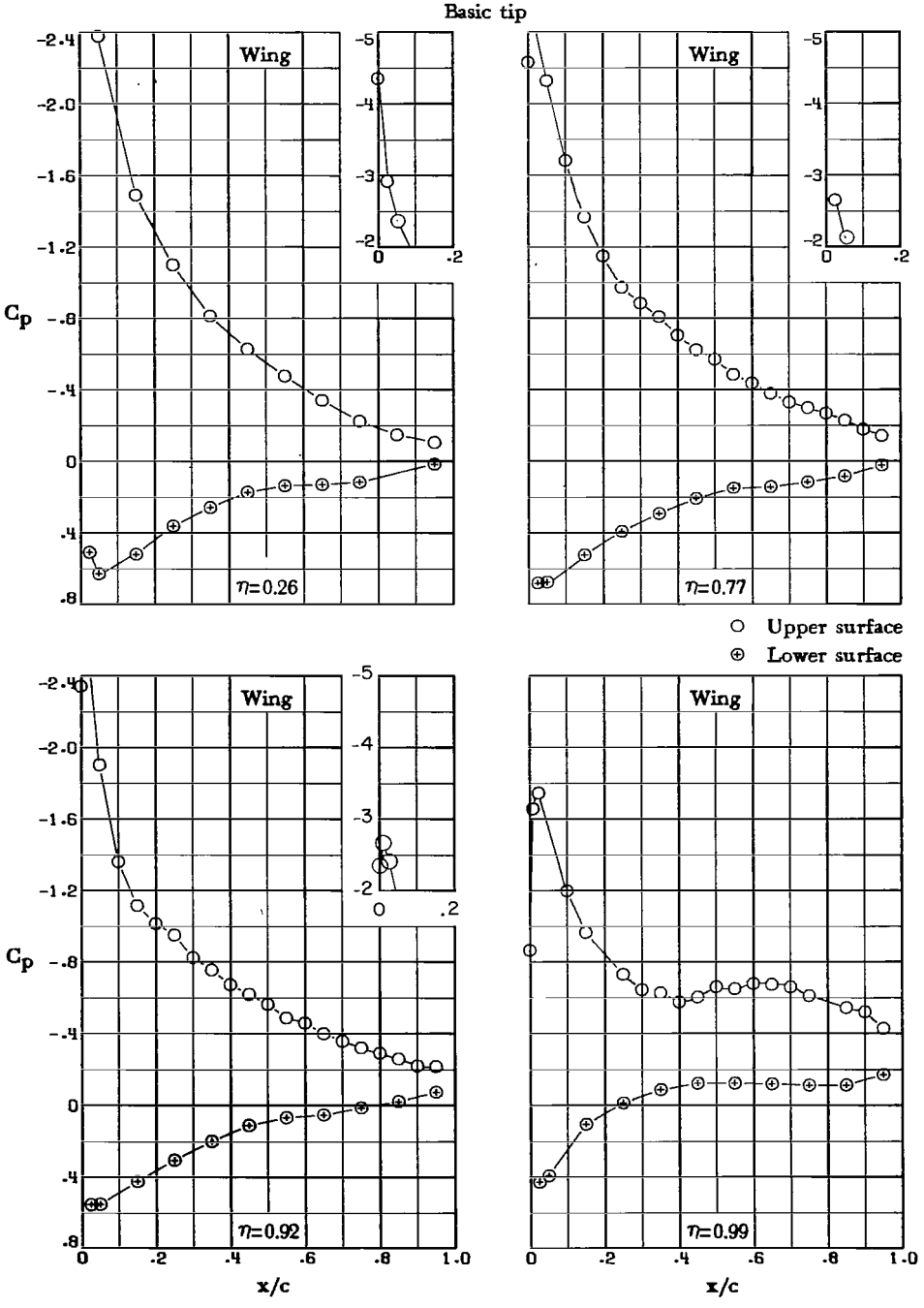

(e) α = 11.8°.

Figure 9.- Concluded.

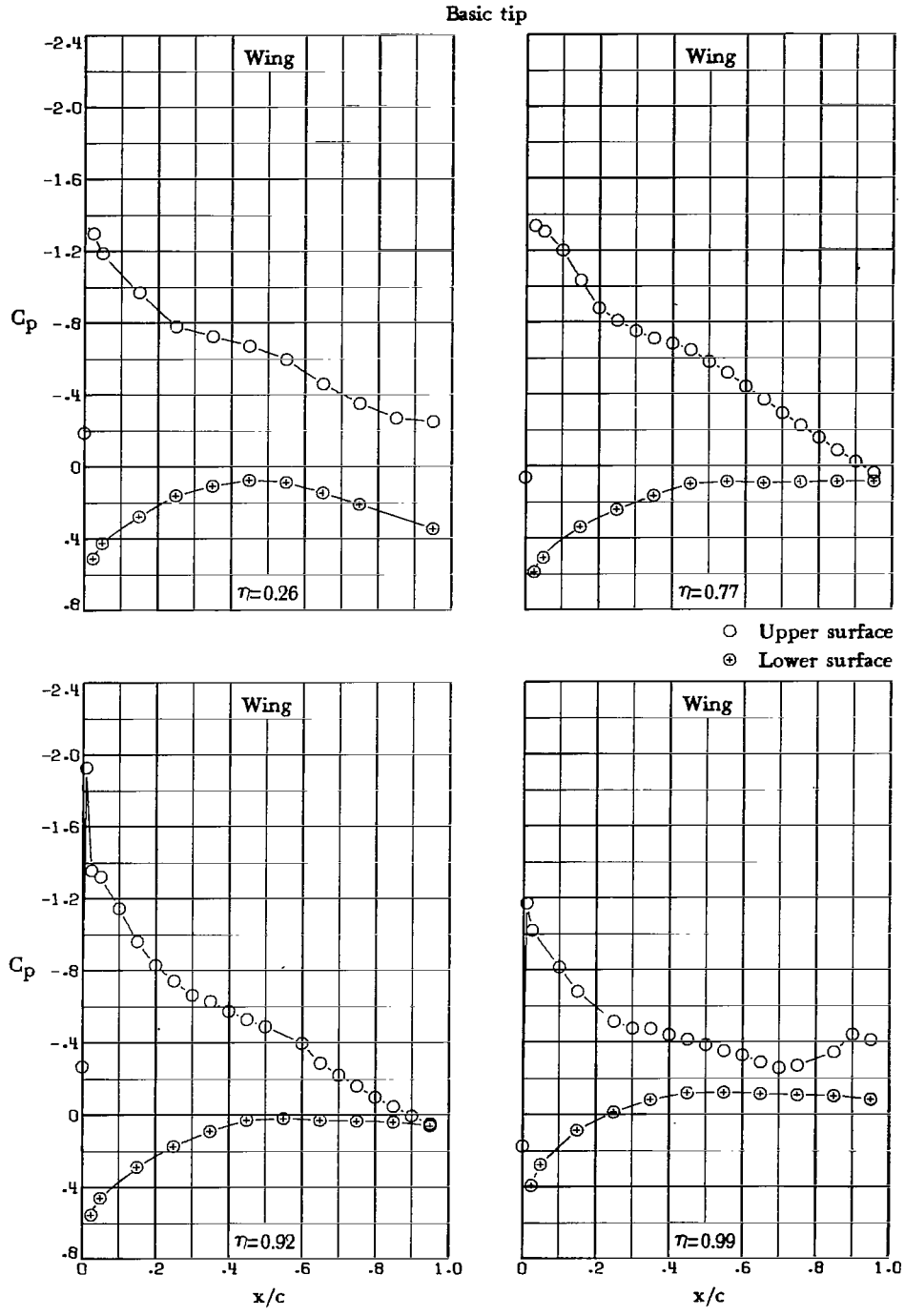

(a) $\alpha = 4.2^{\circ}$.

Figure 10.- Pressure distribution for basic-tip configuration with trailing-edge flaps. Note that vertical scale increment of insert plots is larger.

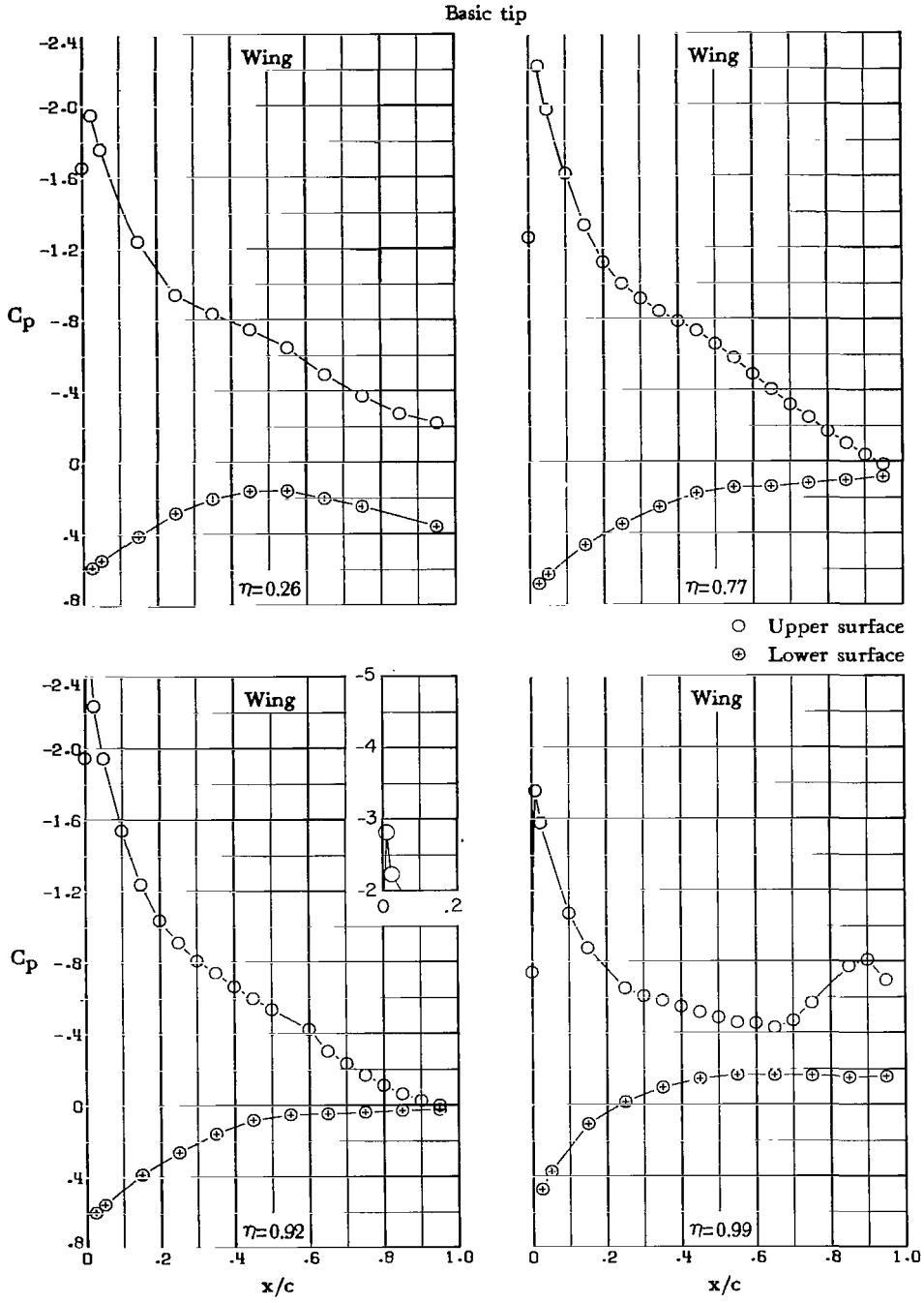

(b) $\alpha = 7.0^{\circ}$.

Figure 10.- Continued.

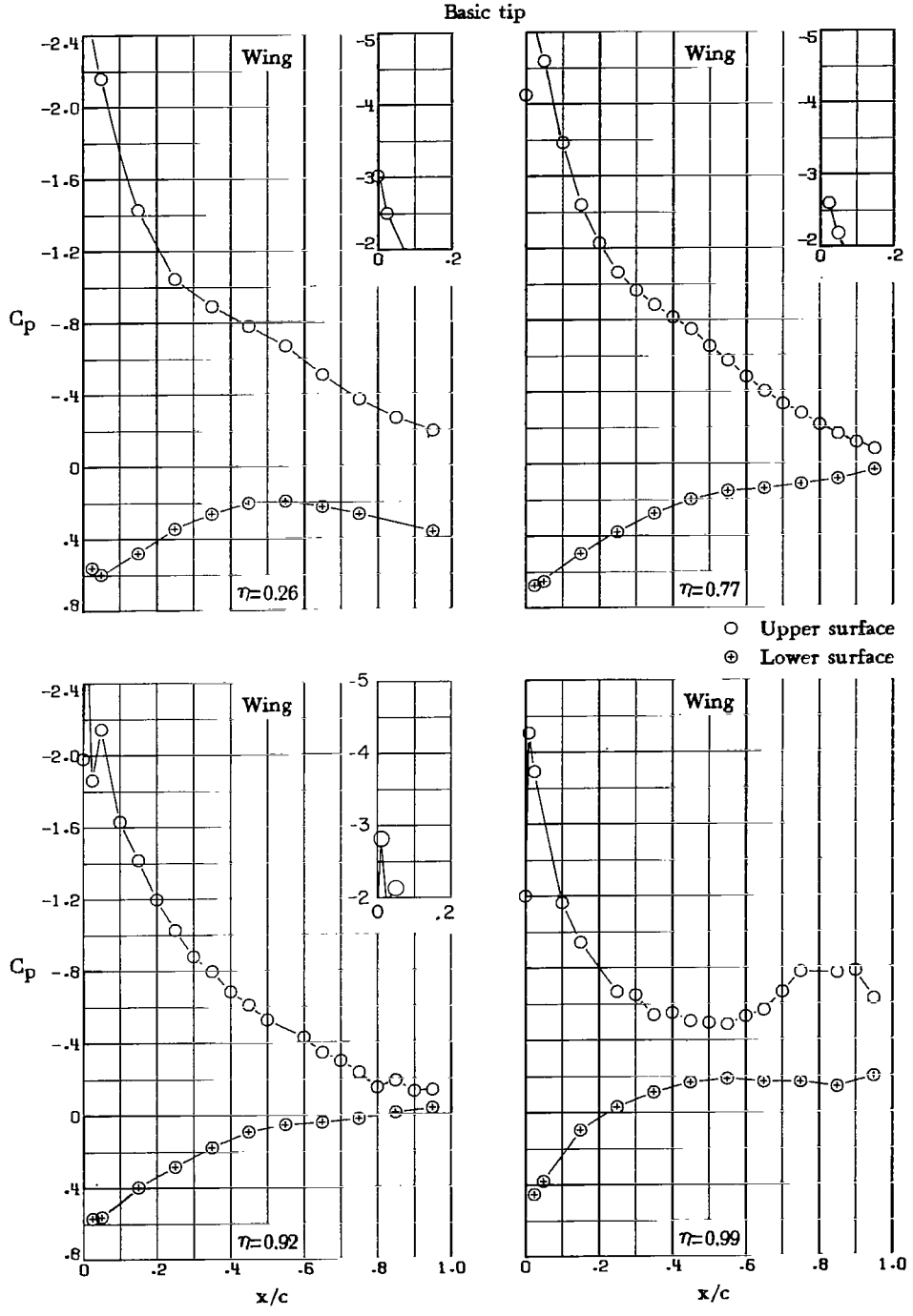

(c) $\alpha = 9.0^{\circ}$.

Figure 10.- Continued.

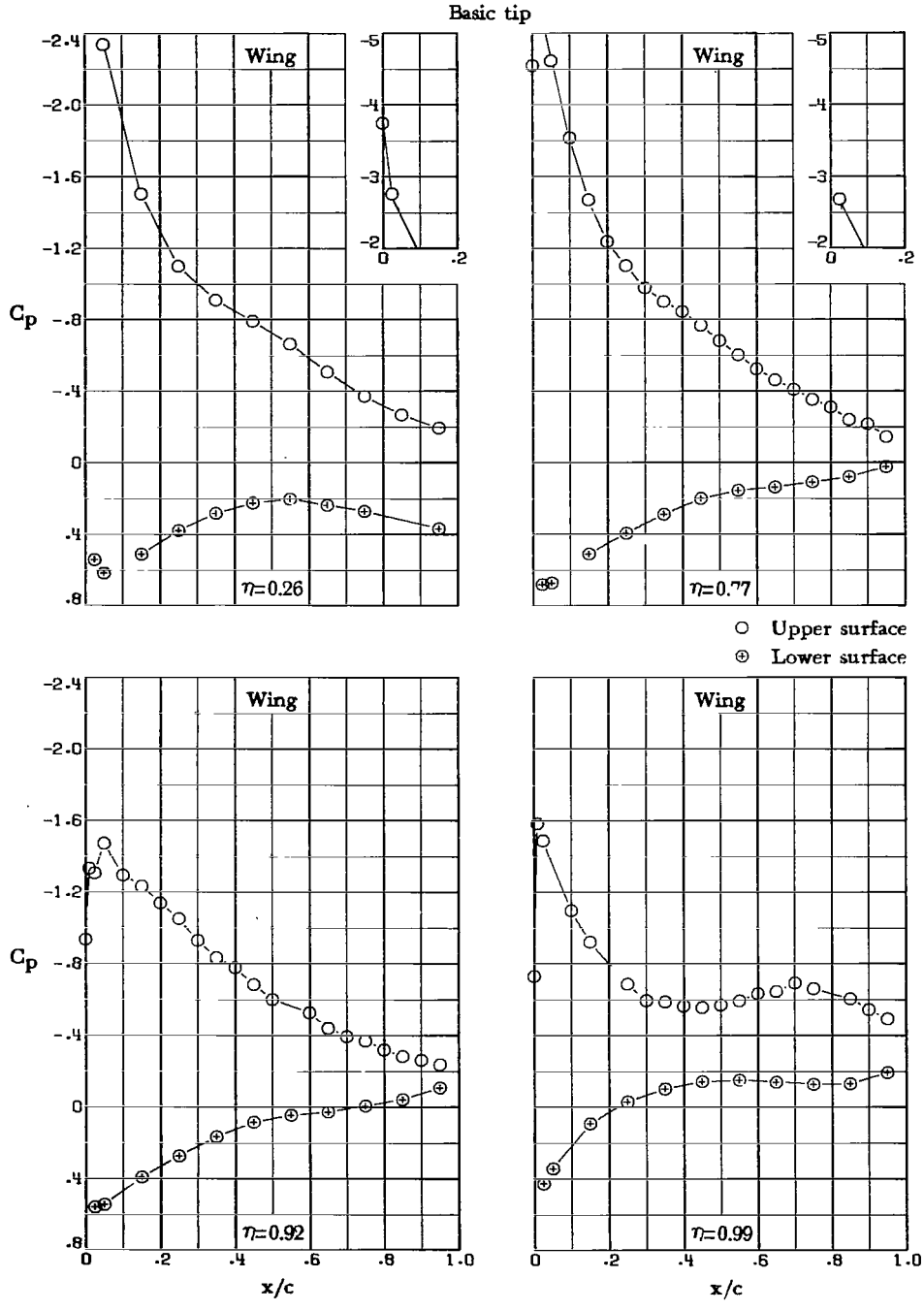

(d) α = 10.0°.

Figure 10.- Continued.

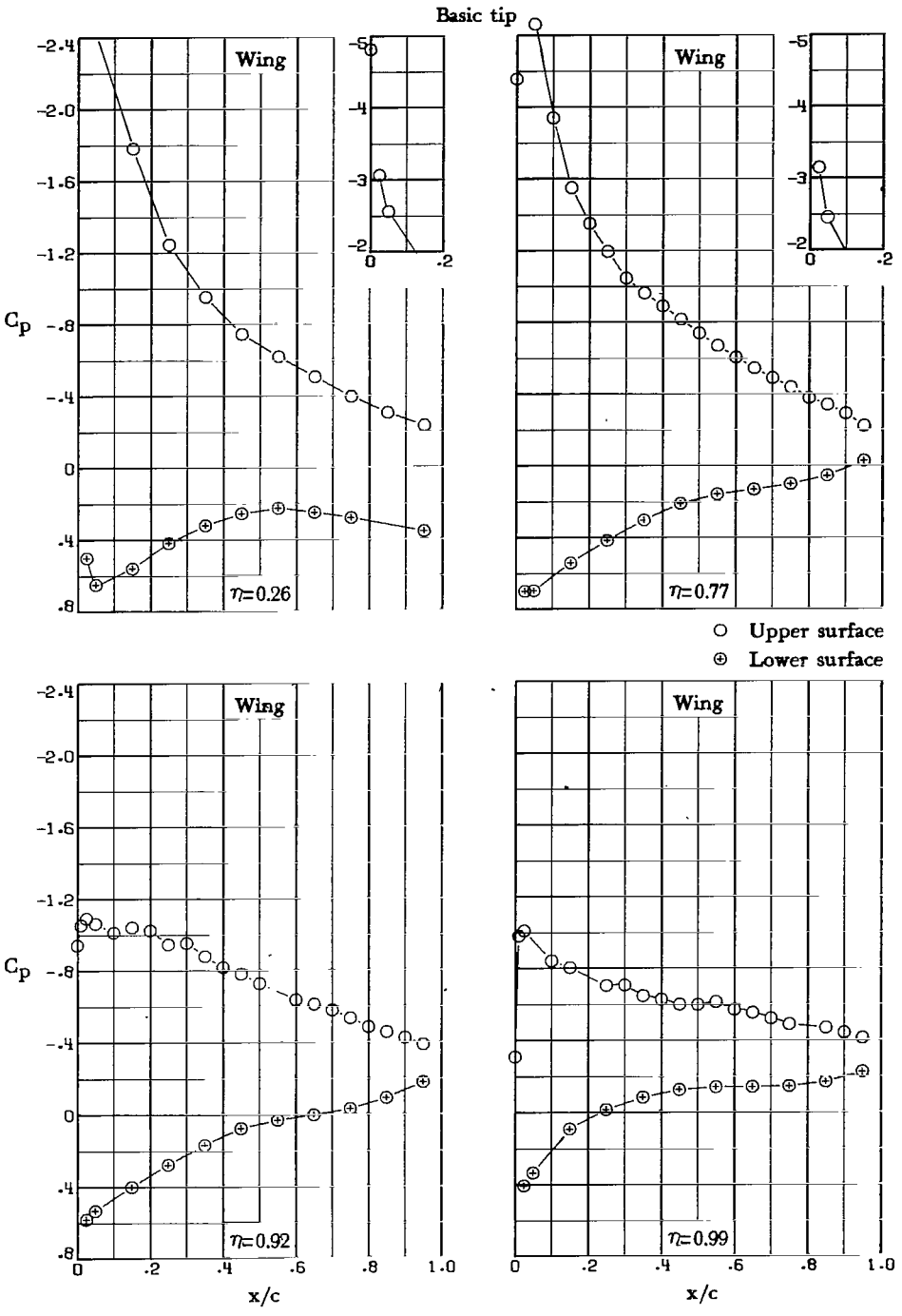

(e) $\alpha = 11.8^{\circ}$.

Figure 10.- Concluded.

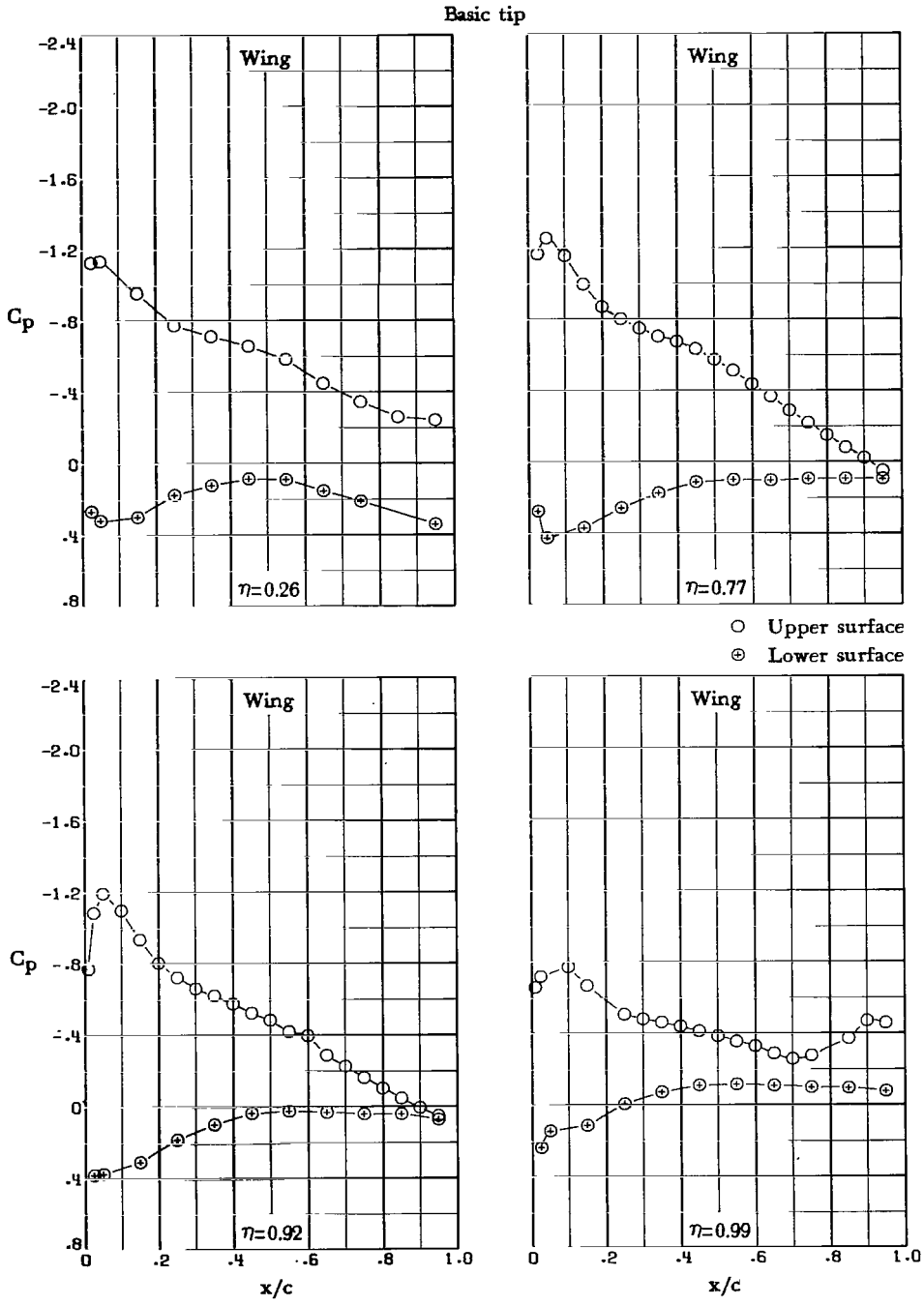

(a) α = 4.2°.

Figure 11.- Pressure distributions for basic-tip configuration with leading- and trailing-edge flaps. Note that vertical scale increment of insert plots is larger.

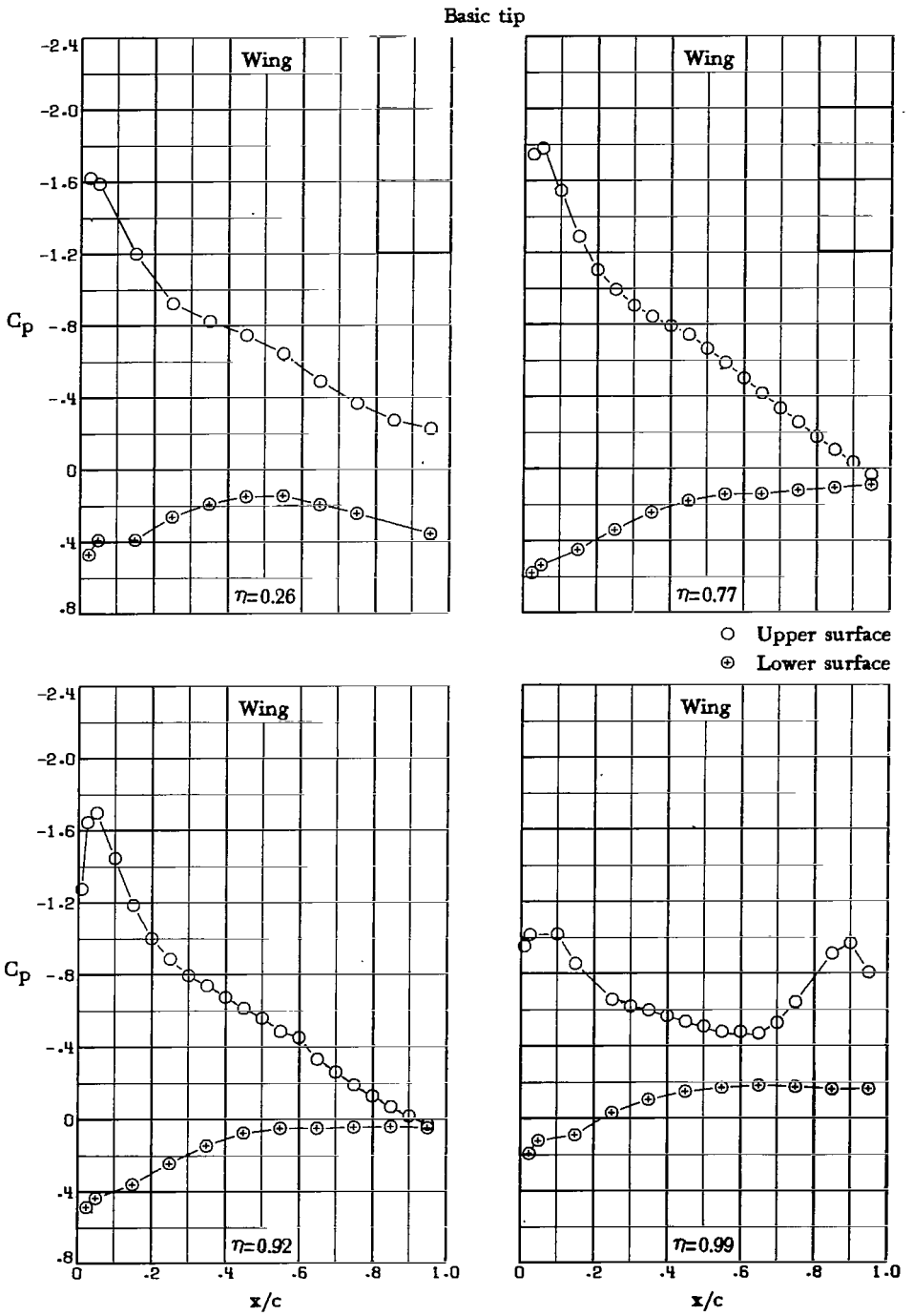

(b) $\alpha = 7.0^{o}$.

Figure 11.- Continued.

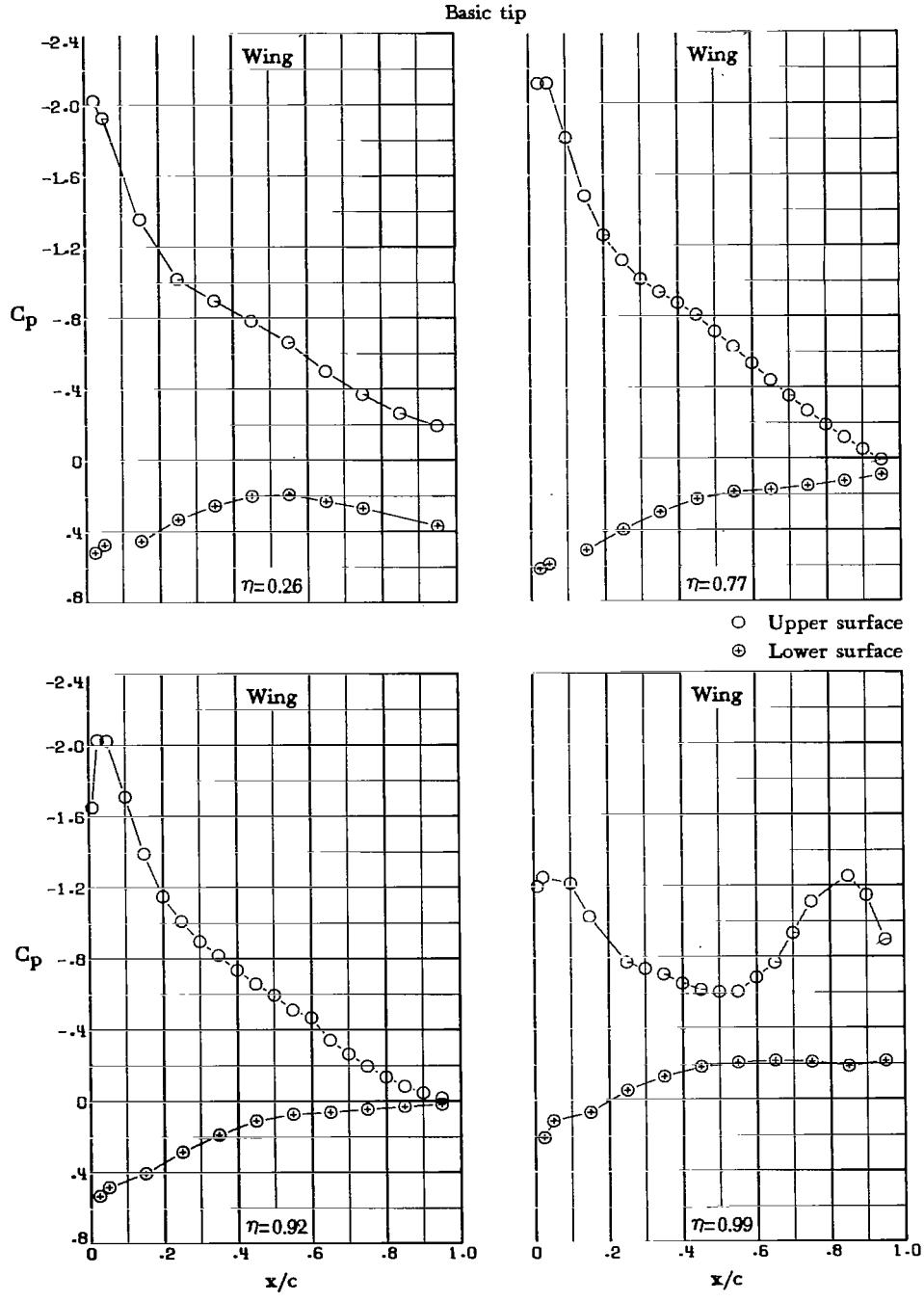

(c) α = 9.0°.

Figure 11.- Continued.

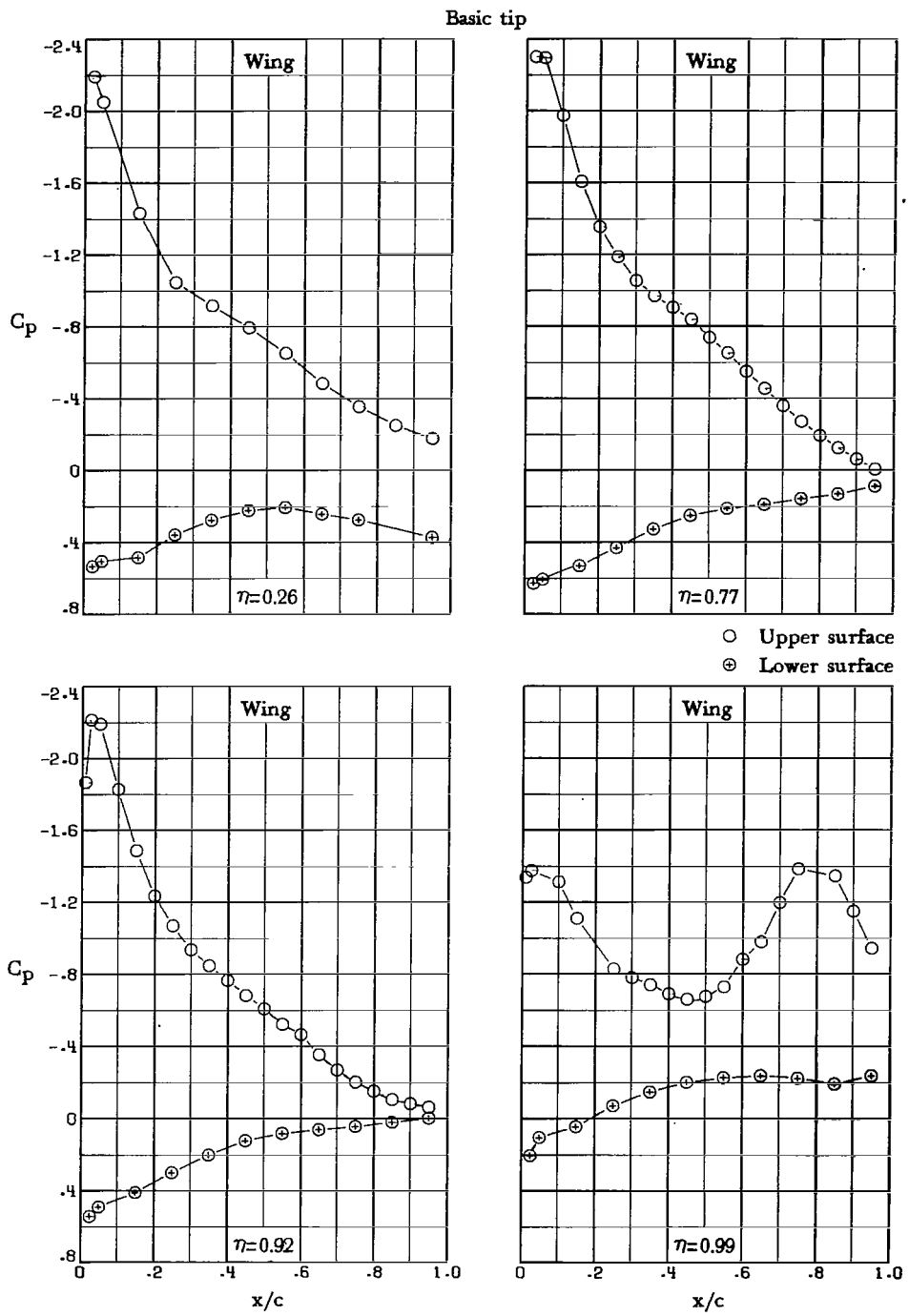

(d) α = 10.0°.

Figure 11.- Continued.

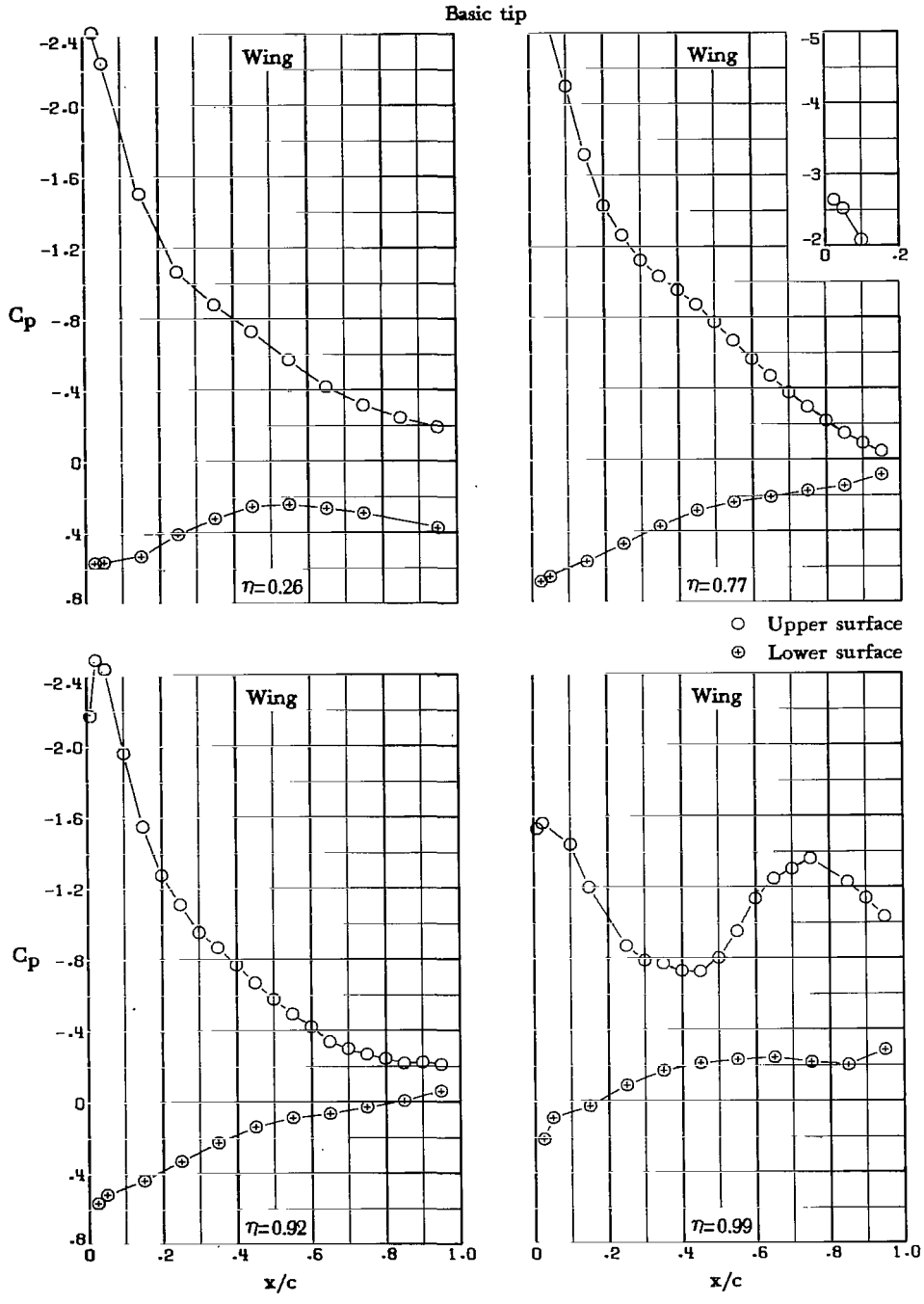

(e) α = 11.8°.

Figure 11.- Concluded.

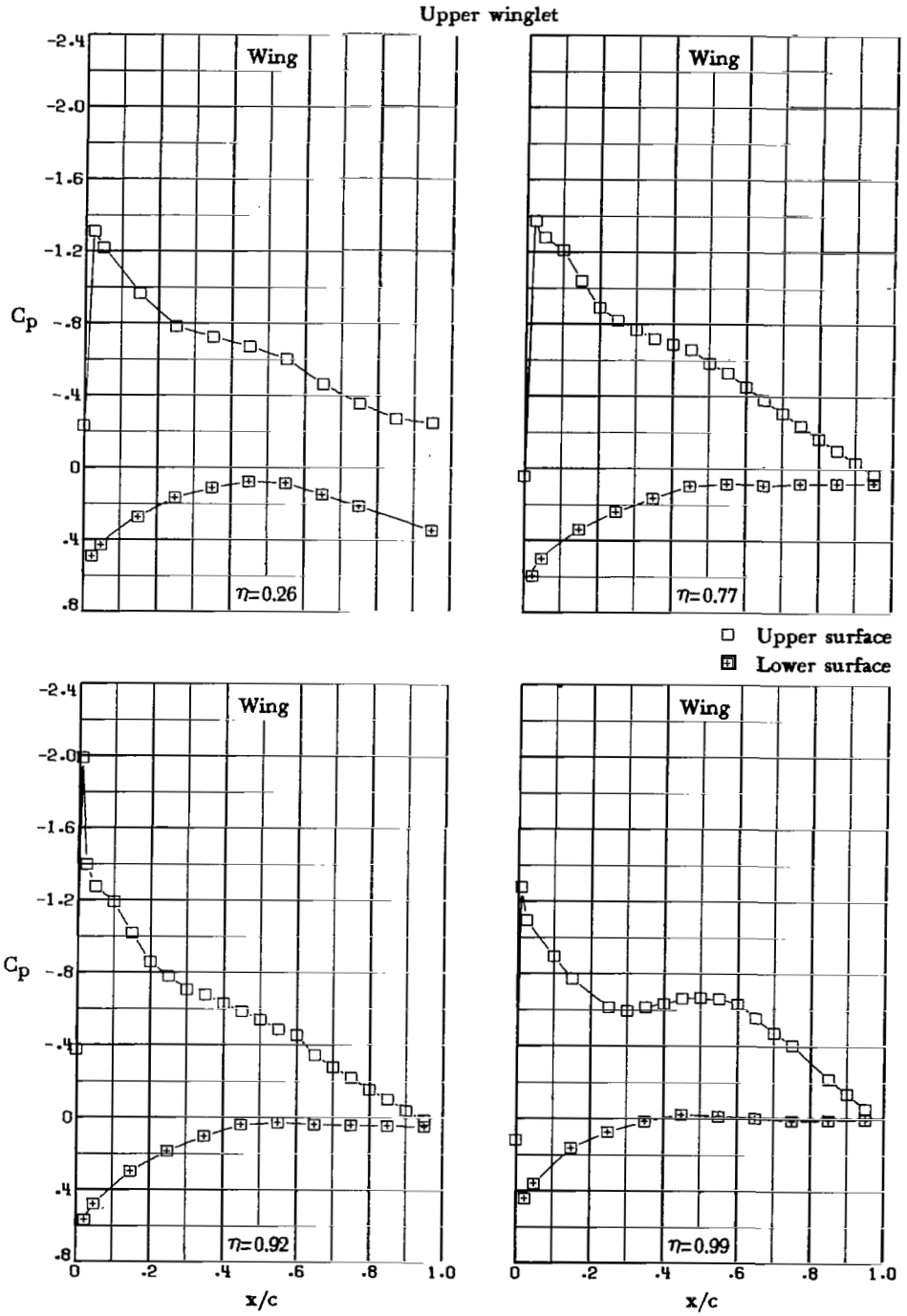

(a) $\alpha = 4.3^{\circ}$.

Figure 12.- Pressure distributions for upper-winglet configuration with trailing-edge flaps. Note that vertical scale increment of insert plots is larger.

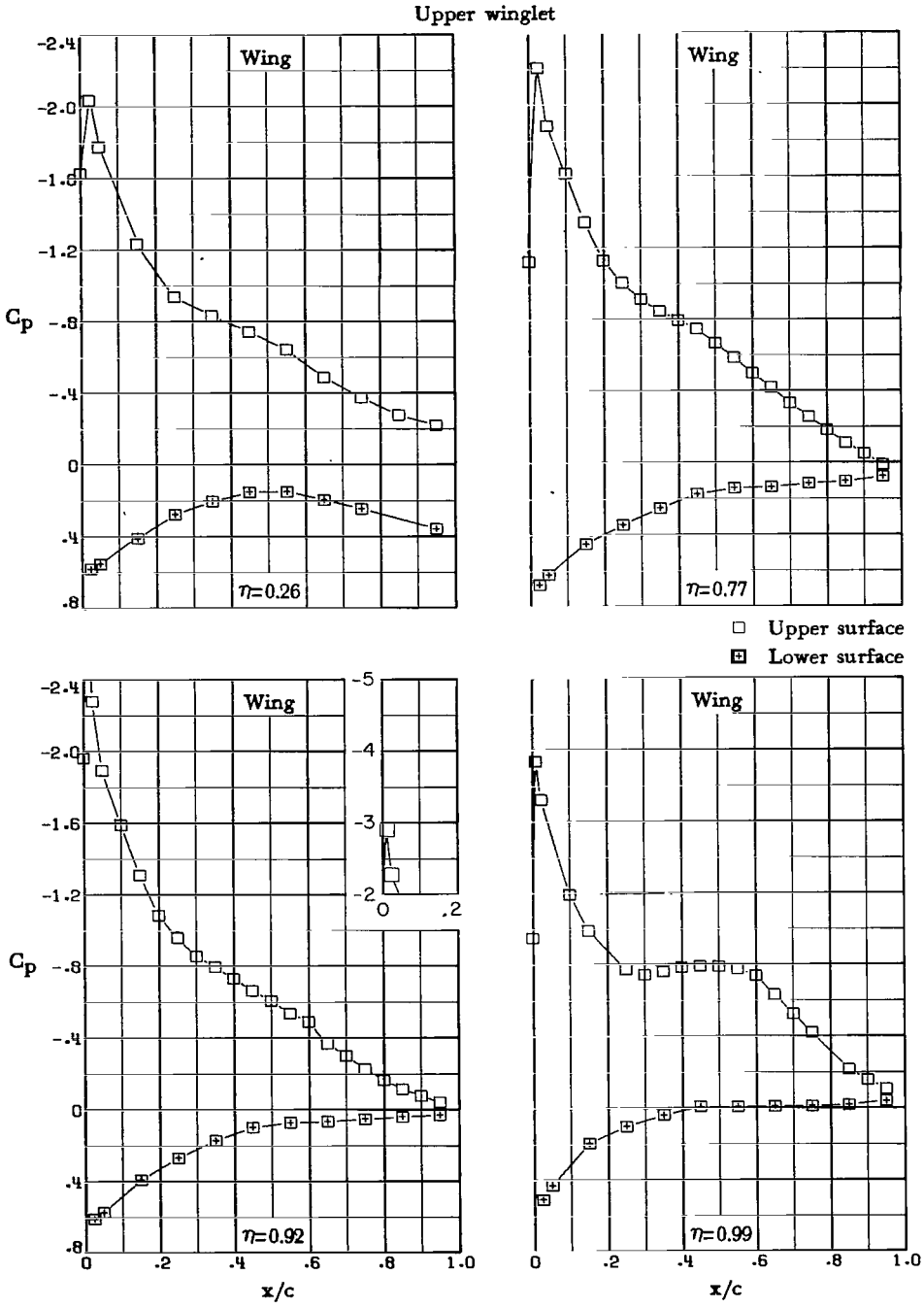

(b) $\alpha = 7.0^{o}$.

Figure 12.- Continued.

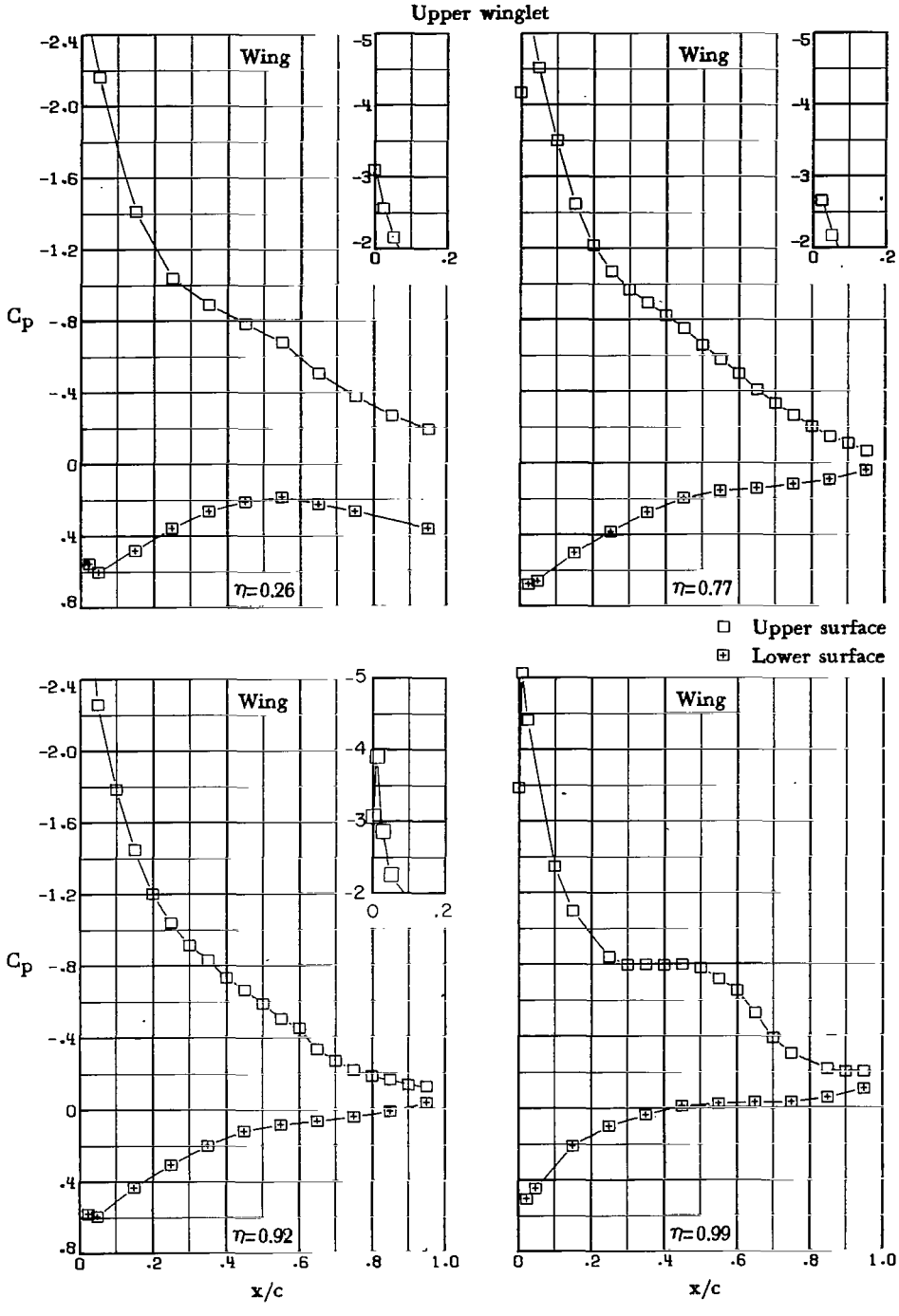

(c) $\alpha = 9.0^{\circ}$.

Figure 12.- Continued.

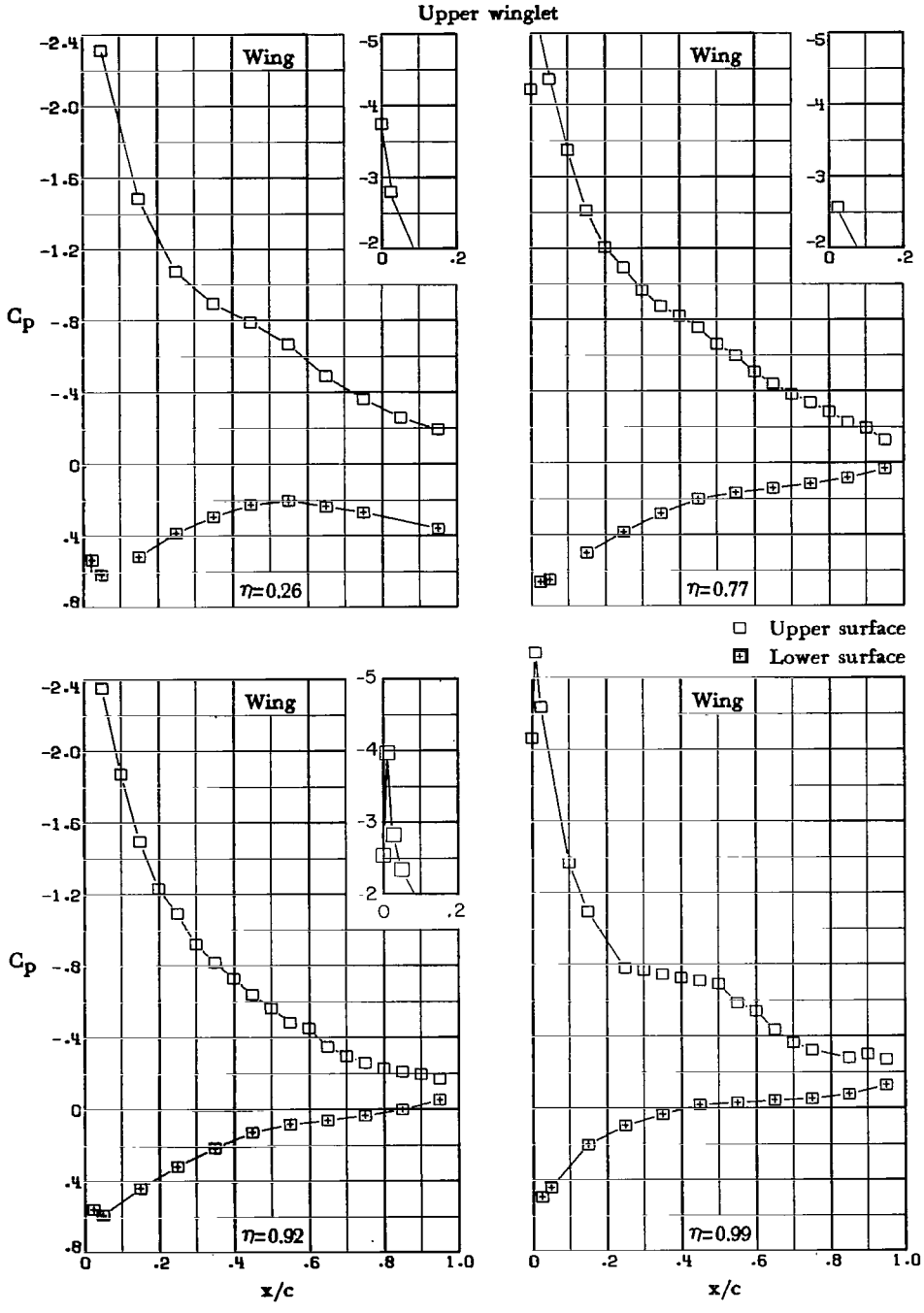

(d) α = 10.0°.

Figure 12.- Continued.

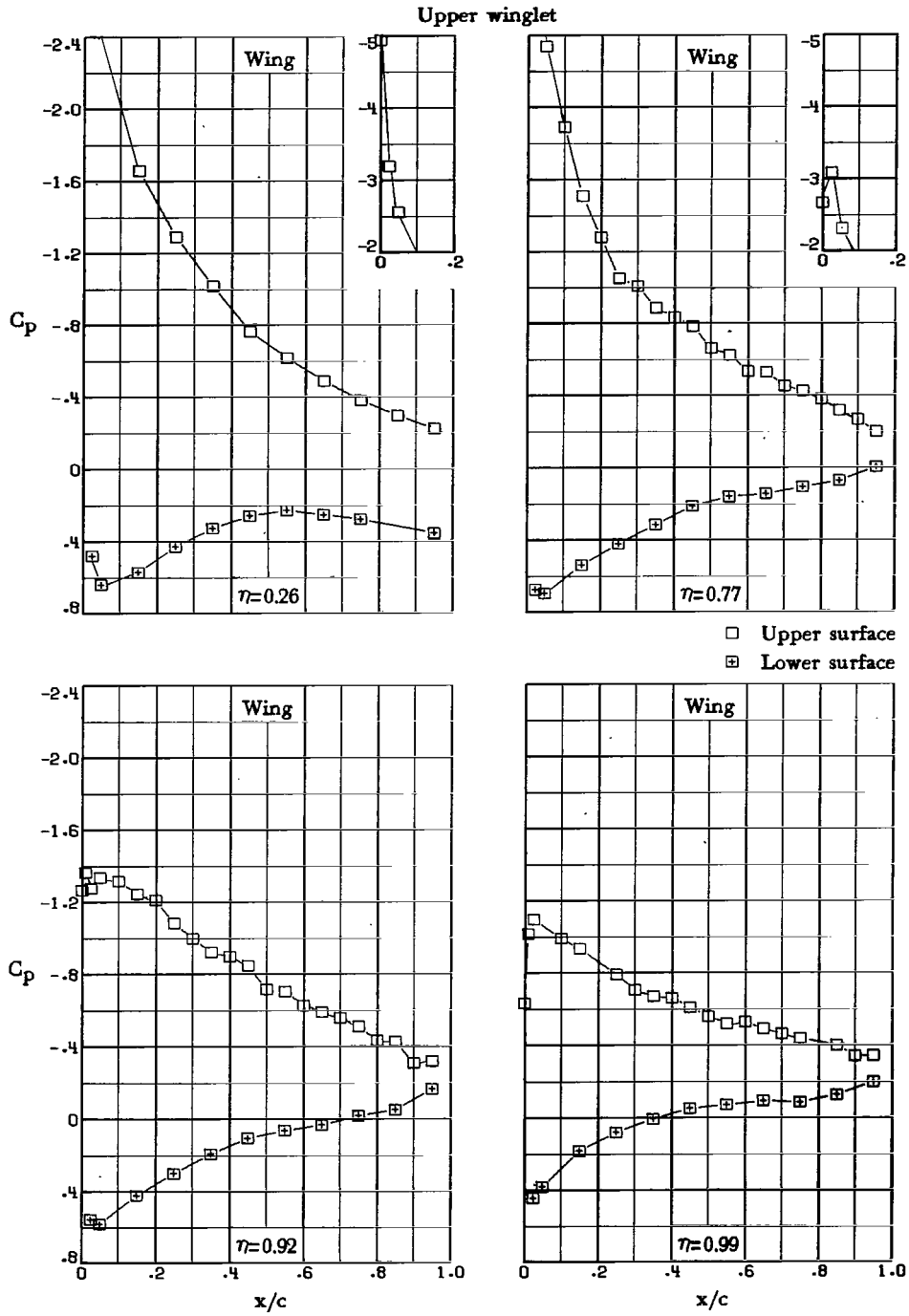

(e) $\alpha = 11.8^{o}$.

Figure 12.- Concluded.

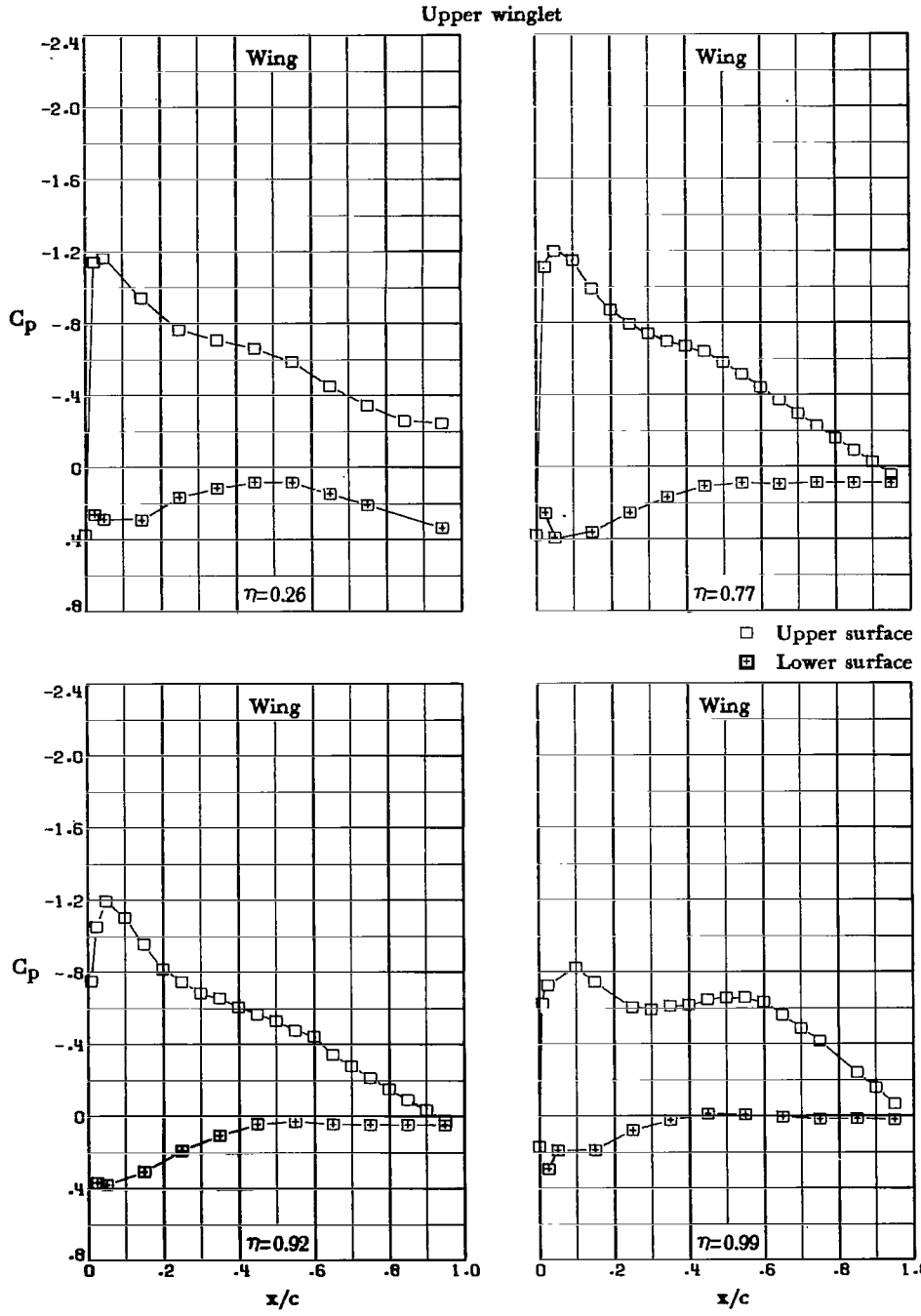

(a) $\alpha = 4.1^{\circ}$.

Figure 13.- Pressure distributions for upper-winglet configuration with leading- and trailing-edge flaps. Note that vertical scale increment of insert plots is larger.

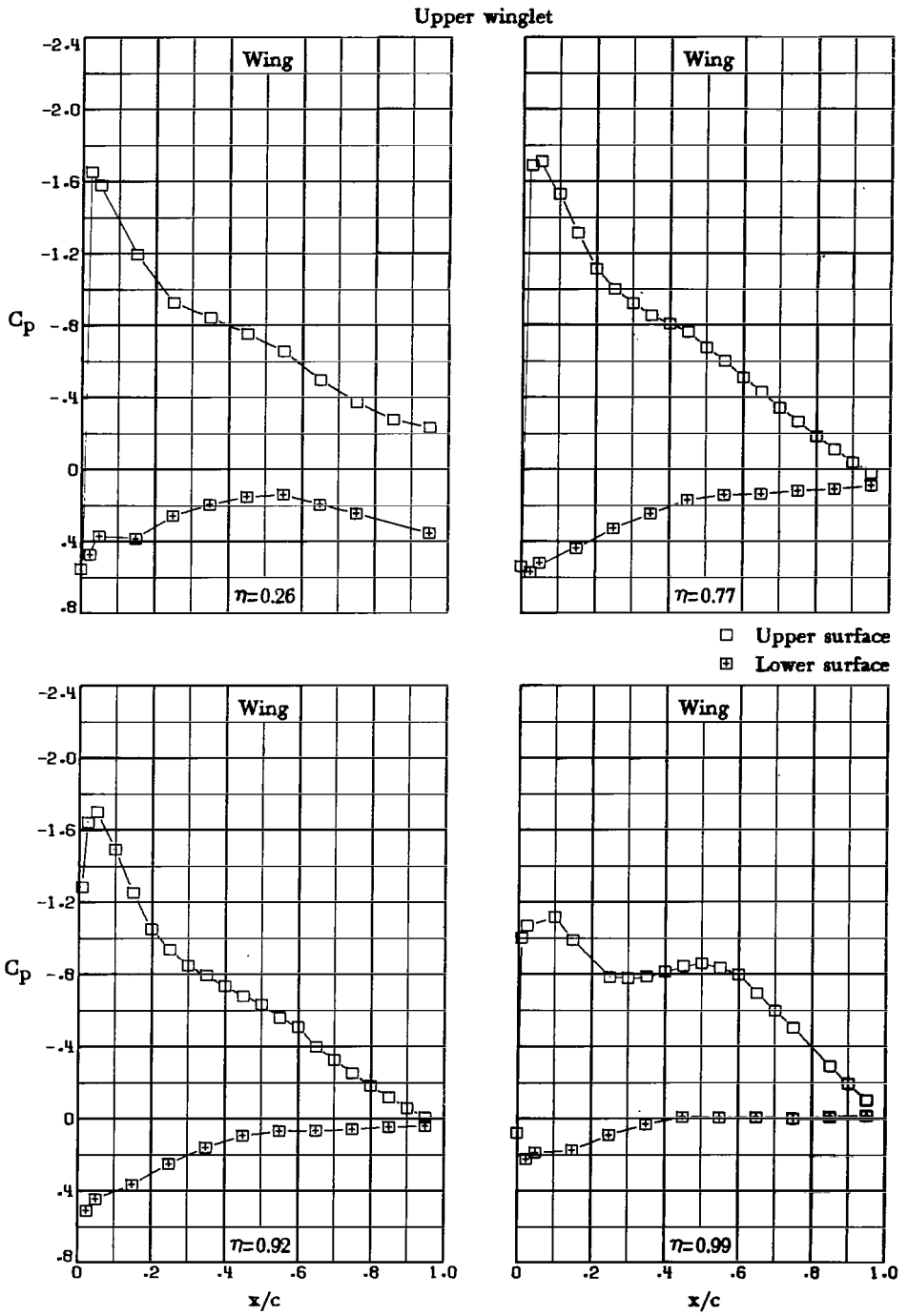

(b) $\alpha = 7.0^{\circ}$.

Figure 13.- Continued.

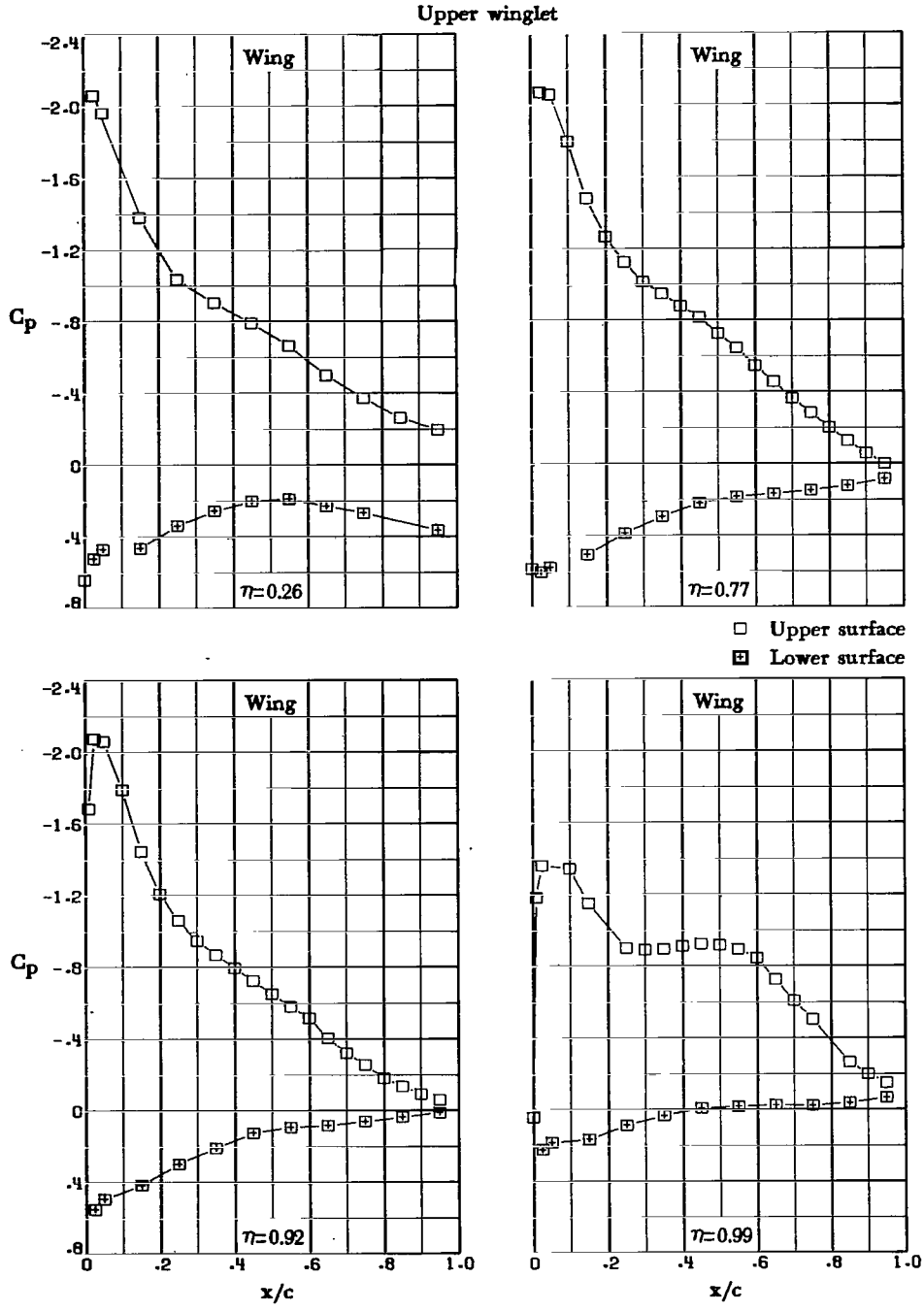

(c) $\alpha = 9.0^{\circ}$.

Figure 13.- Continued.

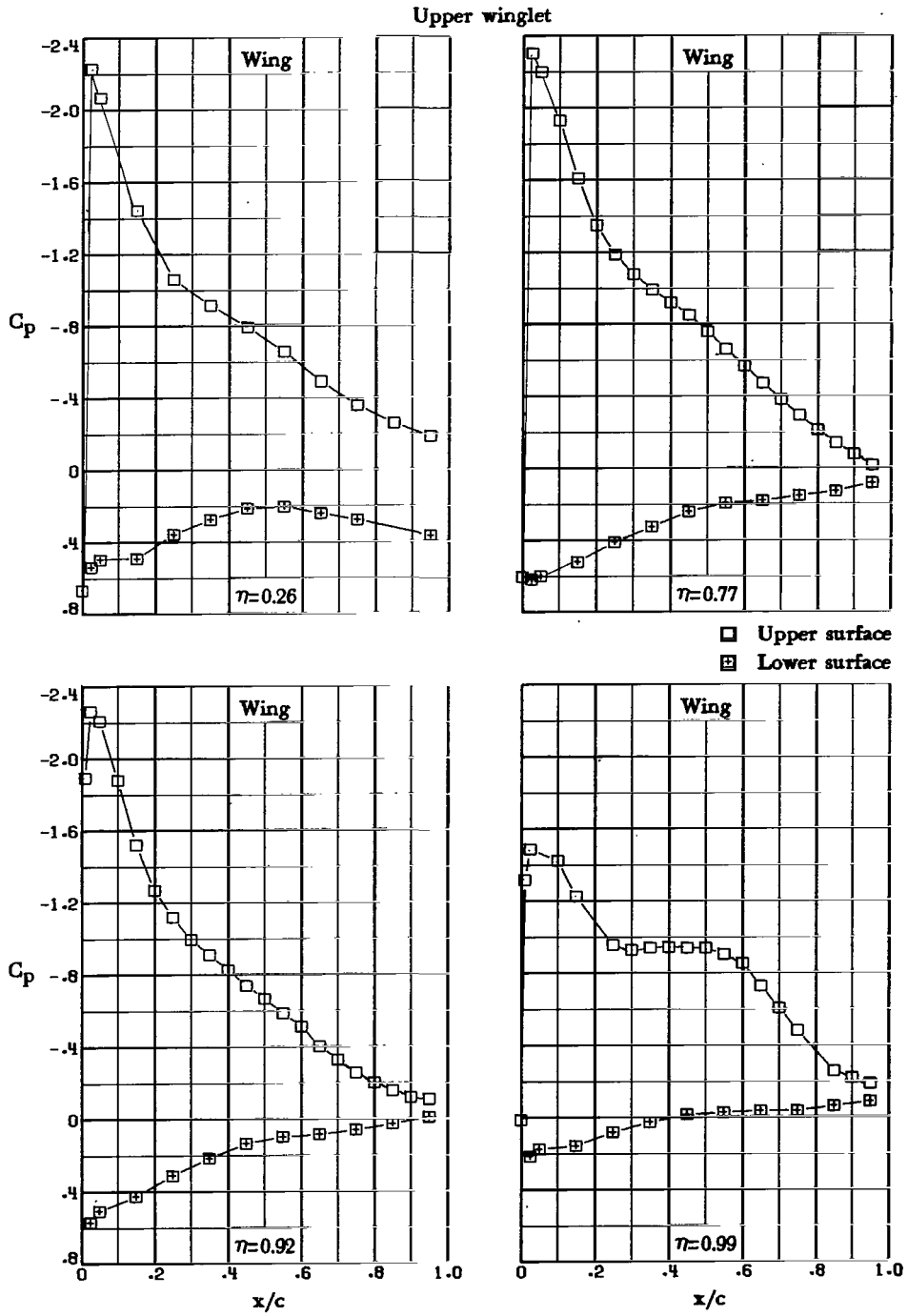

(d) α = 10.0°.

Figure 13.- Continued.

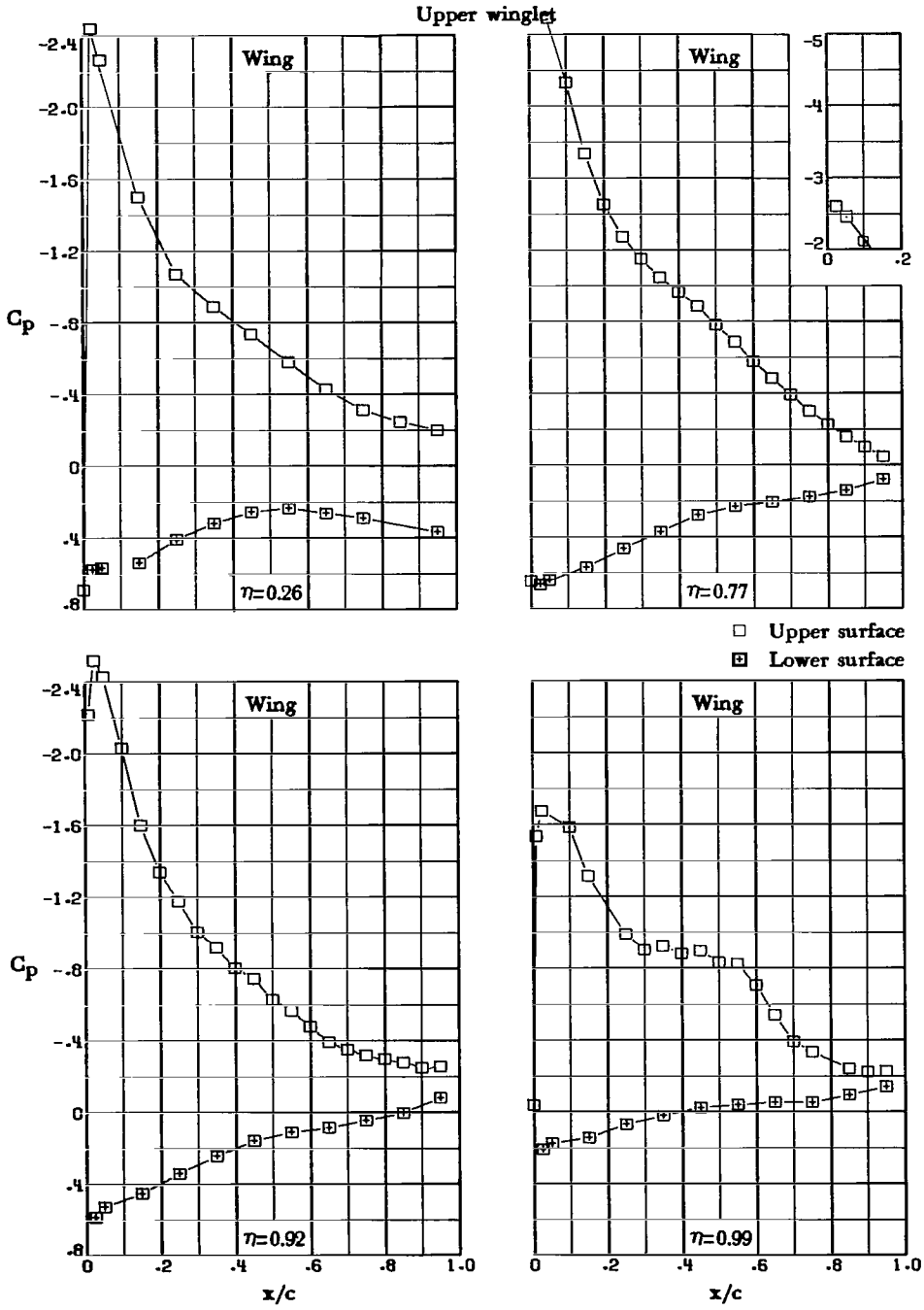

(e) α = 11.8°.

Figure 13.- Concluded.

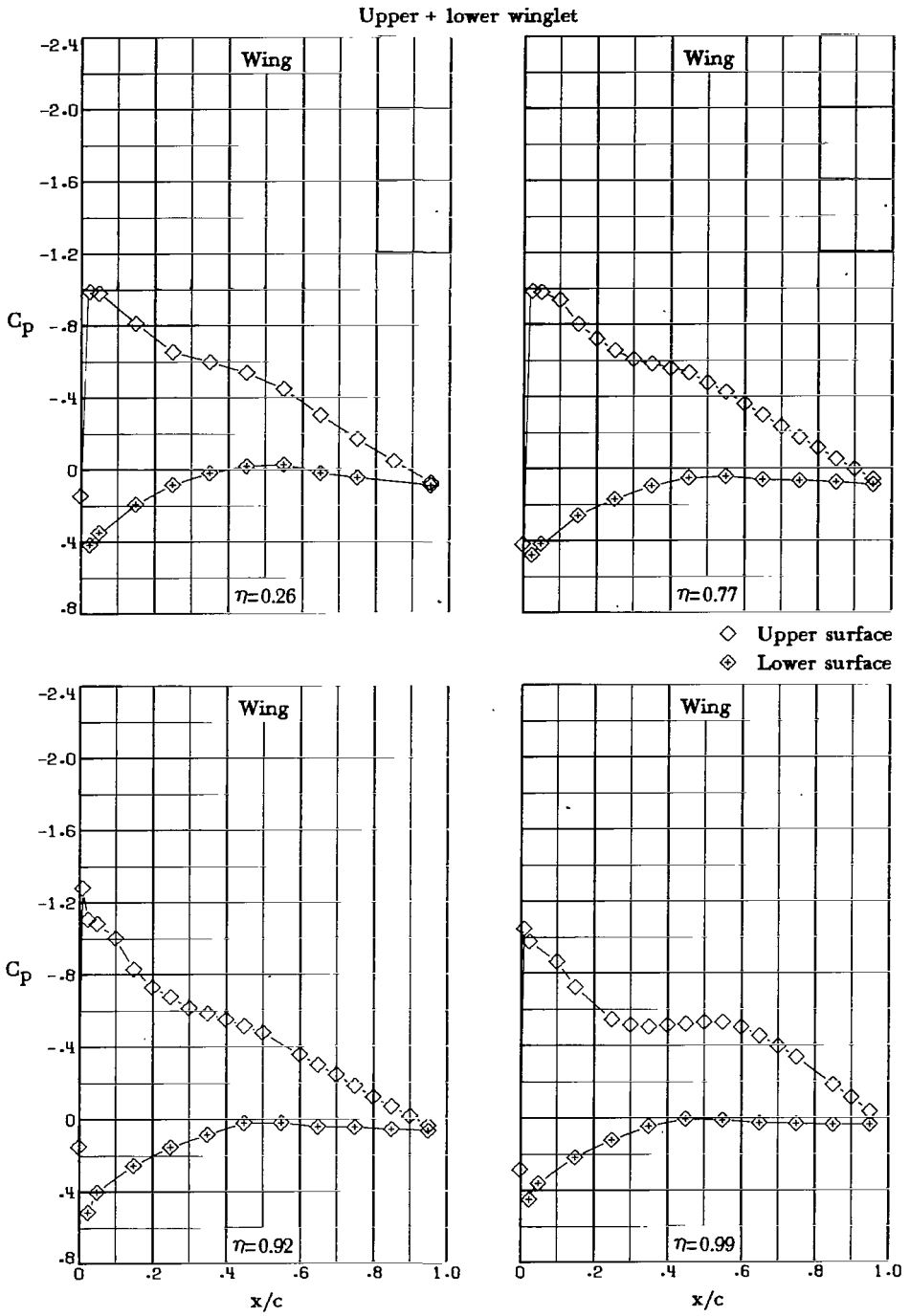

(a) $\alpha = 4.0^{\circ}$.

Figure 14.- Pressure distributions for upper-and-lower-winglet configuration. Note that insert vertical scale increment of insert plots is larger.

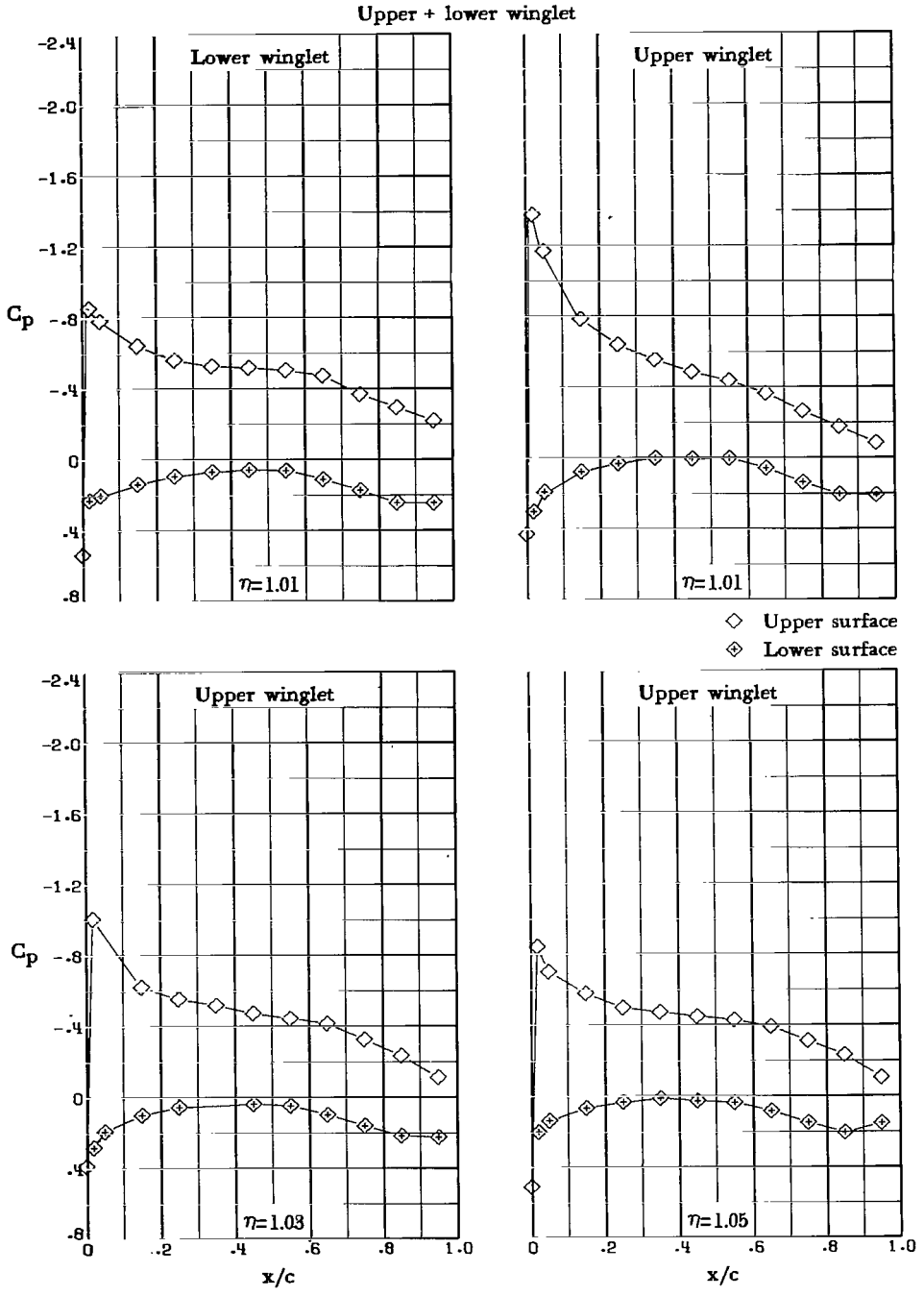

(a) α = 4.0°. Concluded.

Figure 14.- Continued.

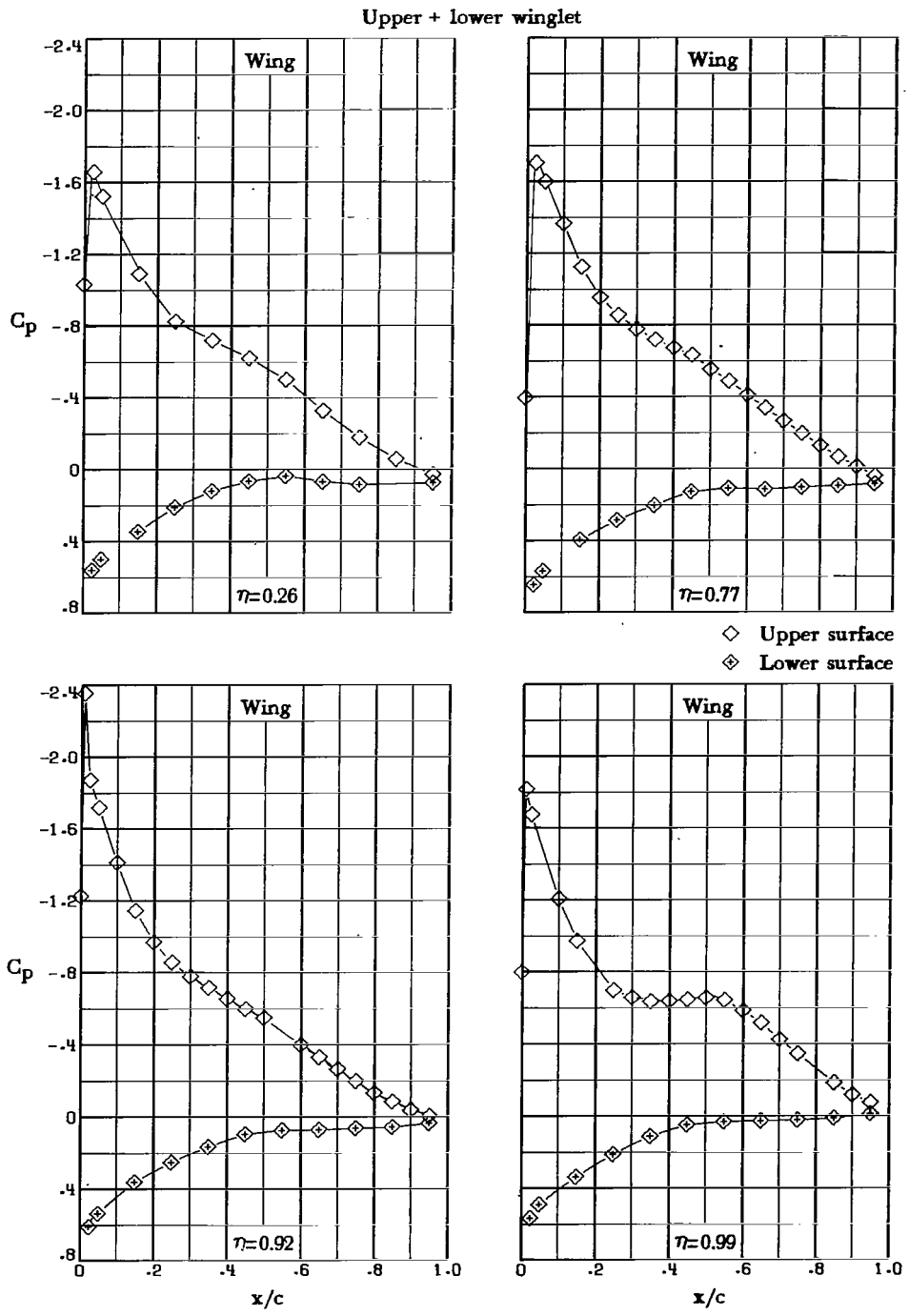

(b) $\alpha = 7.0^{\circ}$.

Figure 14.- Continued.

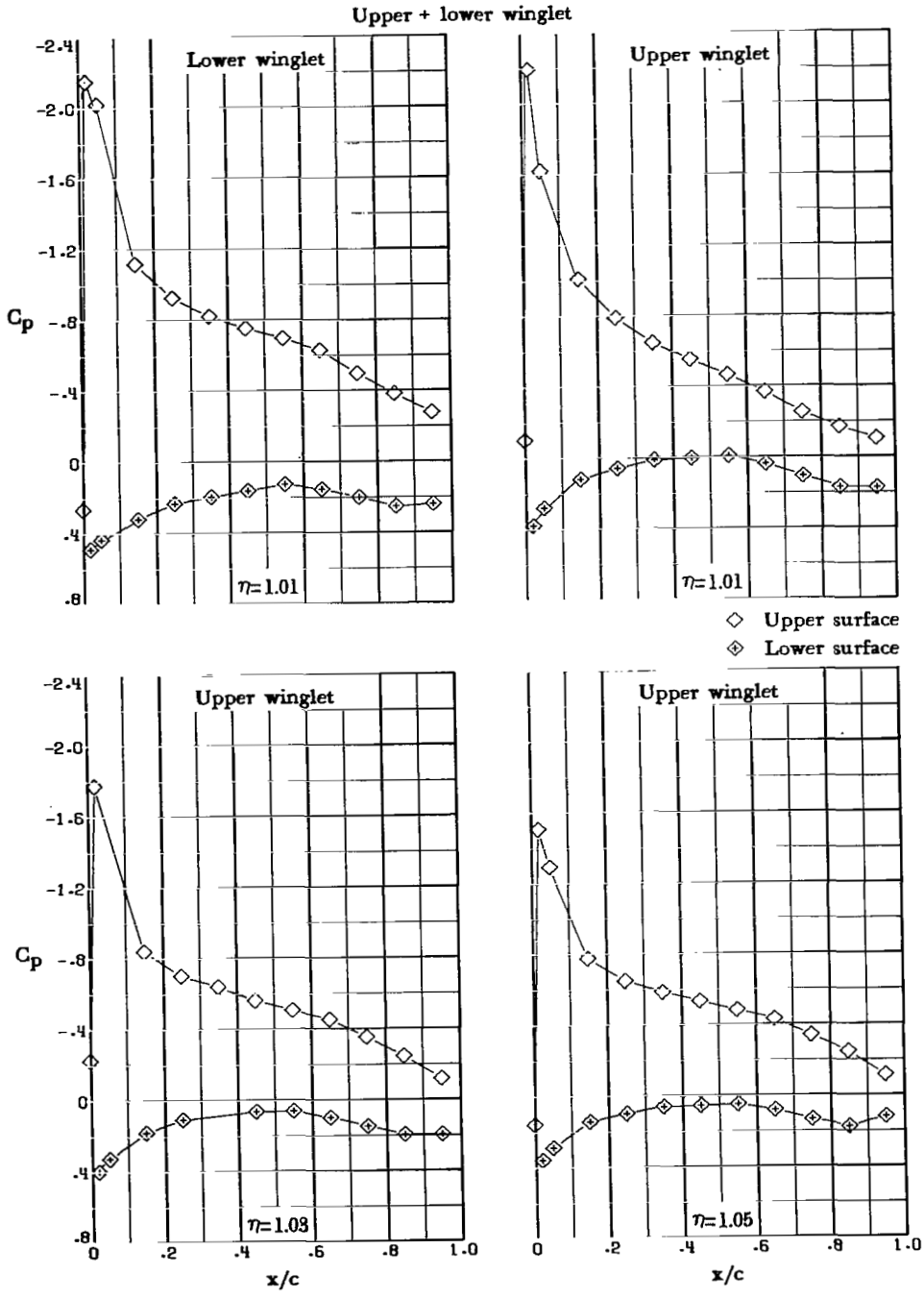

(b) α = 7.0°. Concluded.

Figure 14.- Continued.

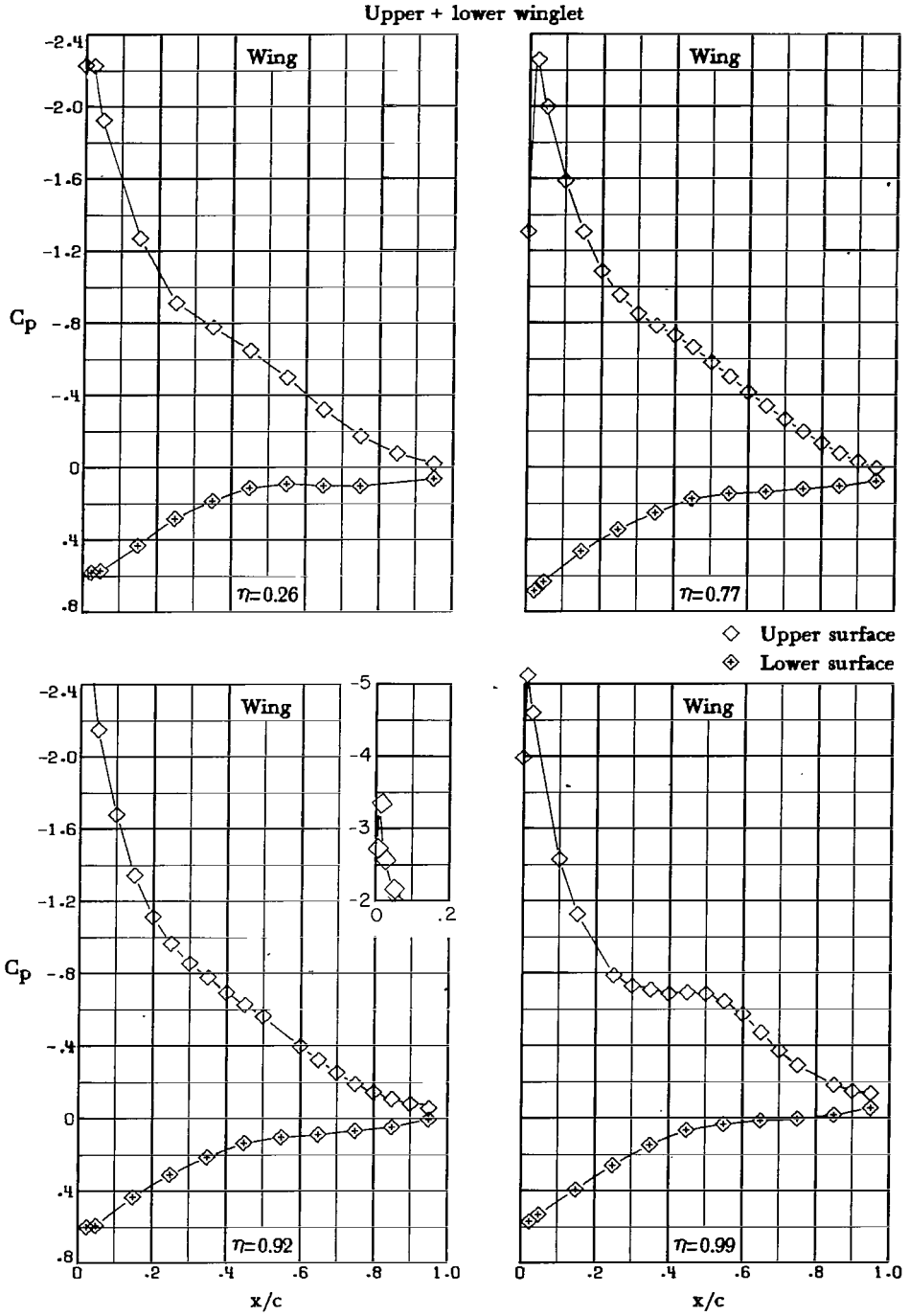

(c) α = 9.0°.

Figure 14.- Continued.

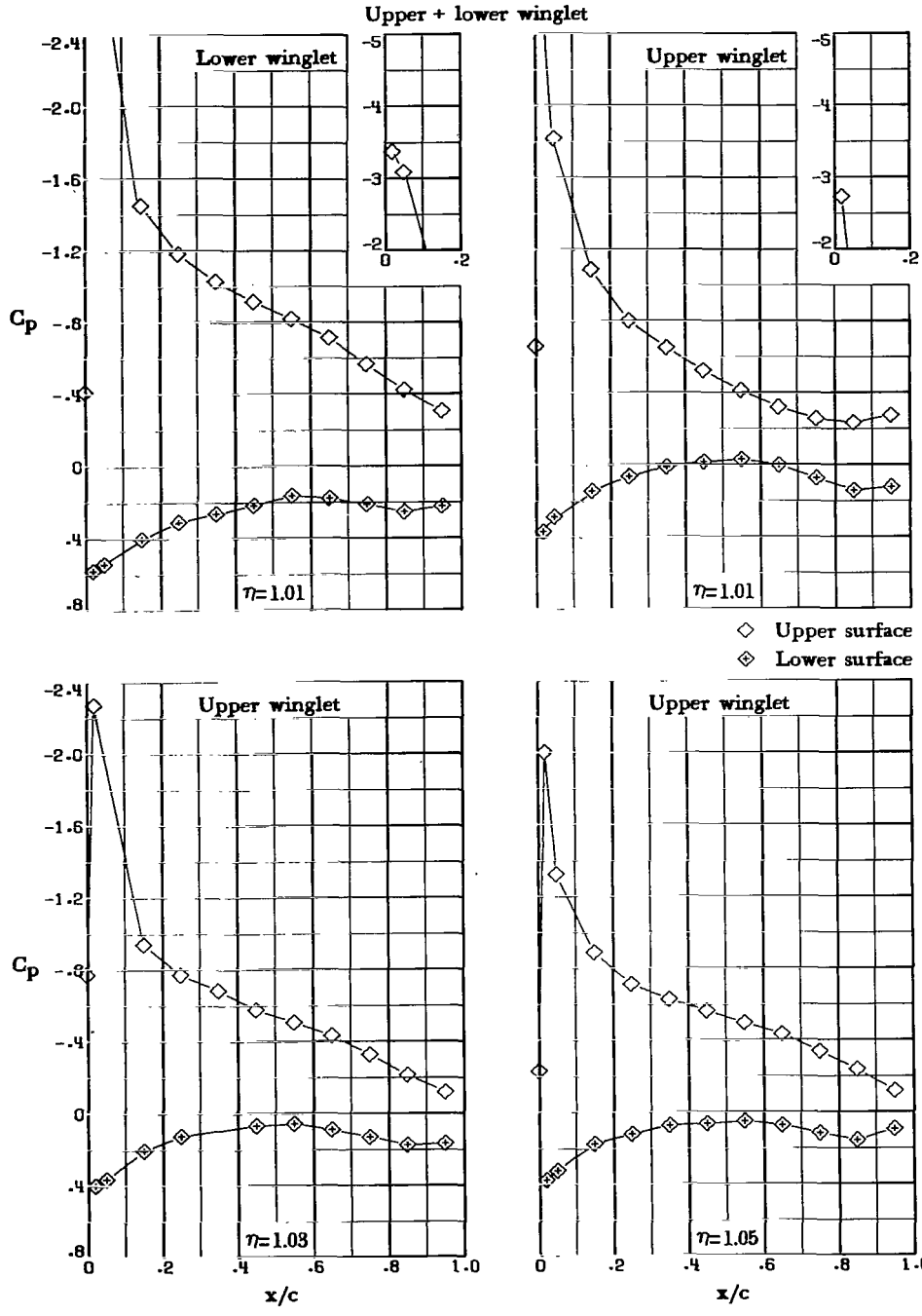

(c) α = 9.0°. Concluded.

Figure 14.- Continued.

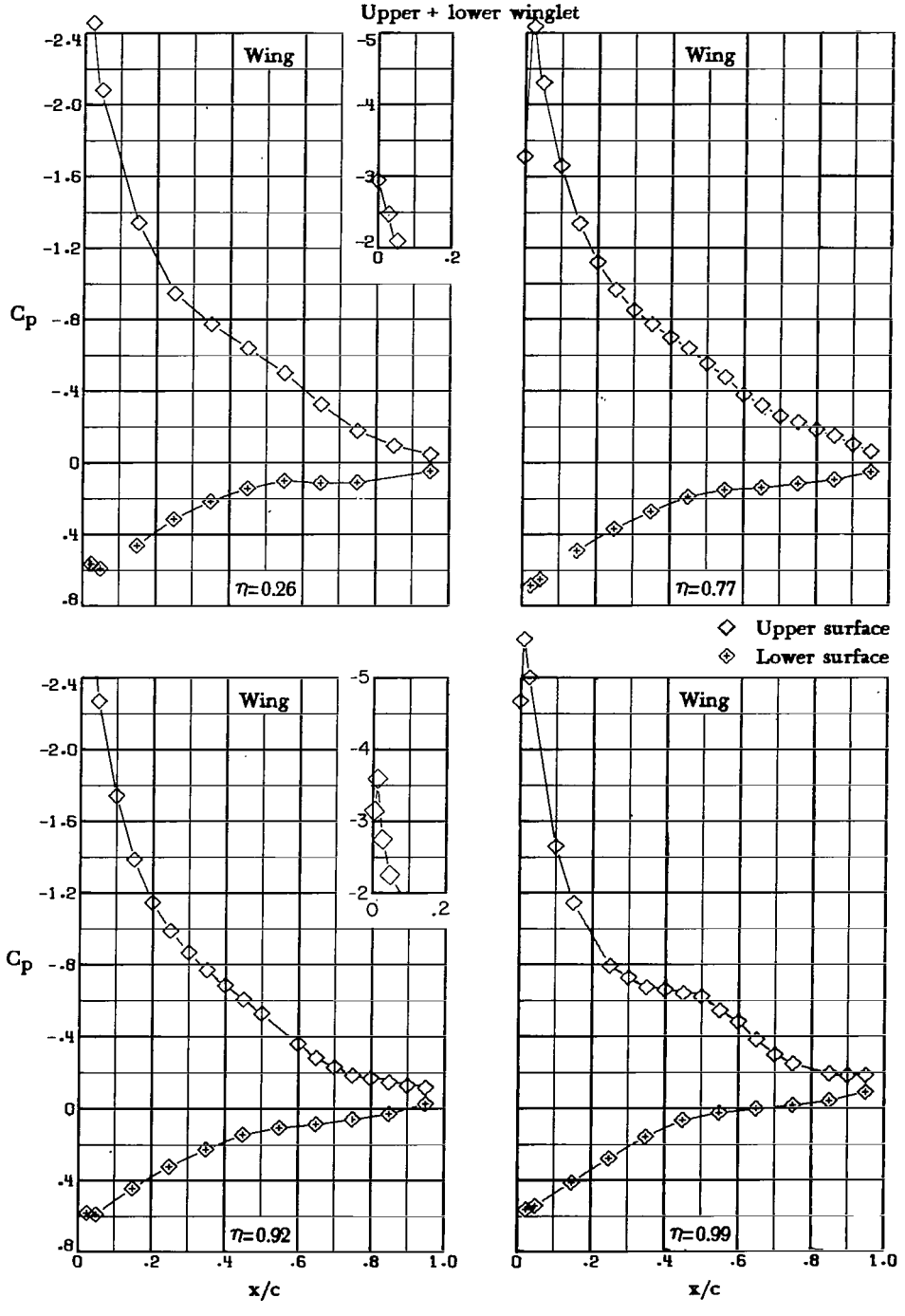

(d) α = 10.0°.

Figure 14.- Continued.

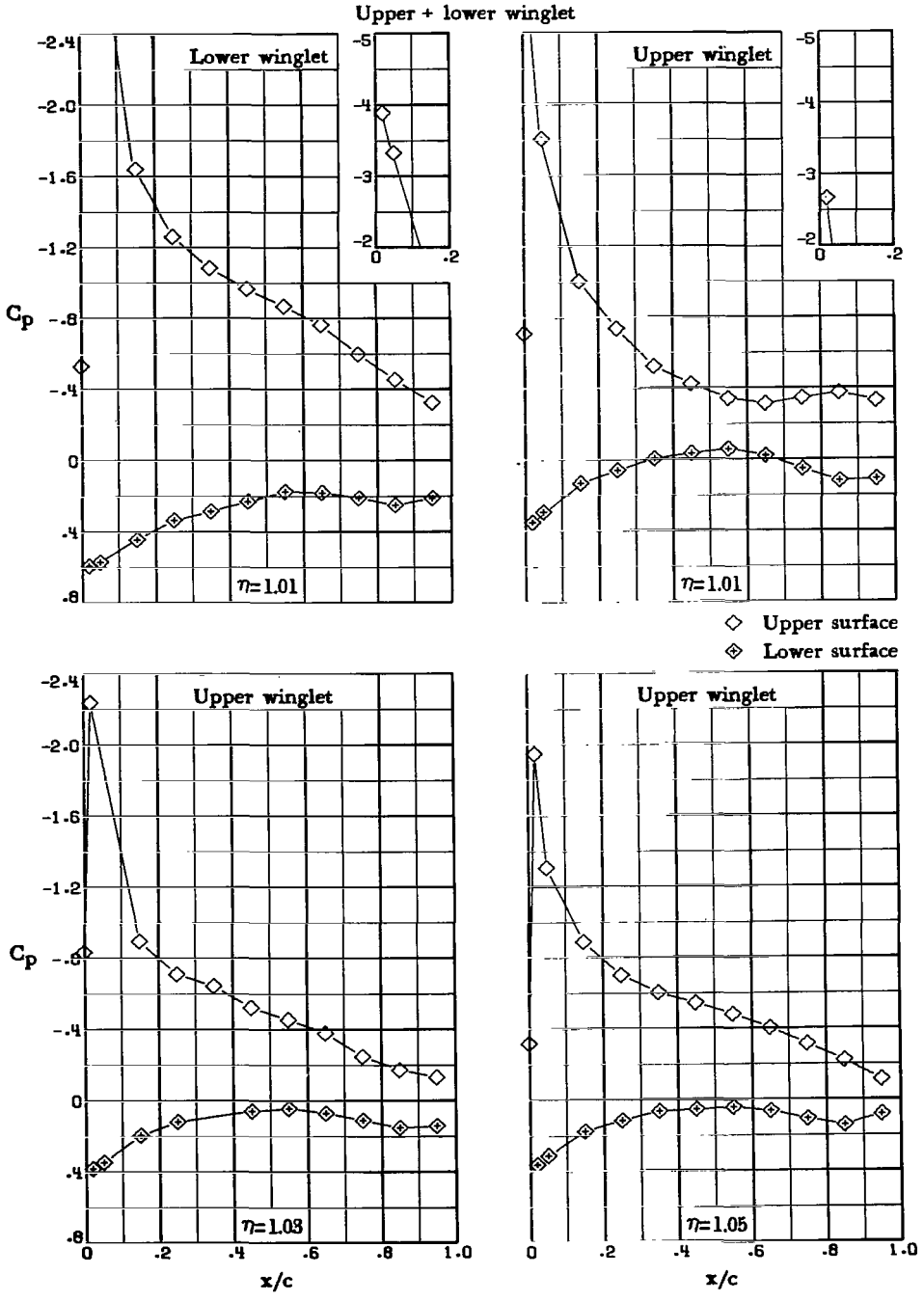

(d) α = 10.0°. Concluded.

Figure 14.- Continued.

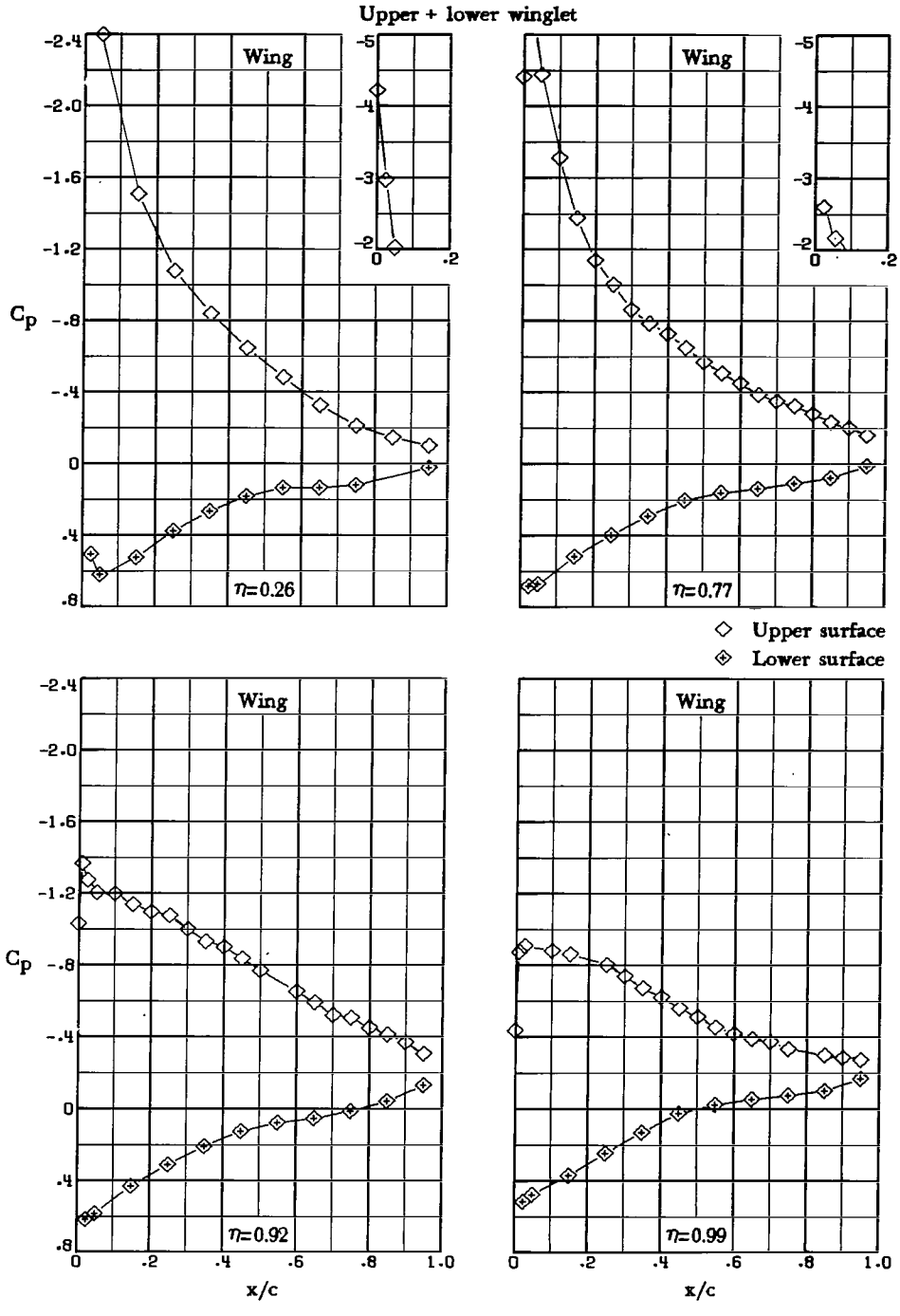

(e) α = 12.0°.

Figure 14.- Continued.

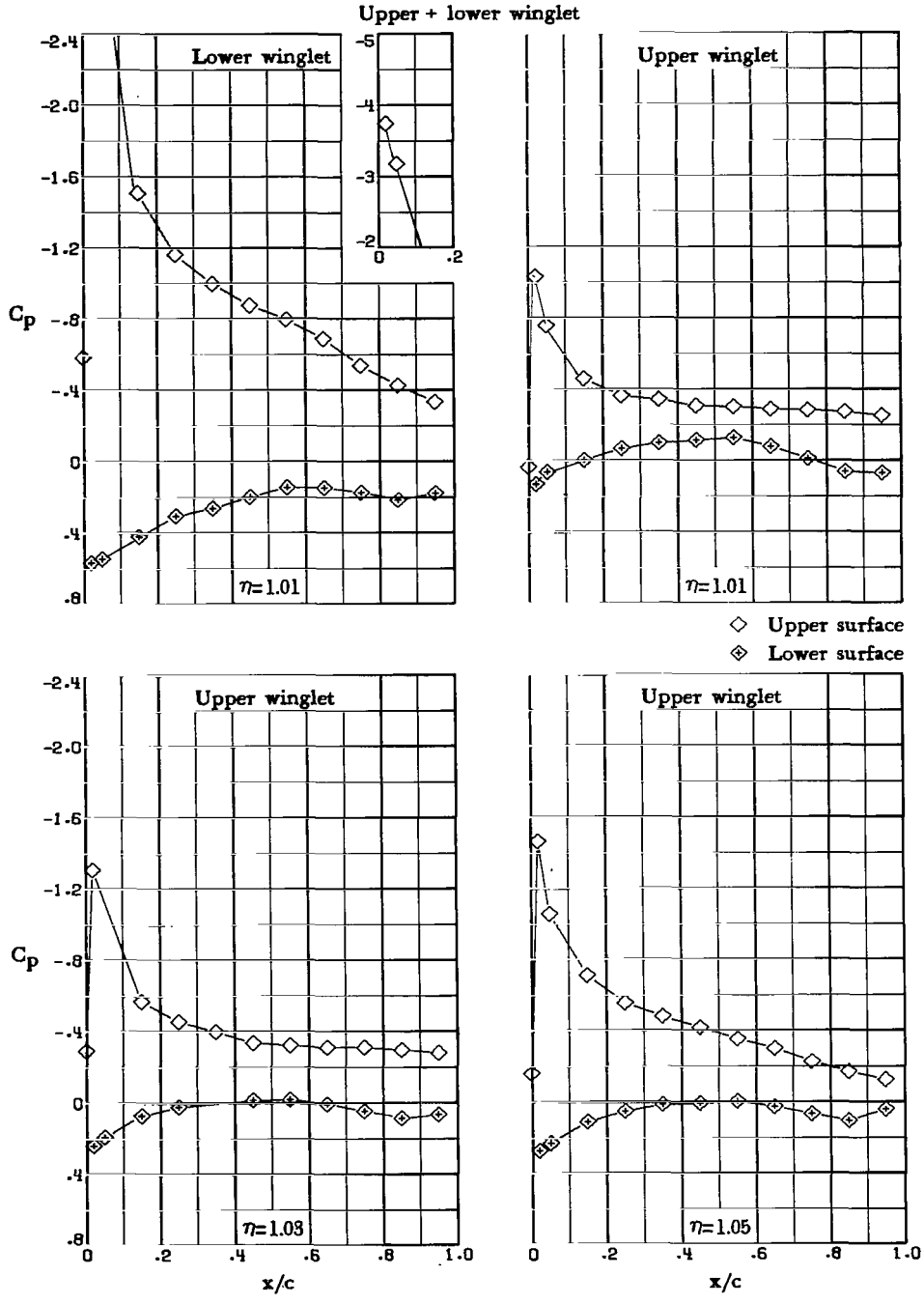

(e) α = 12.0°. Concluded.

Figure 14.- Concluded.

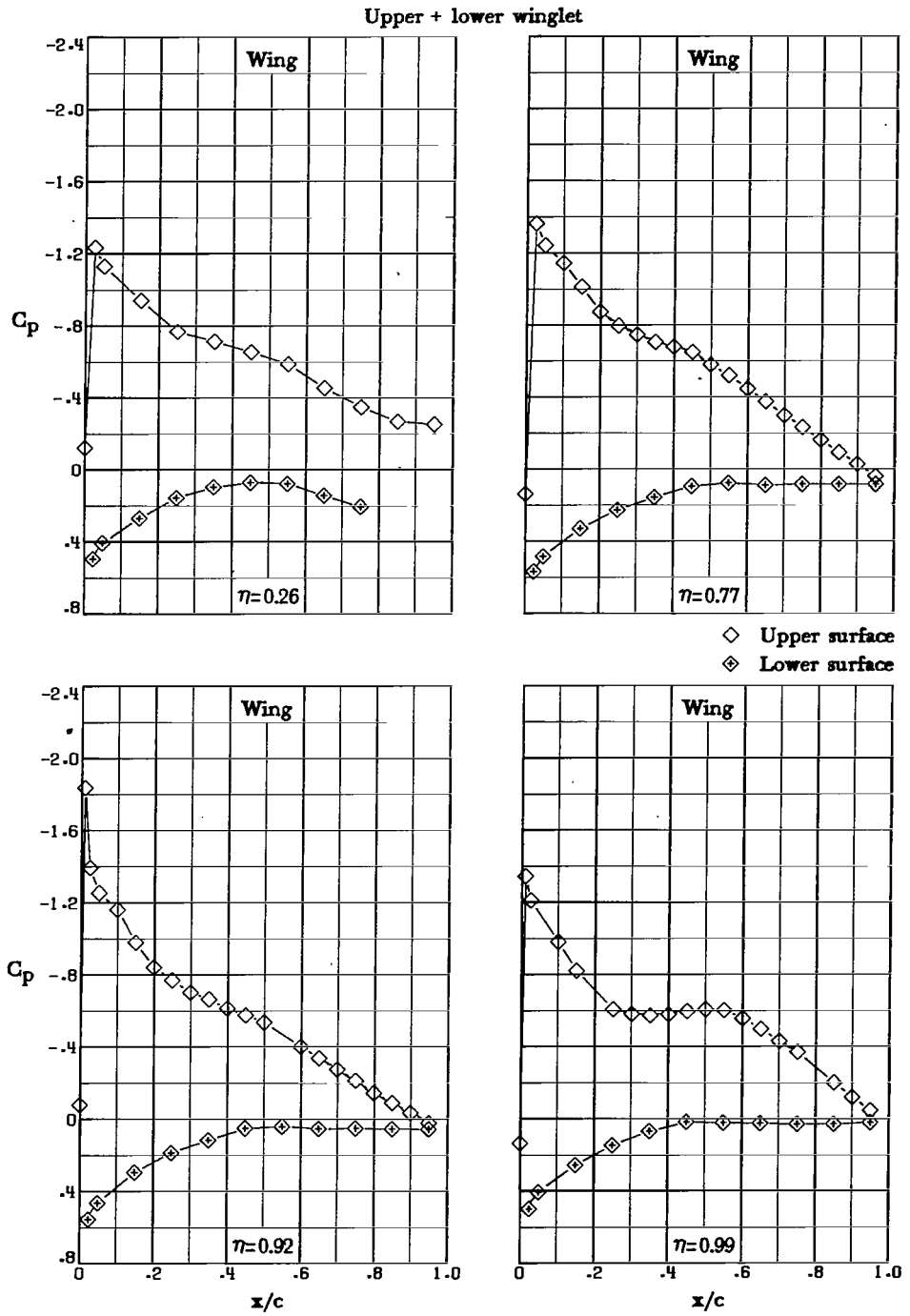

(a) α = 4.0°.

Figure 15.- Pressure distributions for upper-and-lower-winglet configuration with trailing-edge flaps. Note that insert vertical scale increment of insert plots is larger.

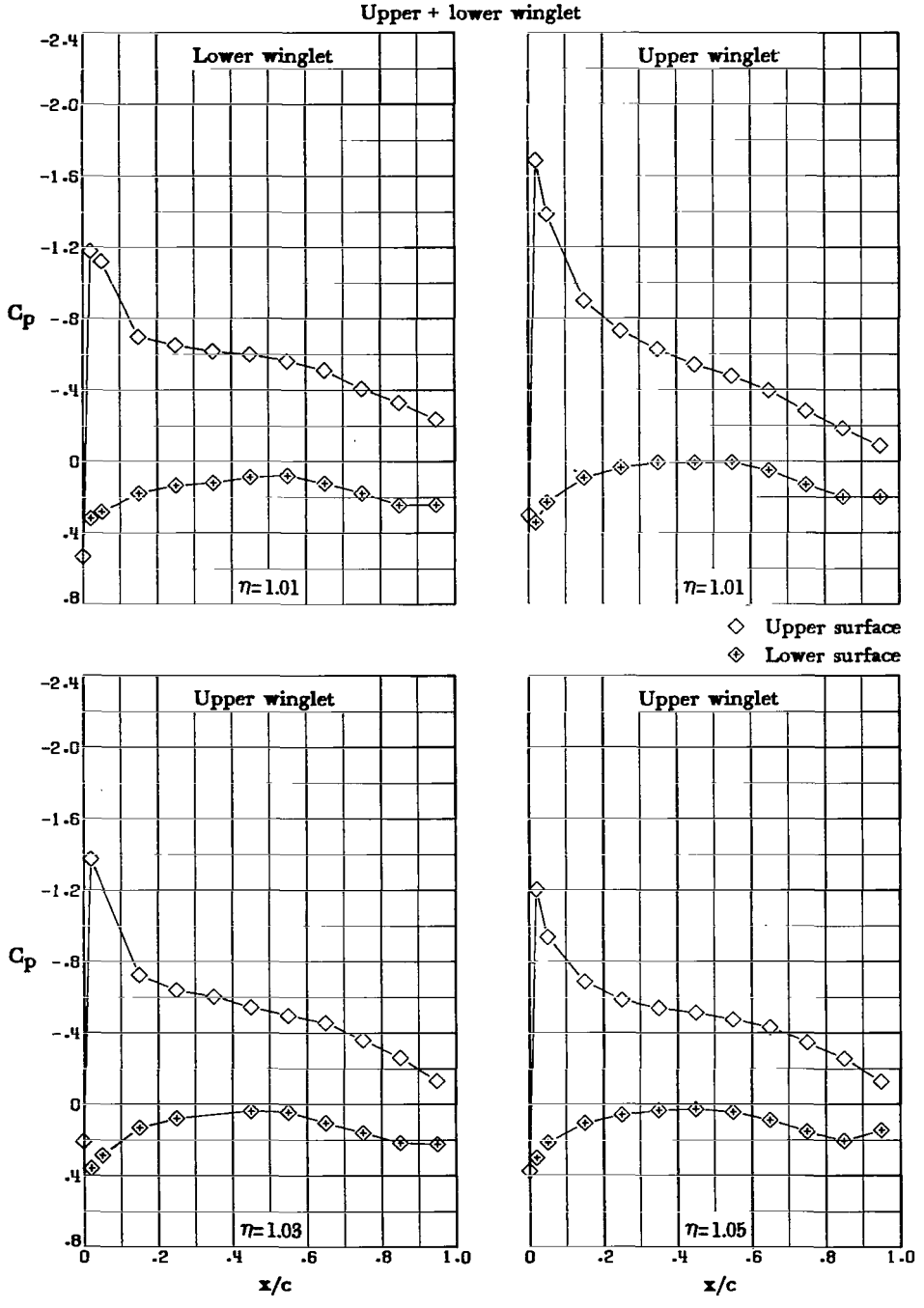

(a) α = 4.0°. Concluded.

Figure 15.- Continued.

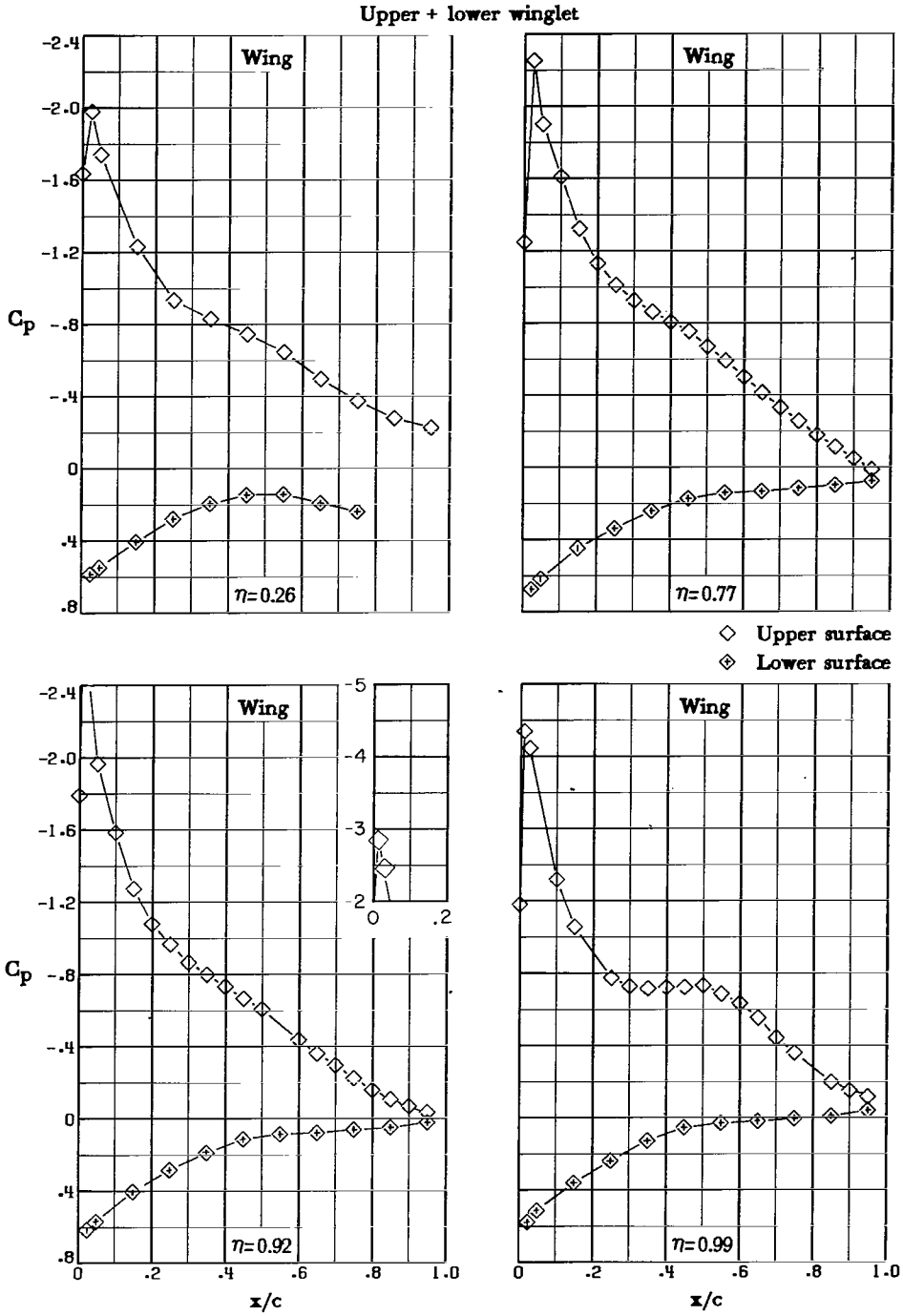

(b) $\alpha = 7.0°$.

Figure 15.- Continued.

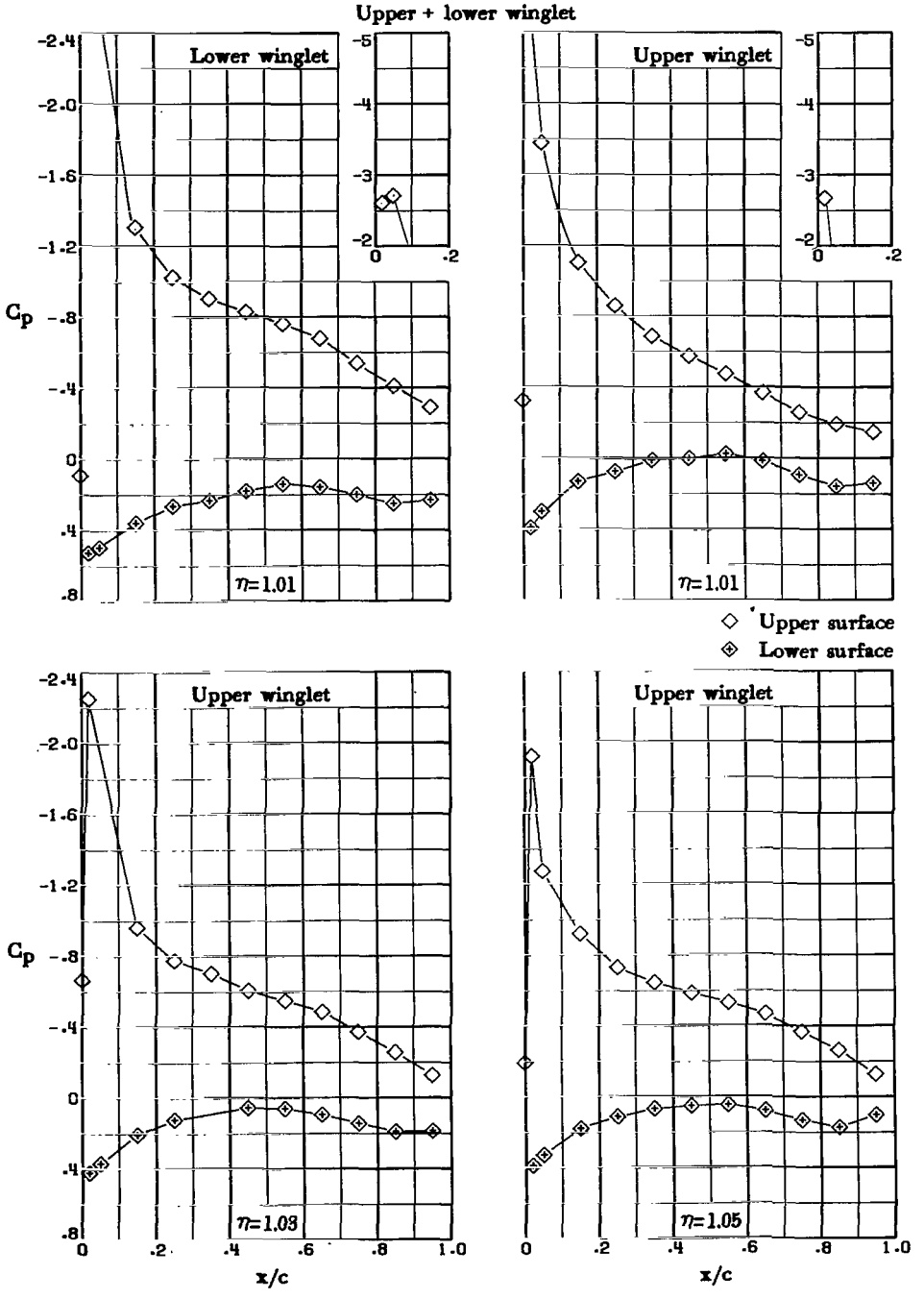

(b) α = 7.0°. Concluded.

Figure 15.- Continued.

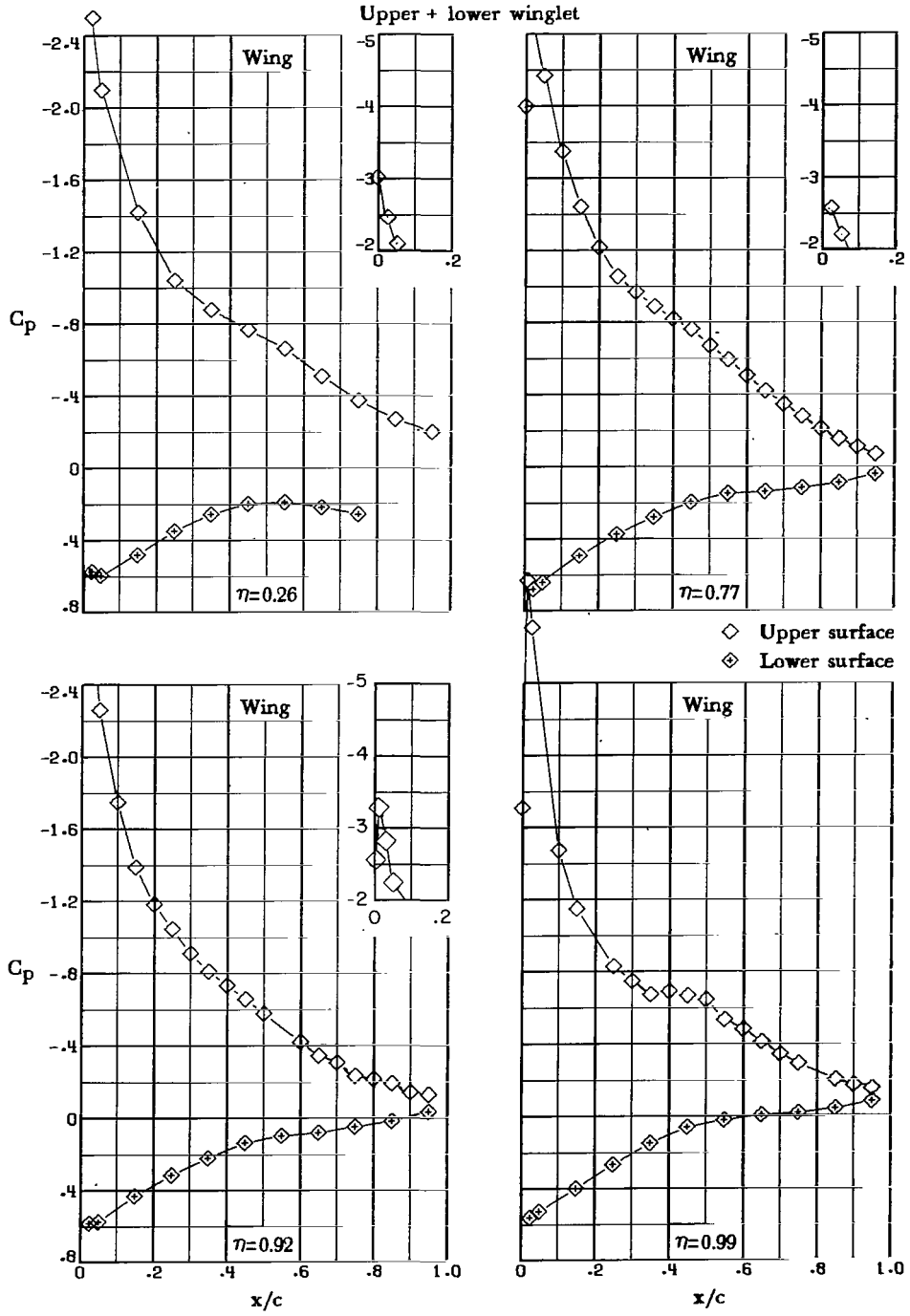

(c) $\alpha = 9.0^{\circ}$.

Figure 15.- Continued.

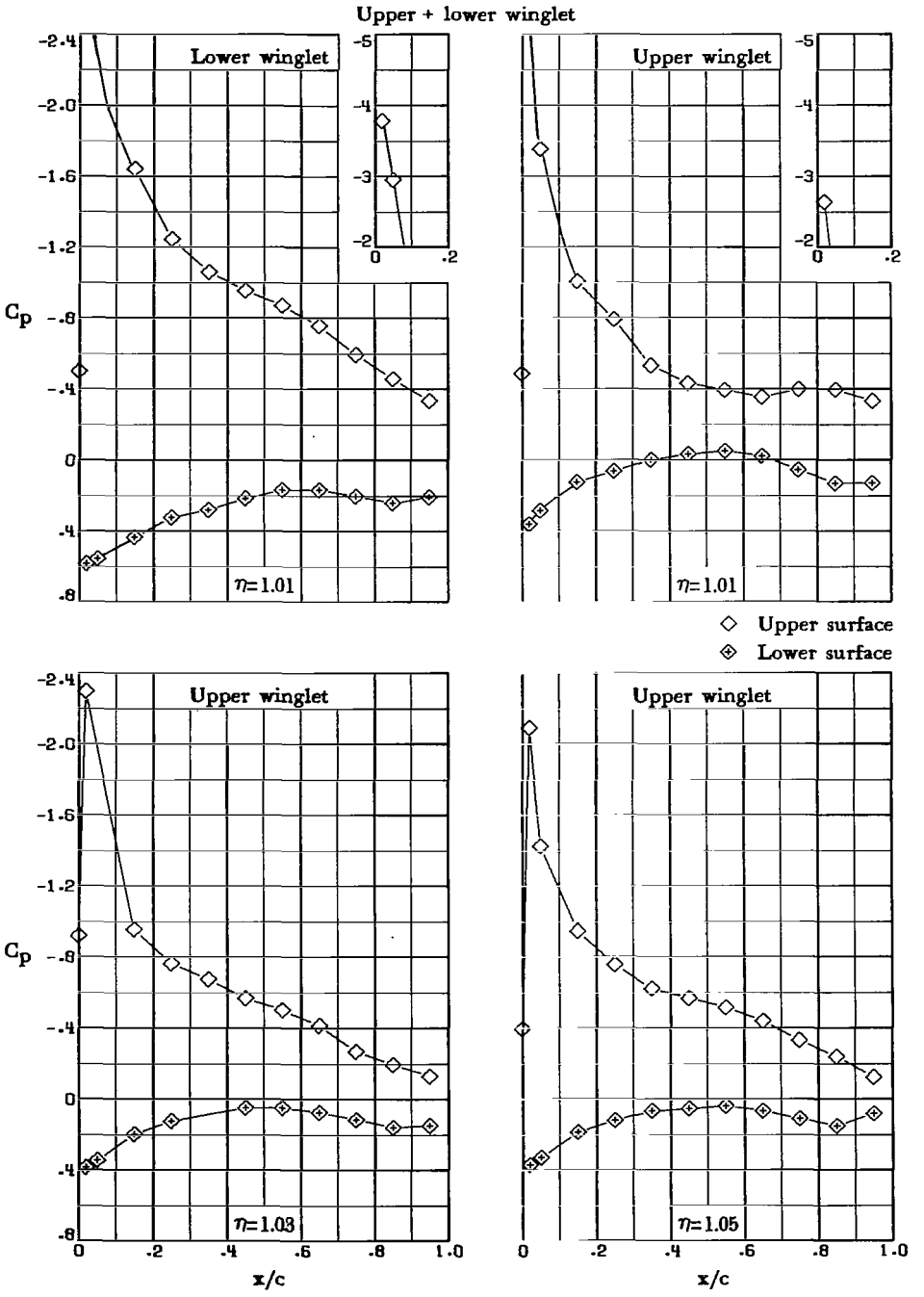

(c) α = 9.0°. Concluded.

Figure 15.- Continued.

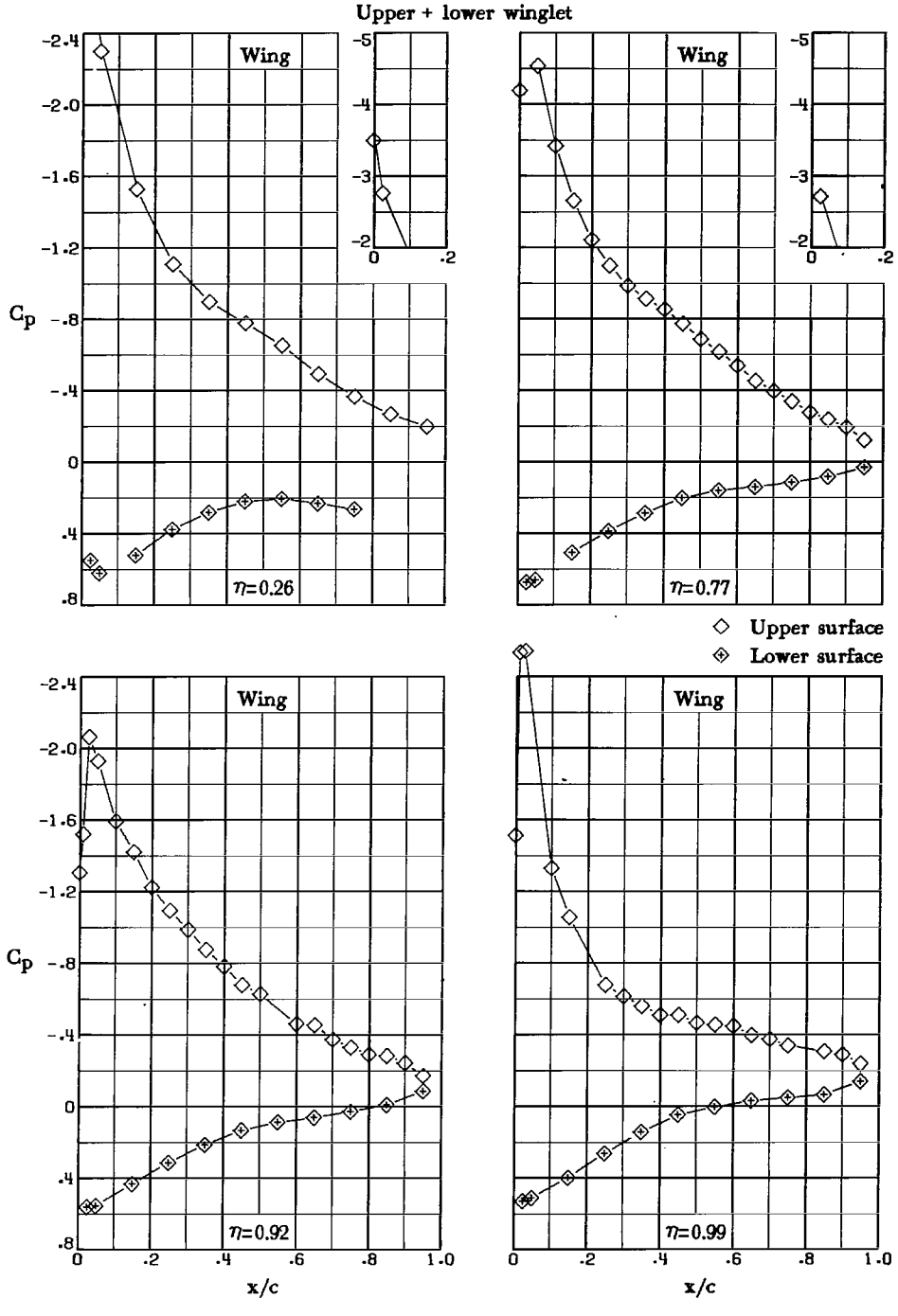

(d) α = 10.0°.

Figure 15.- Continued.

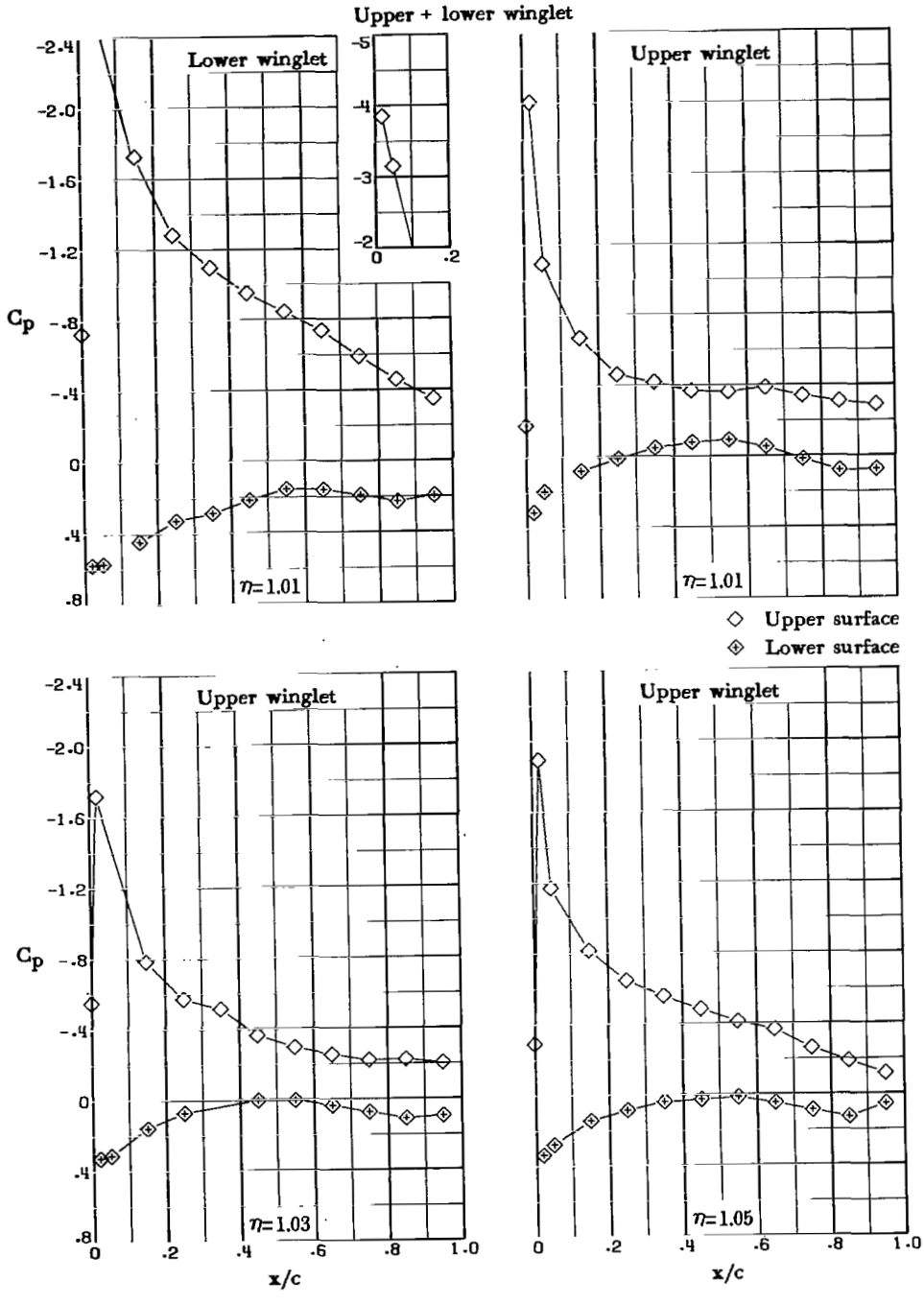

(d) α = 10.0°. Concluded.

Figure 15.- Continued.

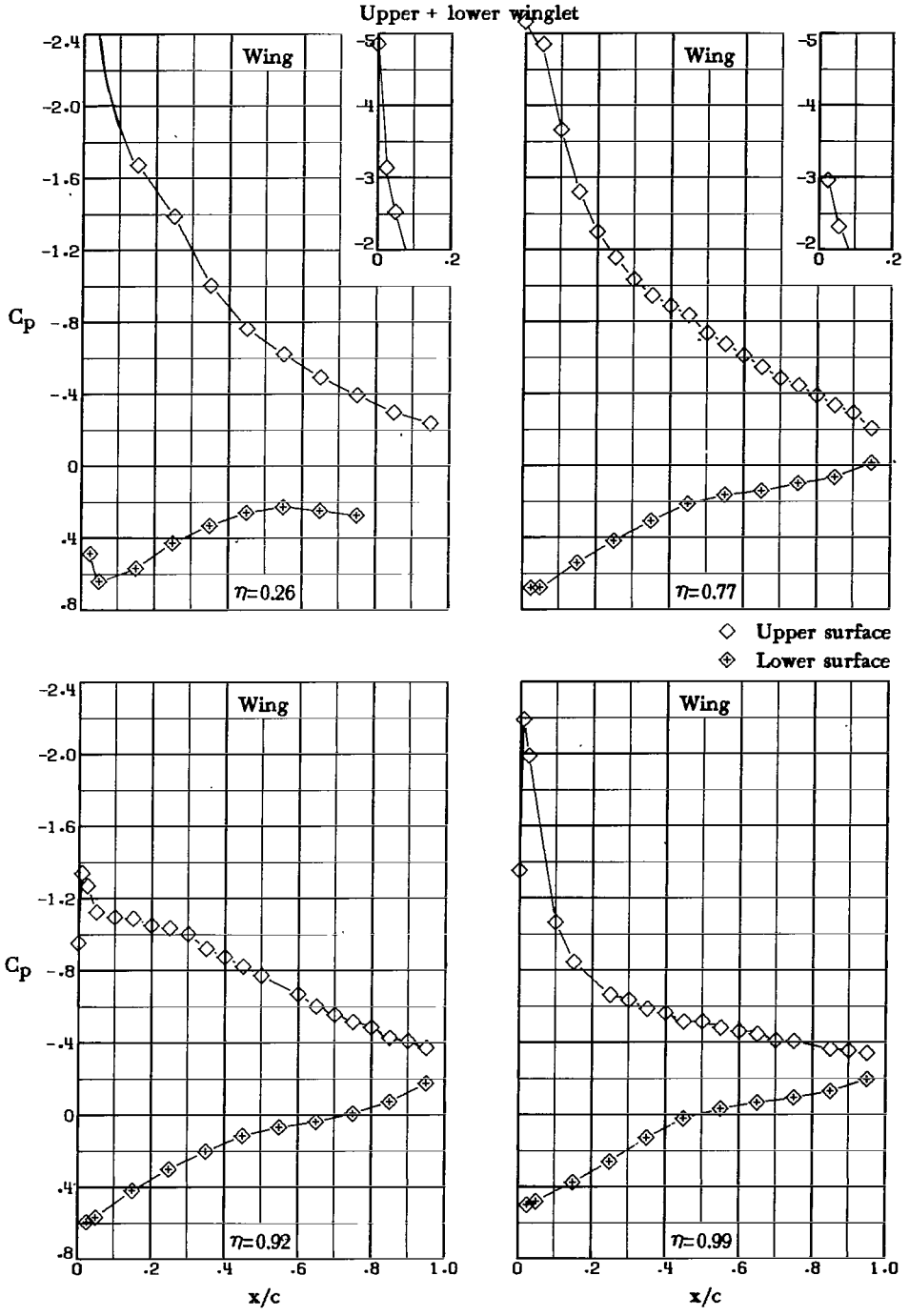

(e) α = 12.0°.

Figure 15.- Continued.

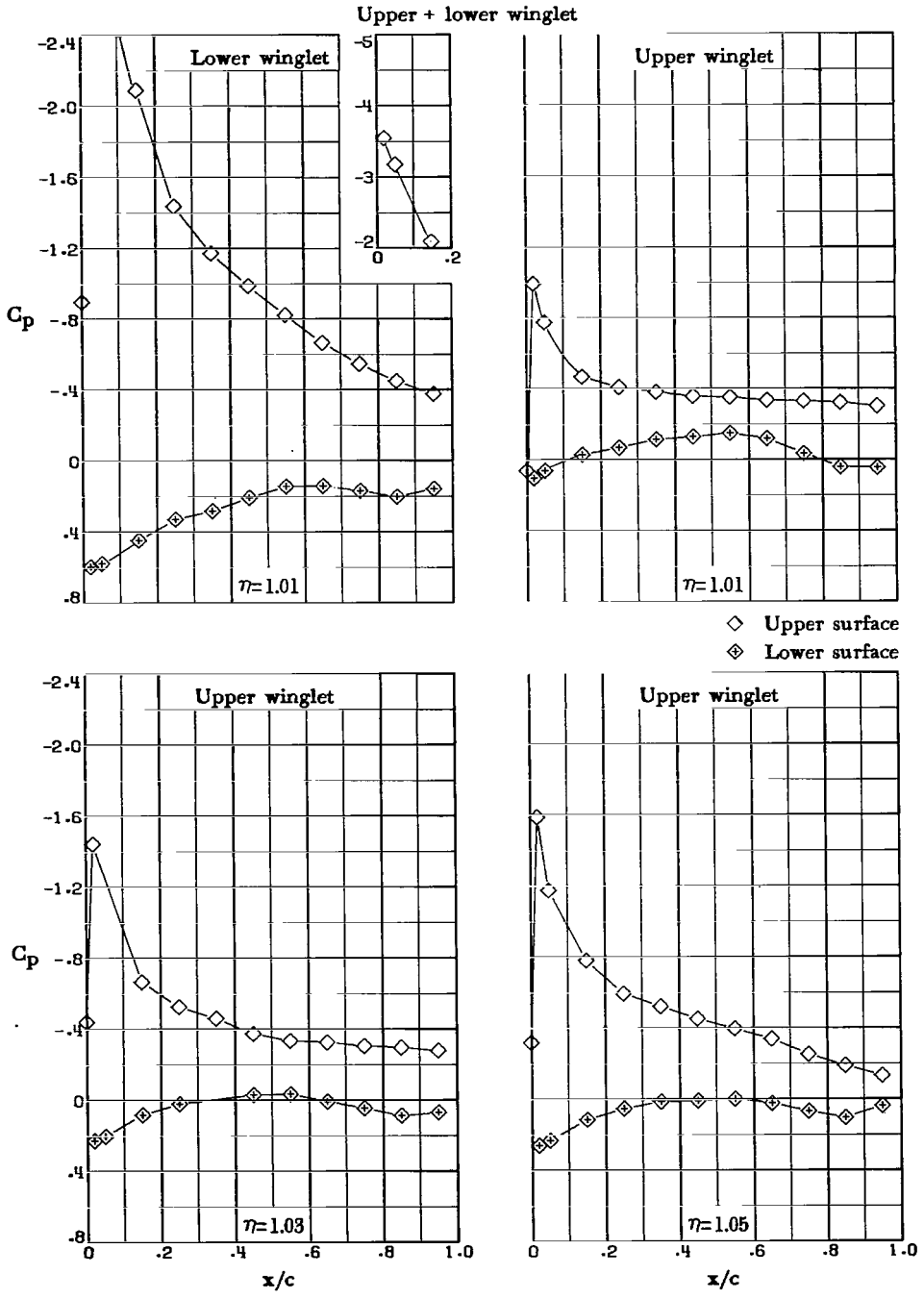

(e) α = 12.0°. Concluded.

Figure 15.- Concluded.

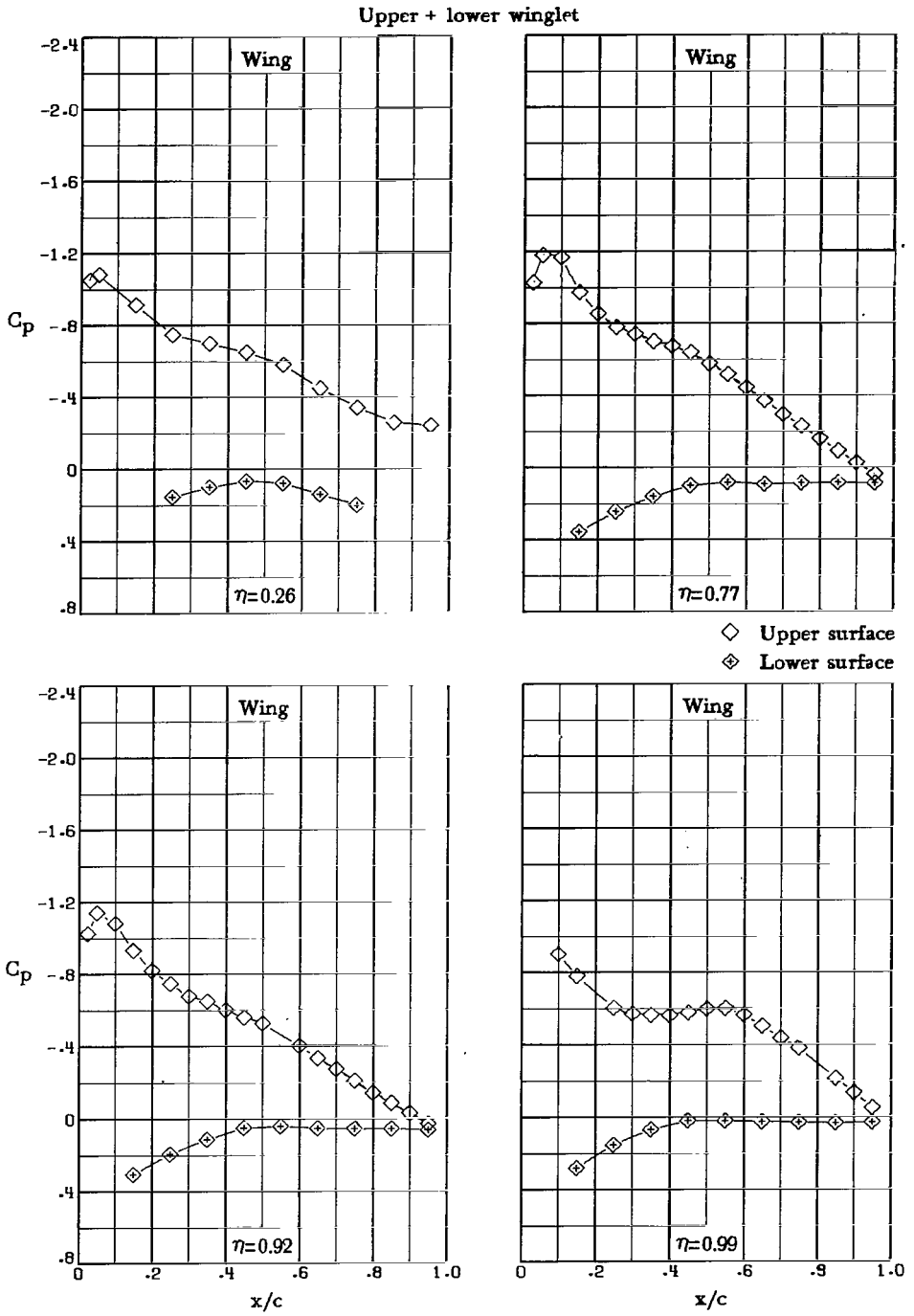

(a) $\alpha = 3.9^{\circ}$.

Figure 16.- Pressure distributions for upper-and-lower-winglet configuration with leading- and trailing-edge flaps. Note that insert vertical scale increment of insert plots is larger.

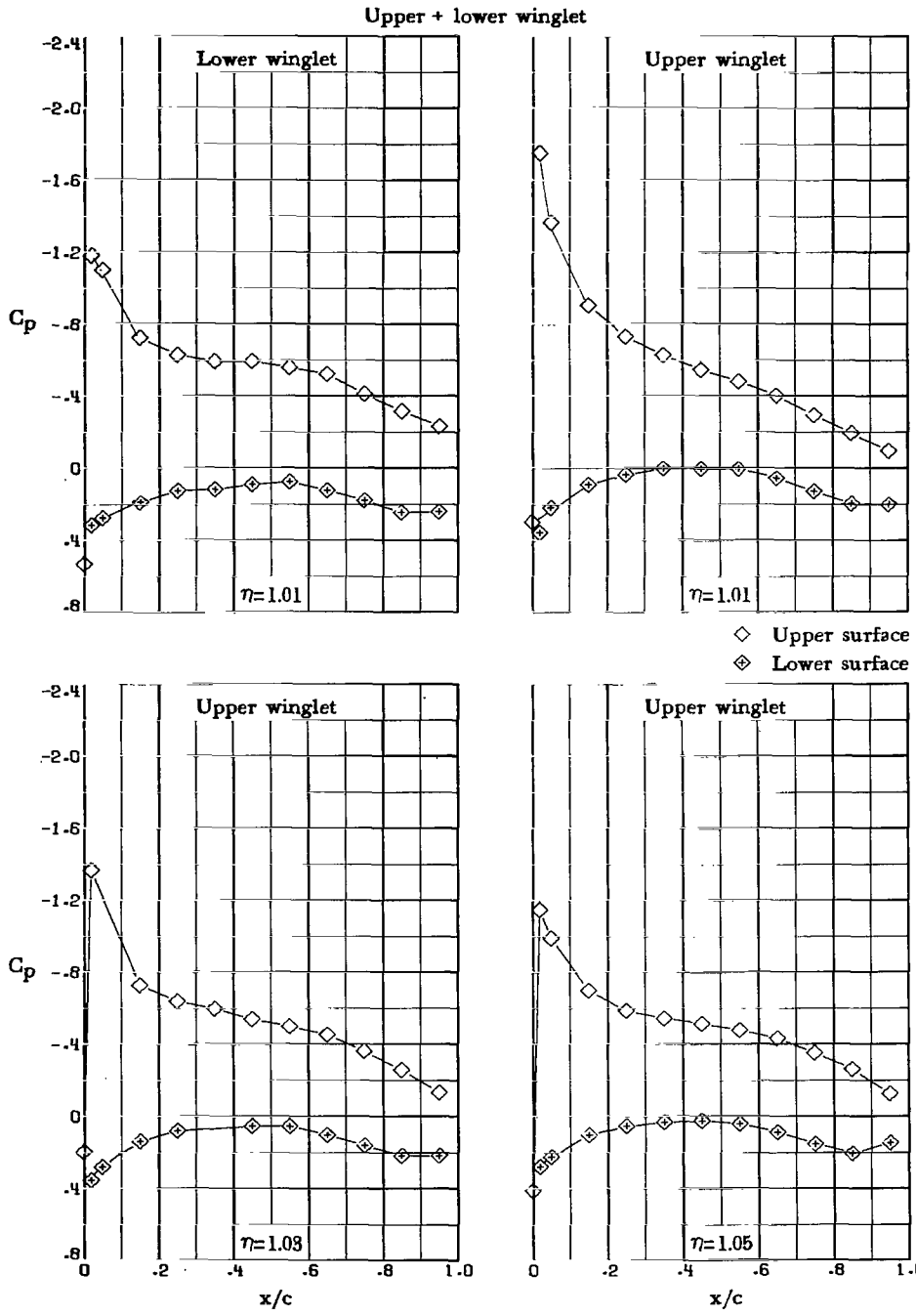

(a) α = 3.9°. Concluded.

Figure 16.- Continued.

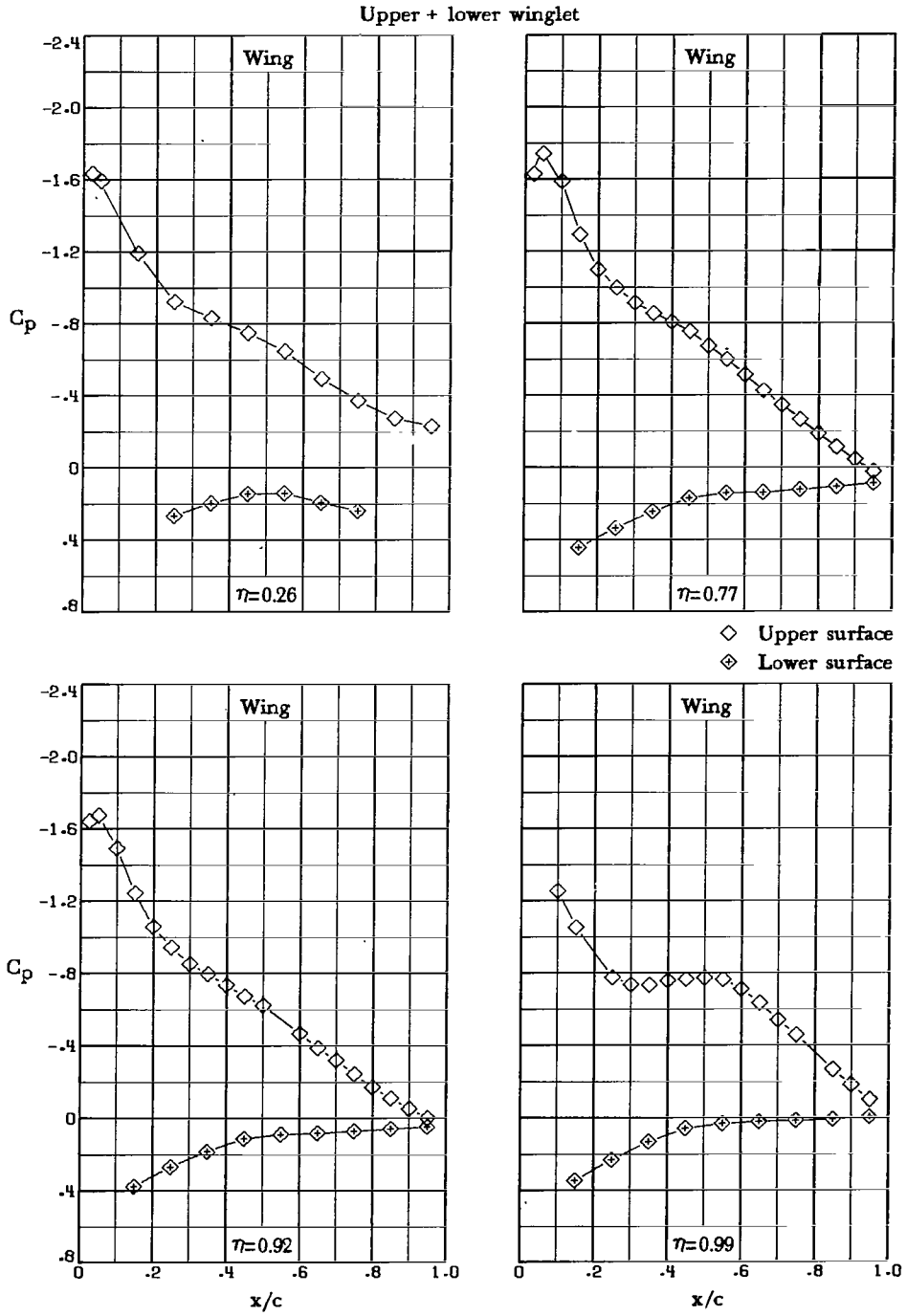

(b) $\alpha = 7.0^{\circ}$.

Figure 16.- Continued.

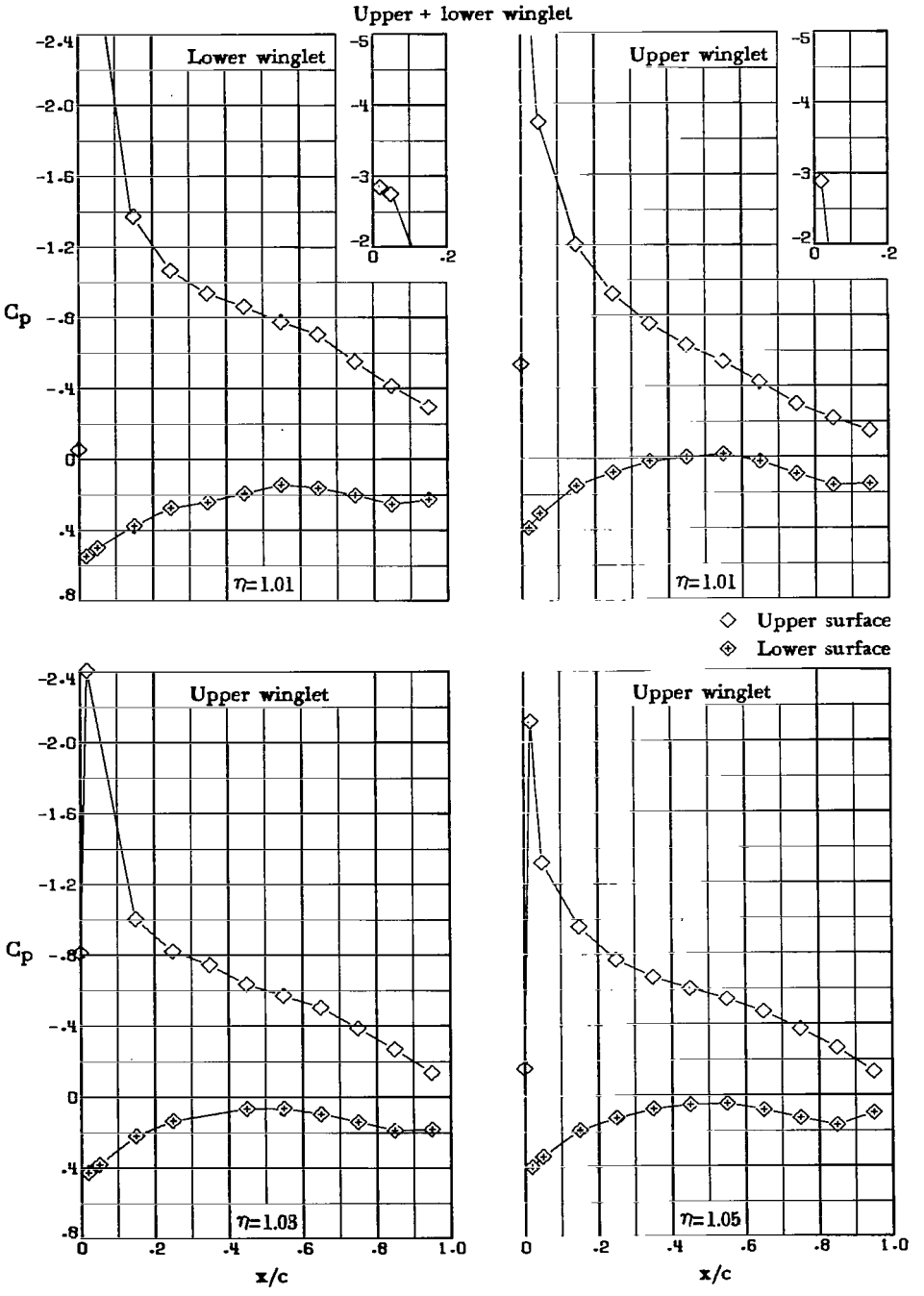

(b) α = 7.0°. Concluded.

Figure 16.- Continued.

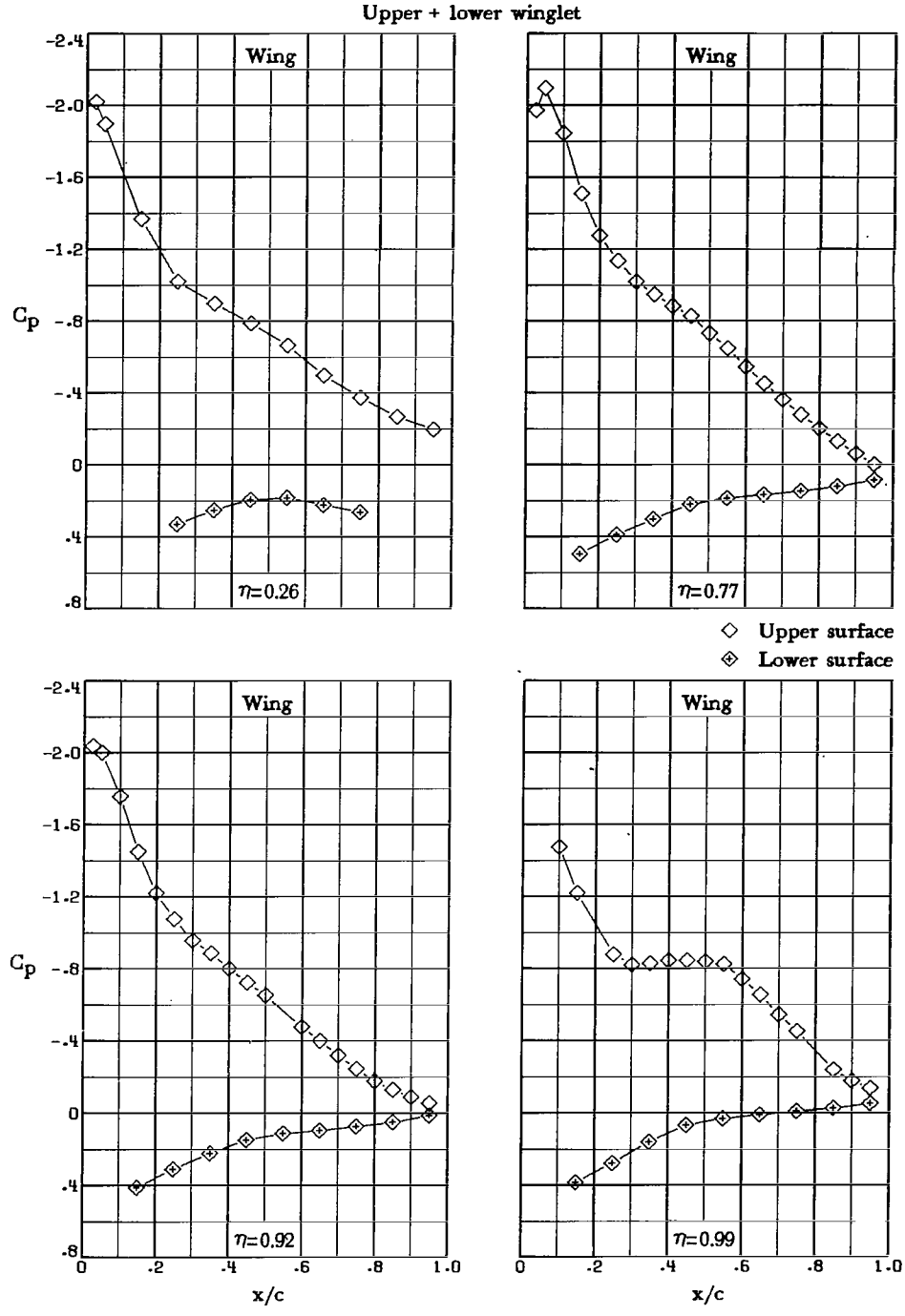

(c) $\alpha = 9.0^{\circ}$.

Figure 16.- Continued.

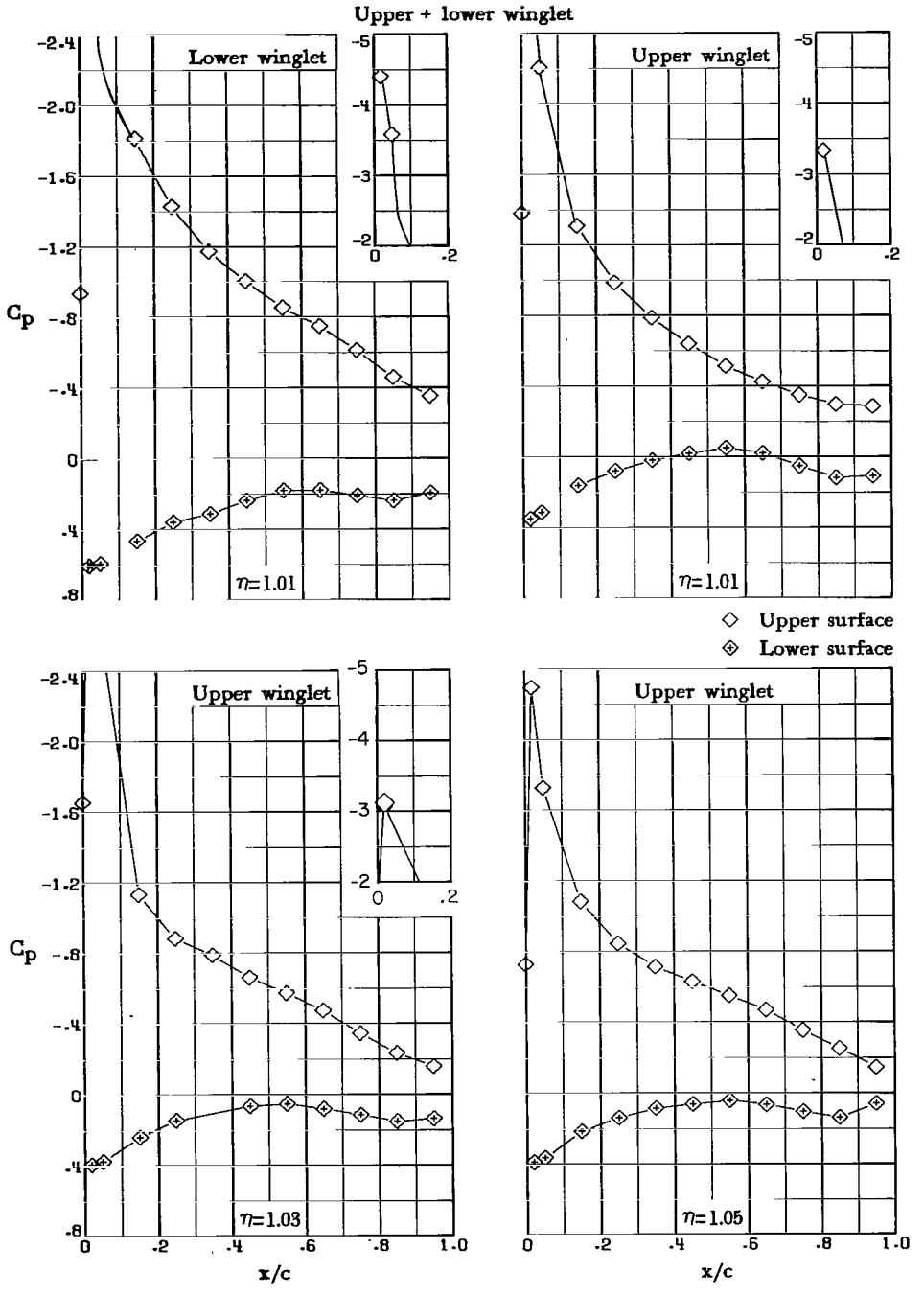

(c) α = 9.0°. Concluded.

Figure 16.- Continued.

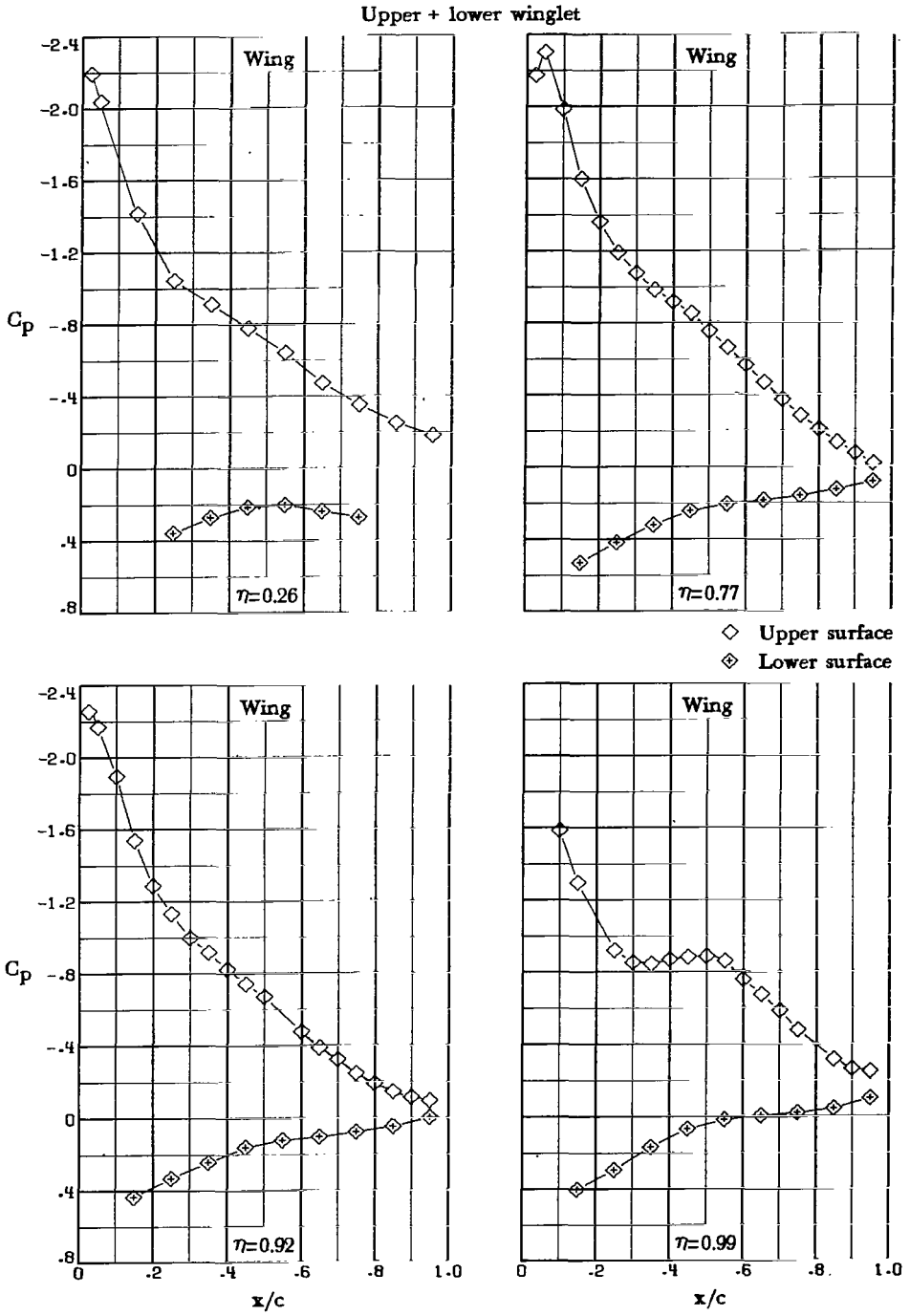

(d) α = 10.0°.

Figure 16.- Continued.

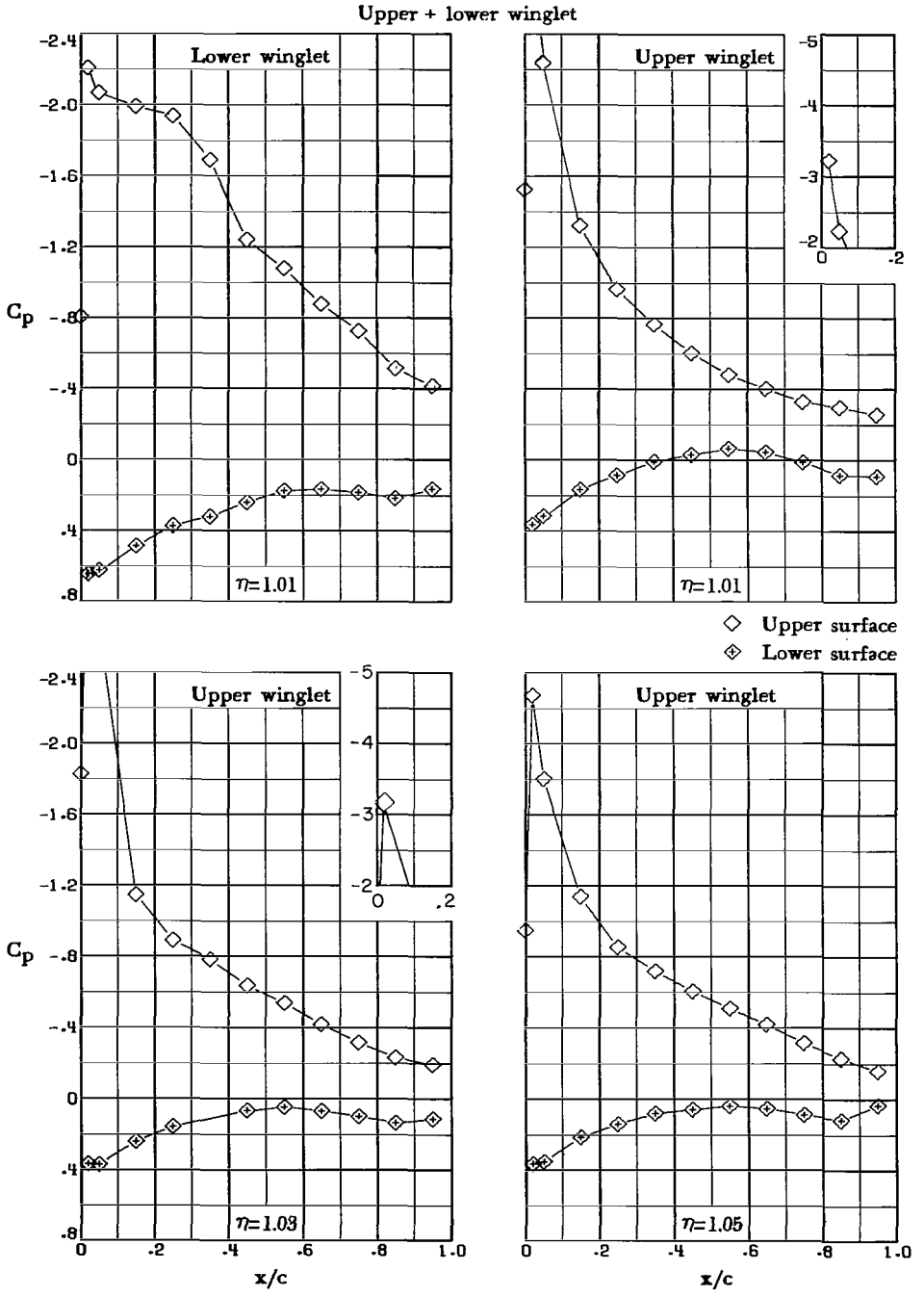

(d) α = 10.0°. Concluded.

Figure 16.- Continued.

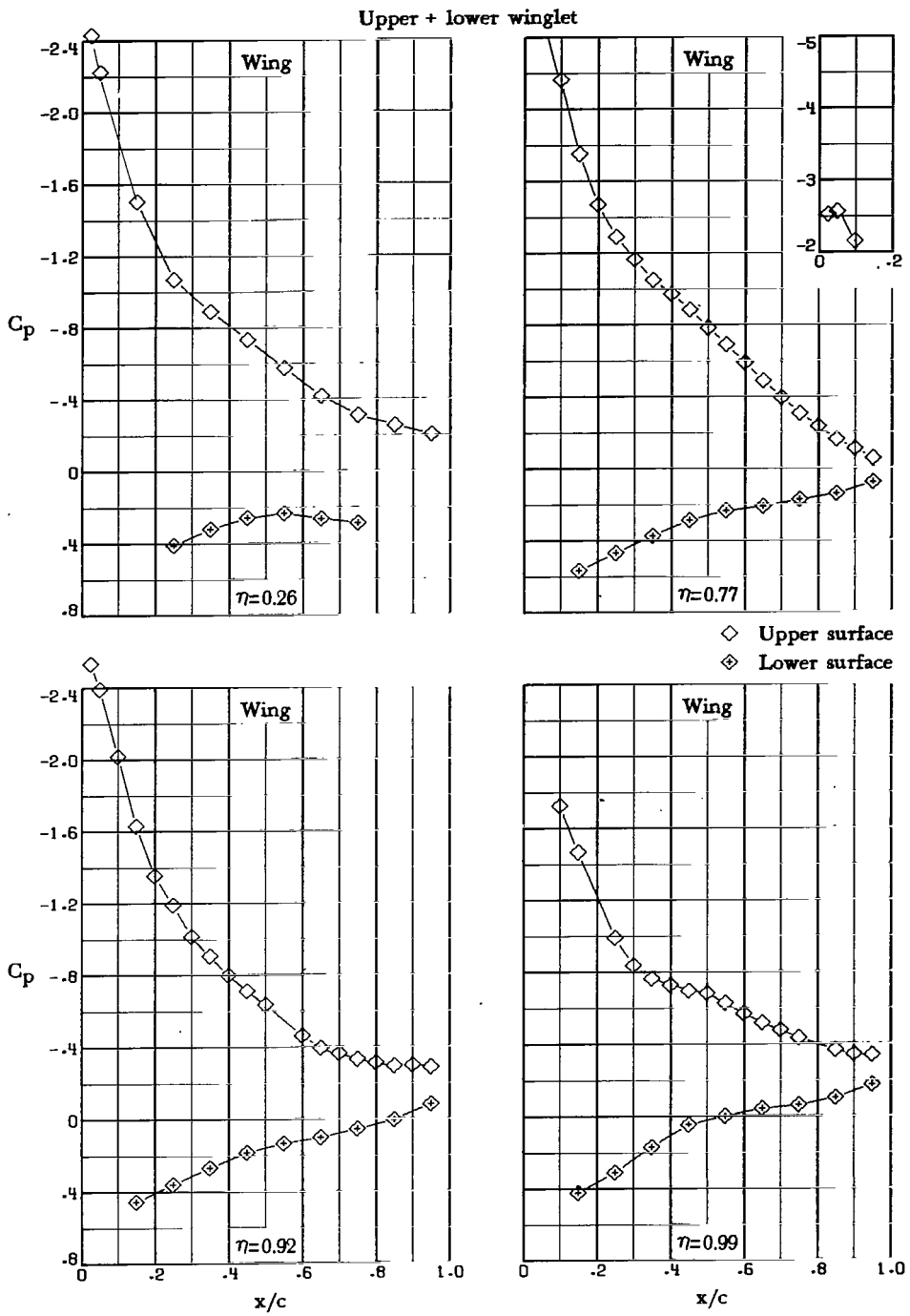

(e) α = 12.0°.

Figure 16.- Continued.

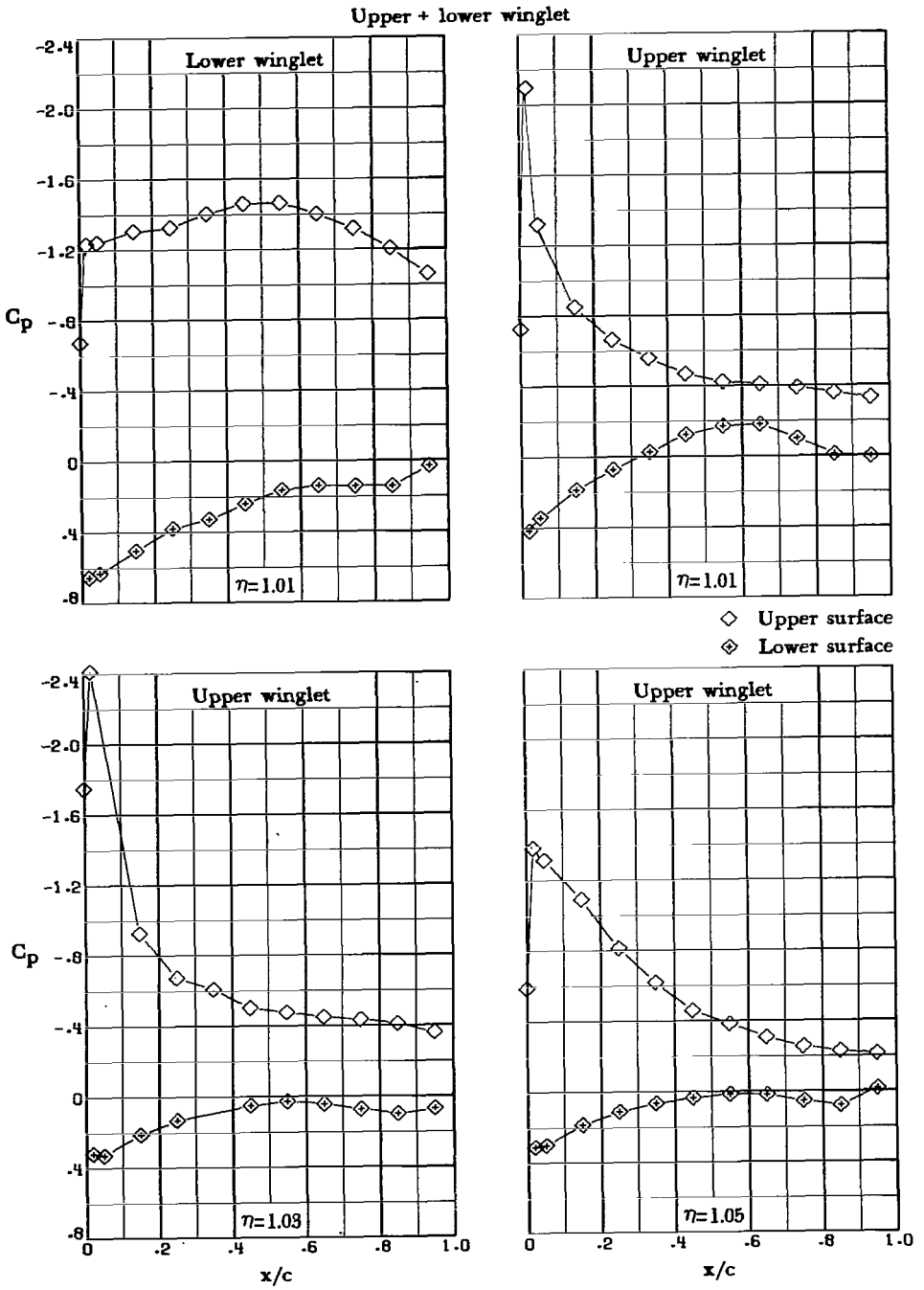

(e) α = 12.0°. Concluded.

Figure 16.- Concluded.

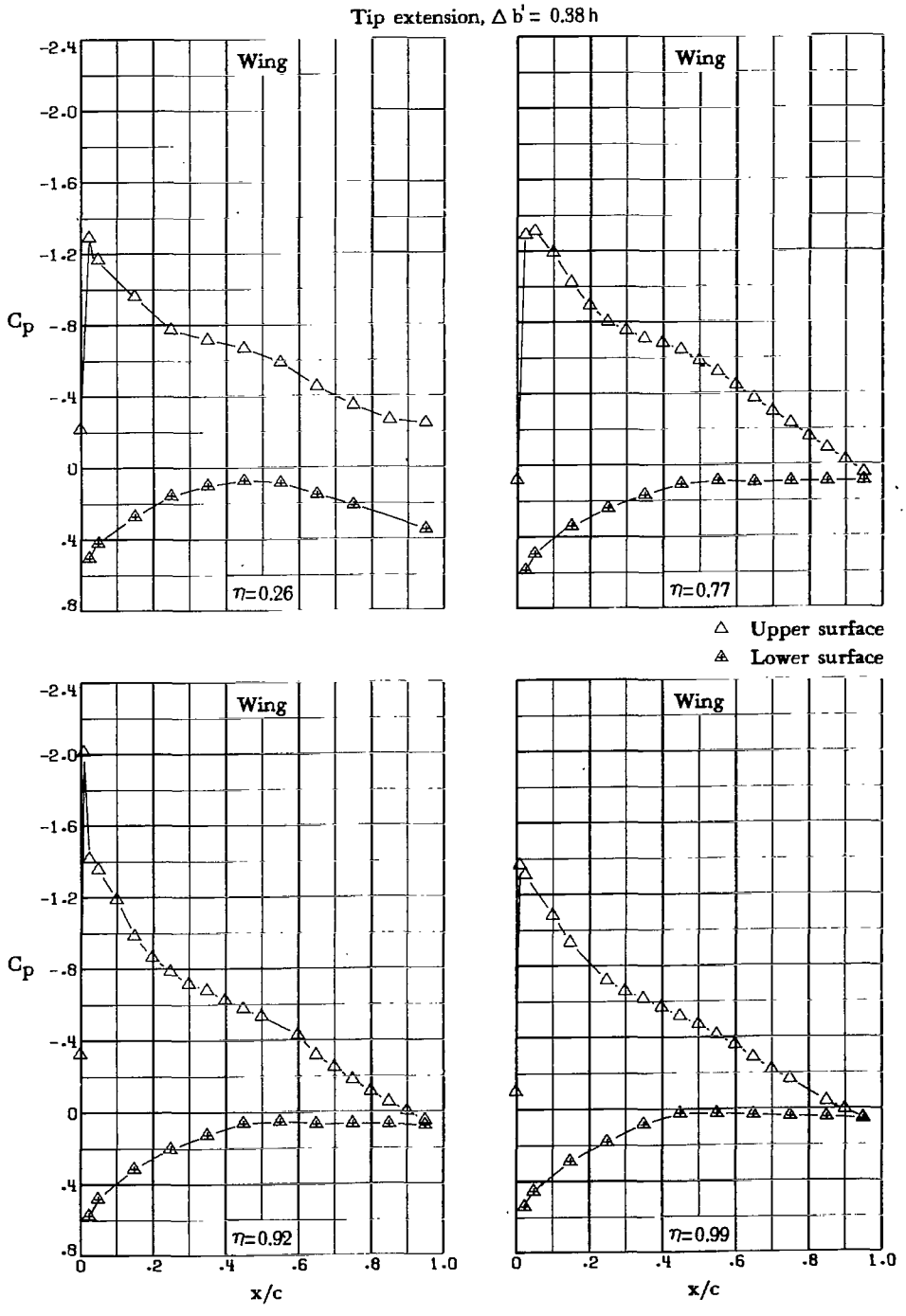

(a) $\alpha = 4.2^{\circ}$.

Figure 17.- Pressure distributions for tip-extension configuration with trailing-edge flaps. Note that insert vertical scale increment of insert plots is larger.

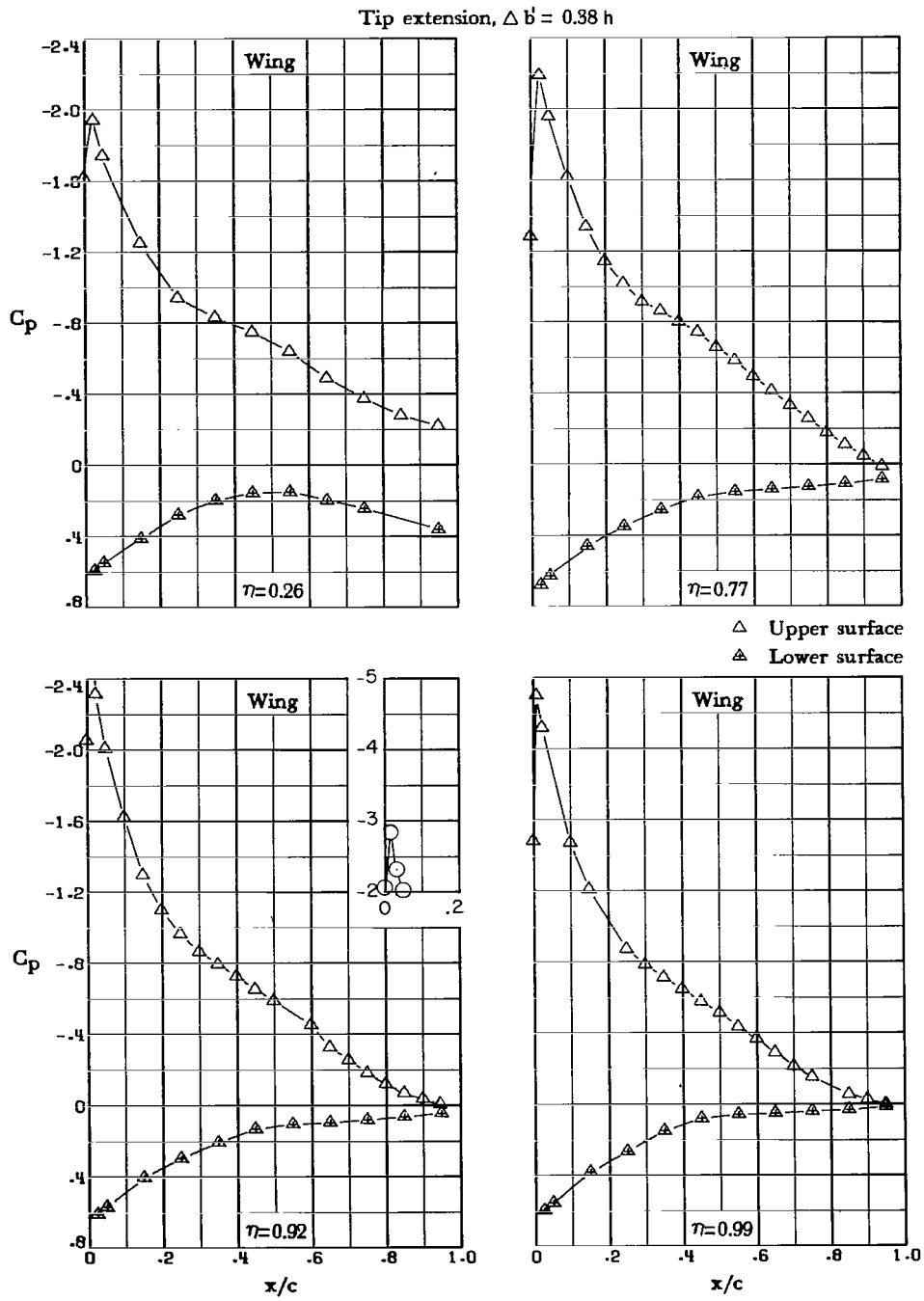

(b) $\alpha = 7.0^{\circ}$.

Figure 17.- Continued.

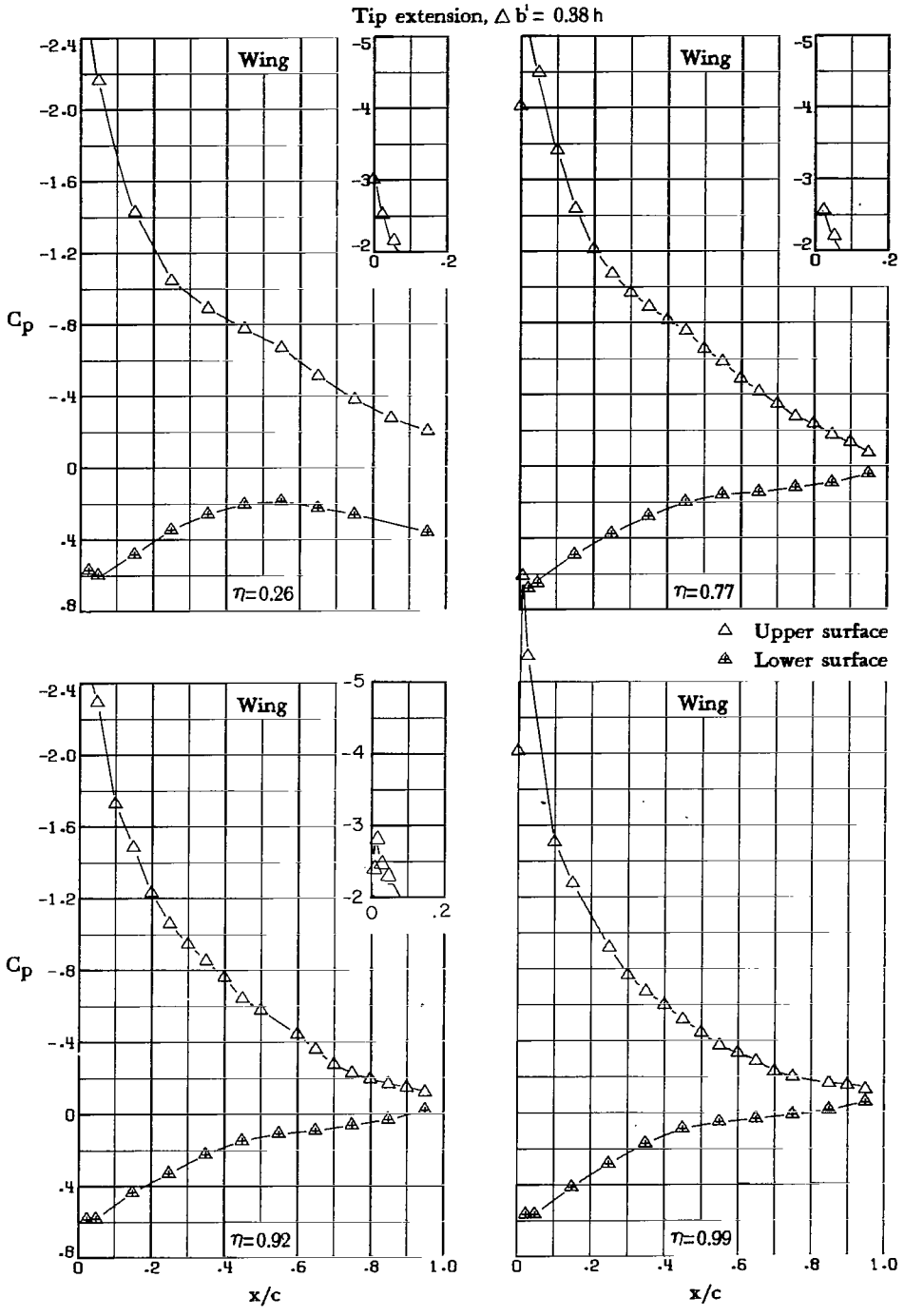

(c) $\alpha = 9.0^{o}$.

Figure 17.- Continued.

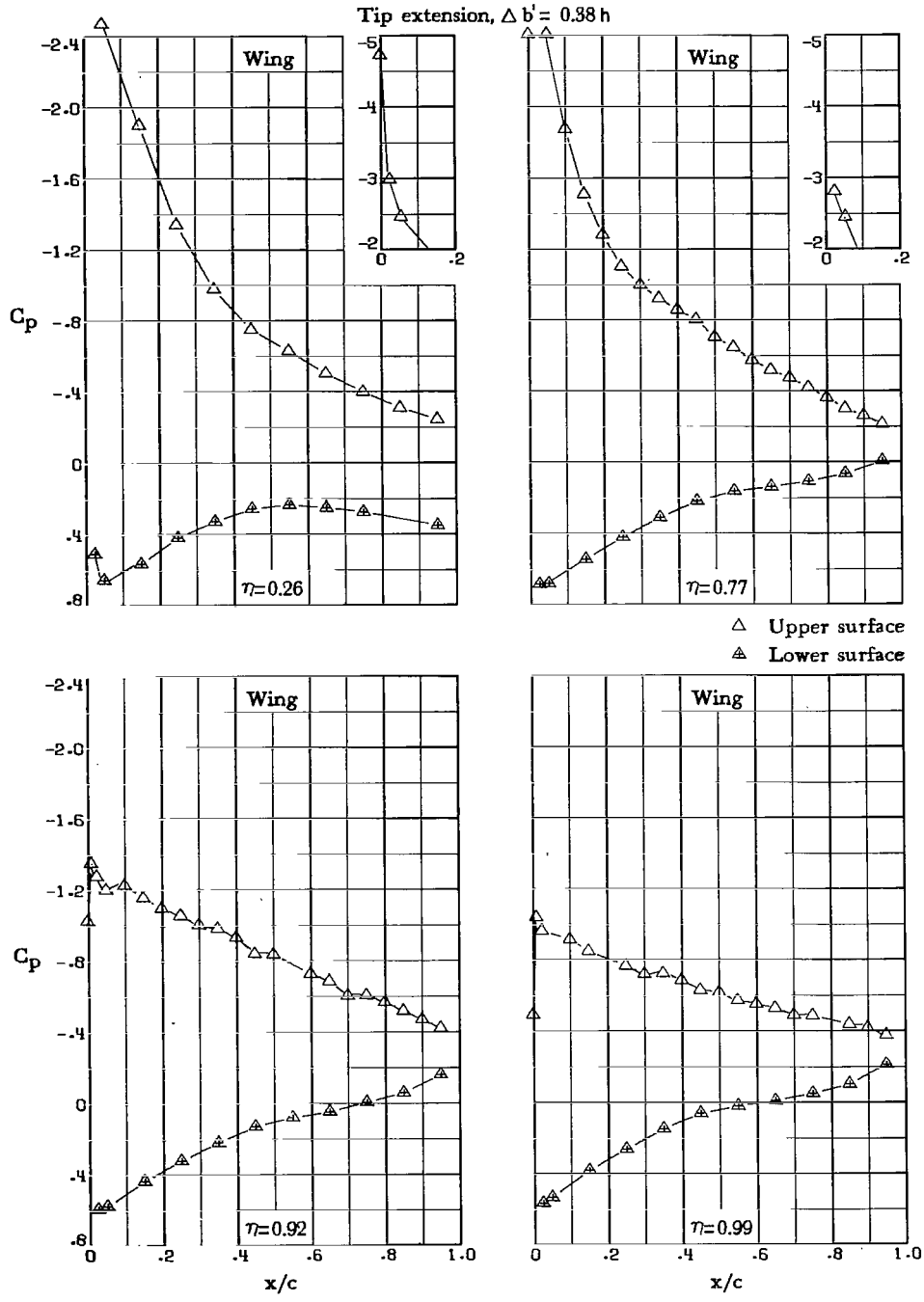

(d) α = 12.0°.

Figure 17.- Concluded.

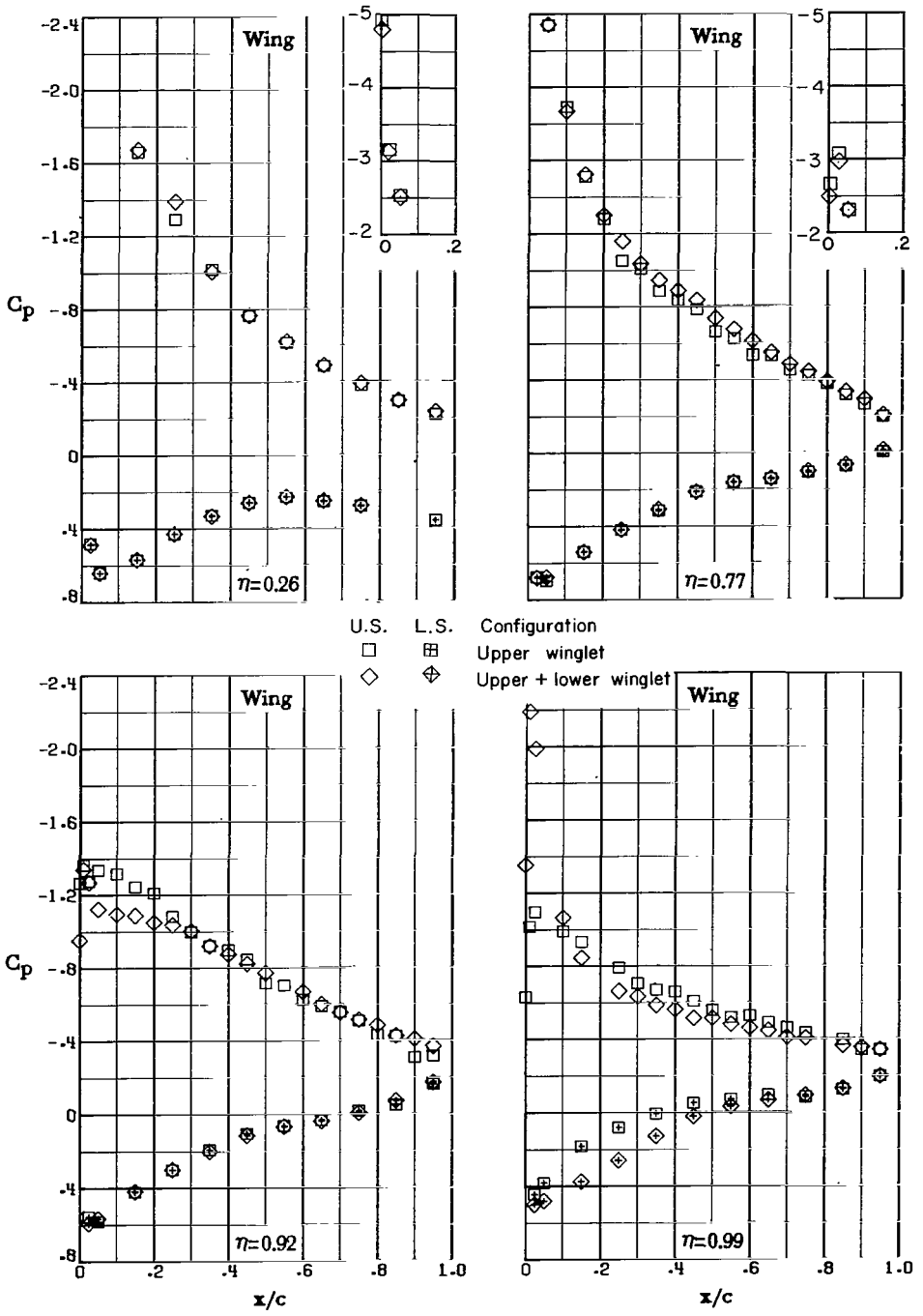

(a) Trailing-edge flaps.

Figure 18.- Comparison of pressure distributions of upper-winglet and upper-and-lower-winglet configurations with trailing-edge flaps and leading- and trailing-edge flaps. $\alpha \approx 12^{o}$. Note that insert vertical scale increment of insert plots is larger.

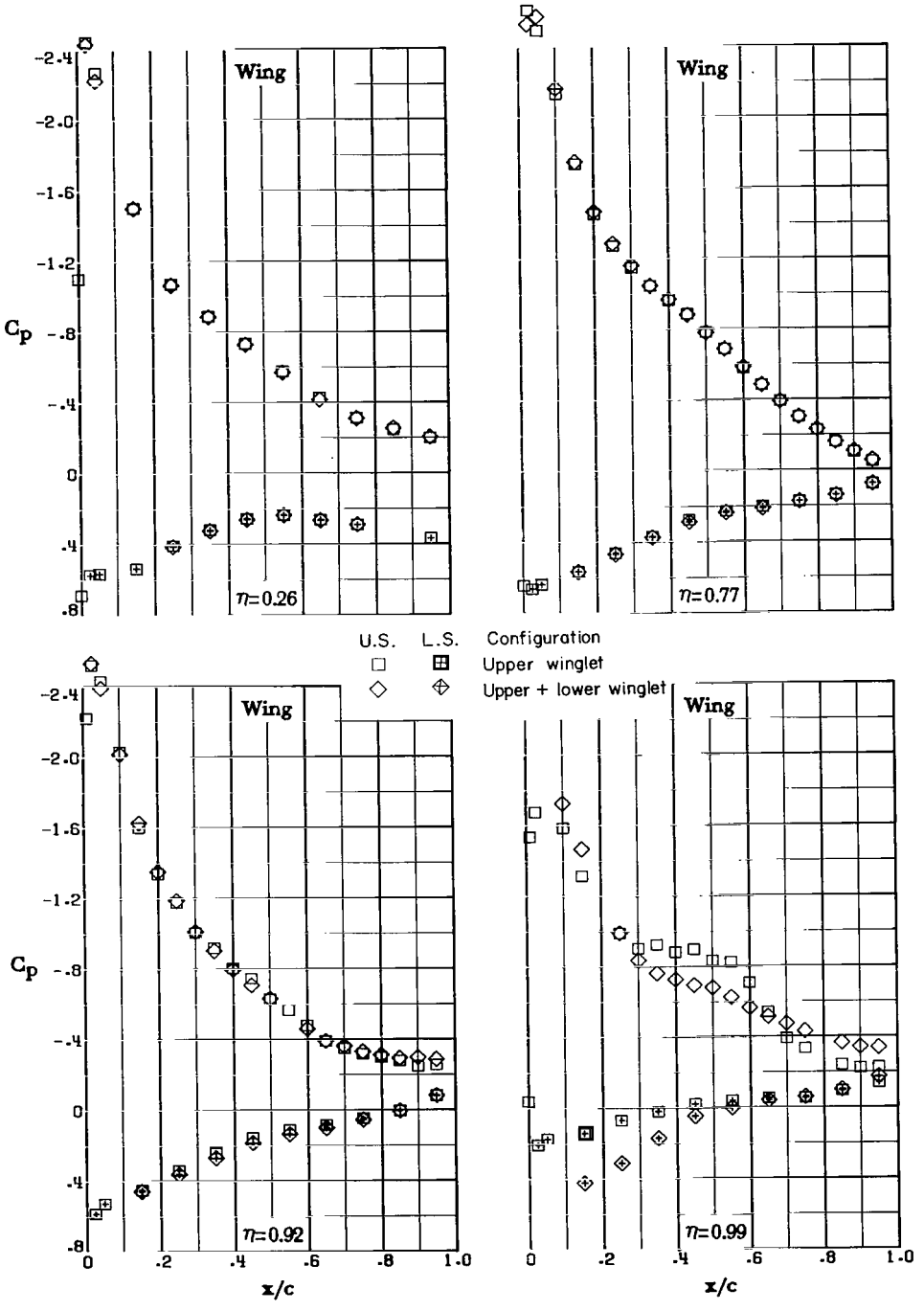

(b) Leading- and trailing-edge flaps.

Figure 18.- Concluded.

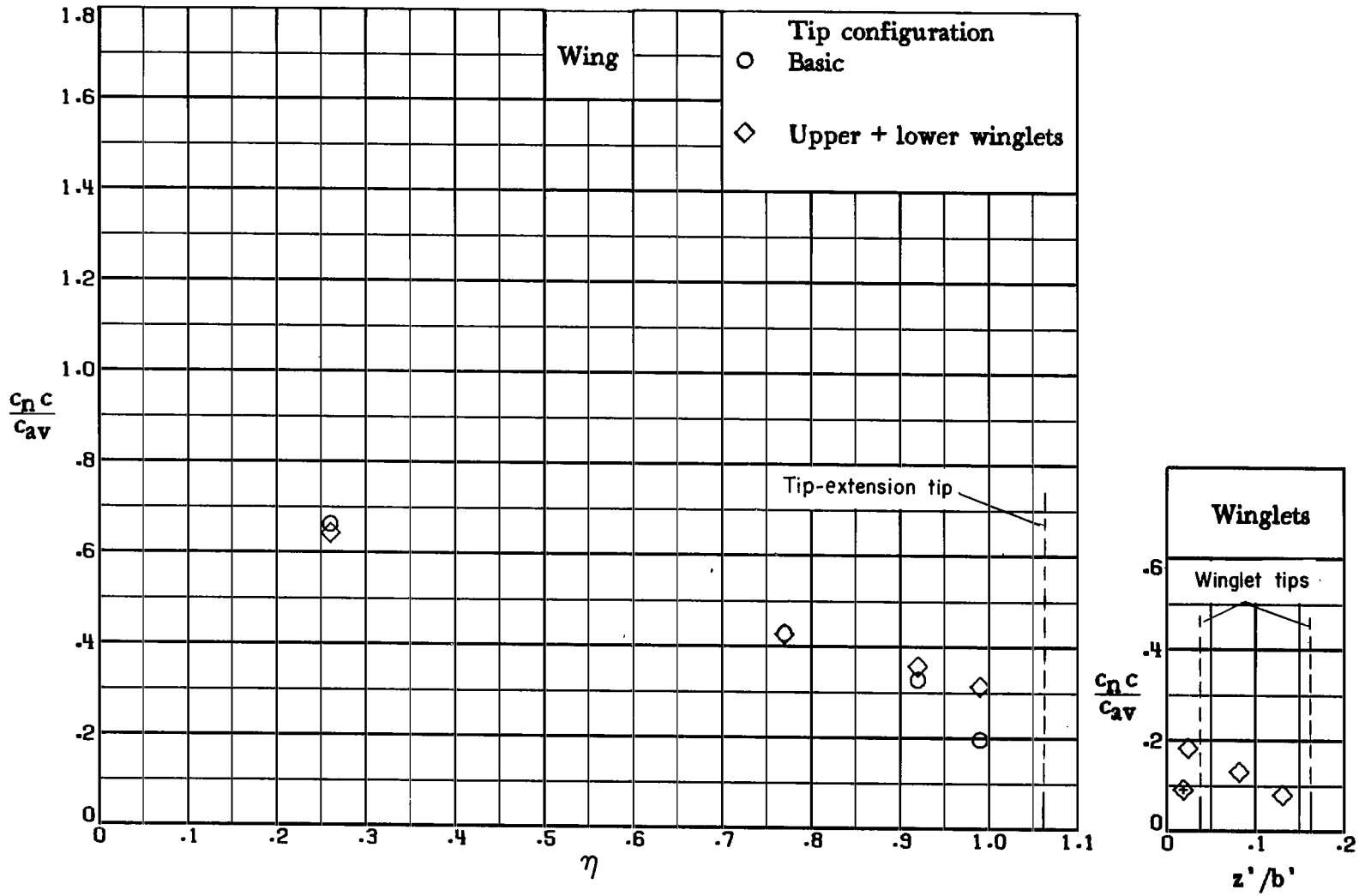

(a) $\alpha = 4.0^{\circ}$.

Figure 19.- Comparison of spanwise load distribution for basic-tip and upper-and-lower-winglet configurations. (⊕ indicates lower-winglet data.)

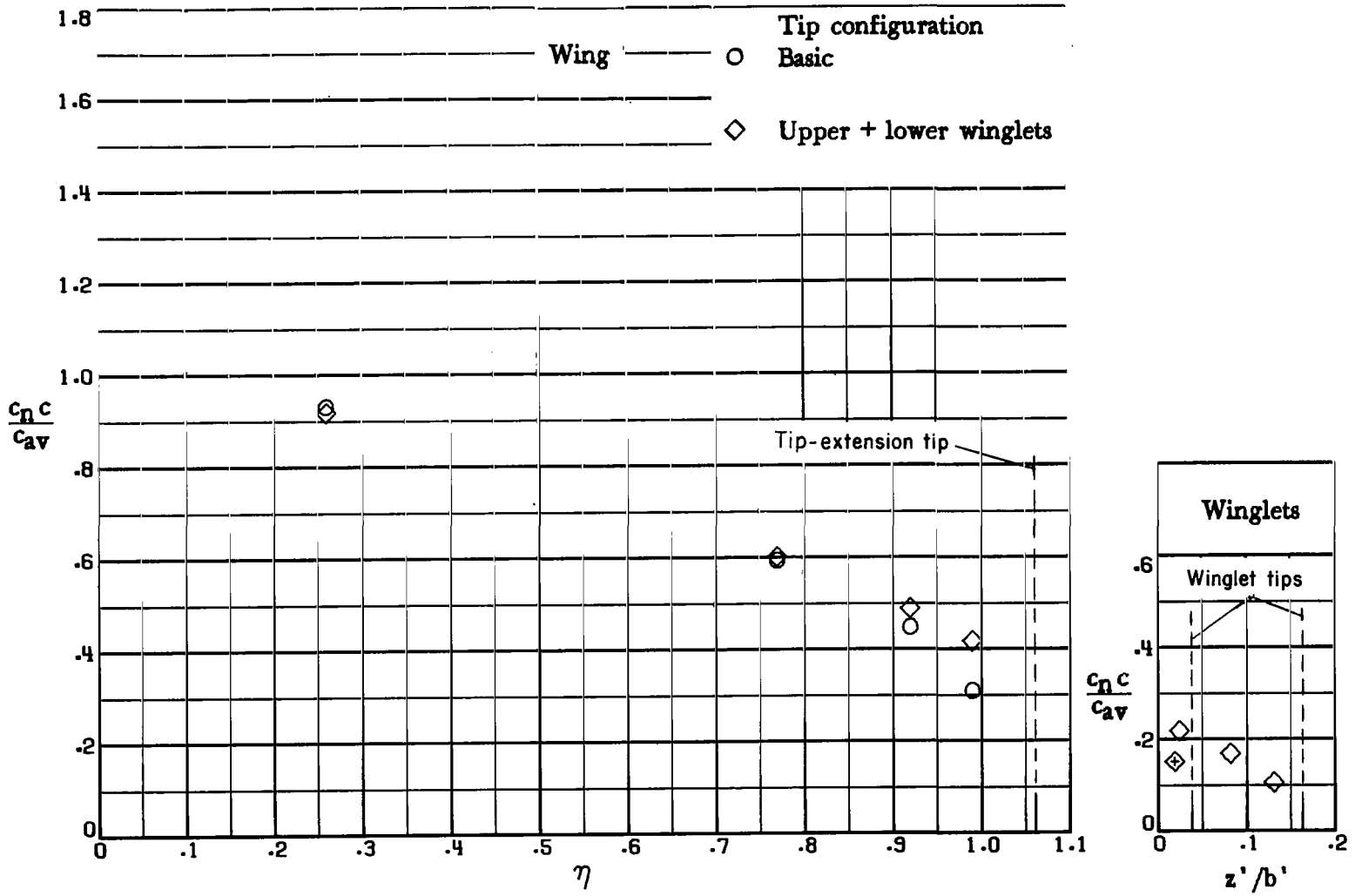

(b) $\alpha = 7.0^{\circ}$.

Figure 19.- Continued.

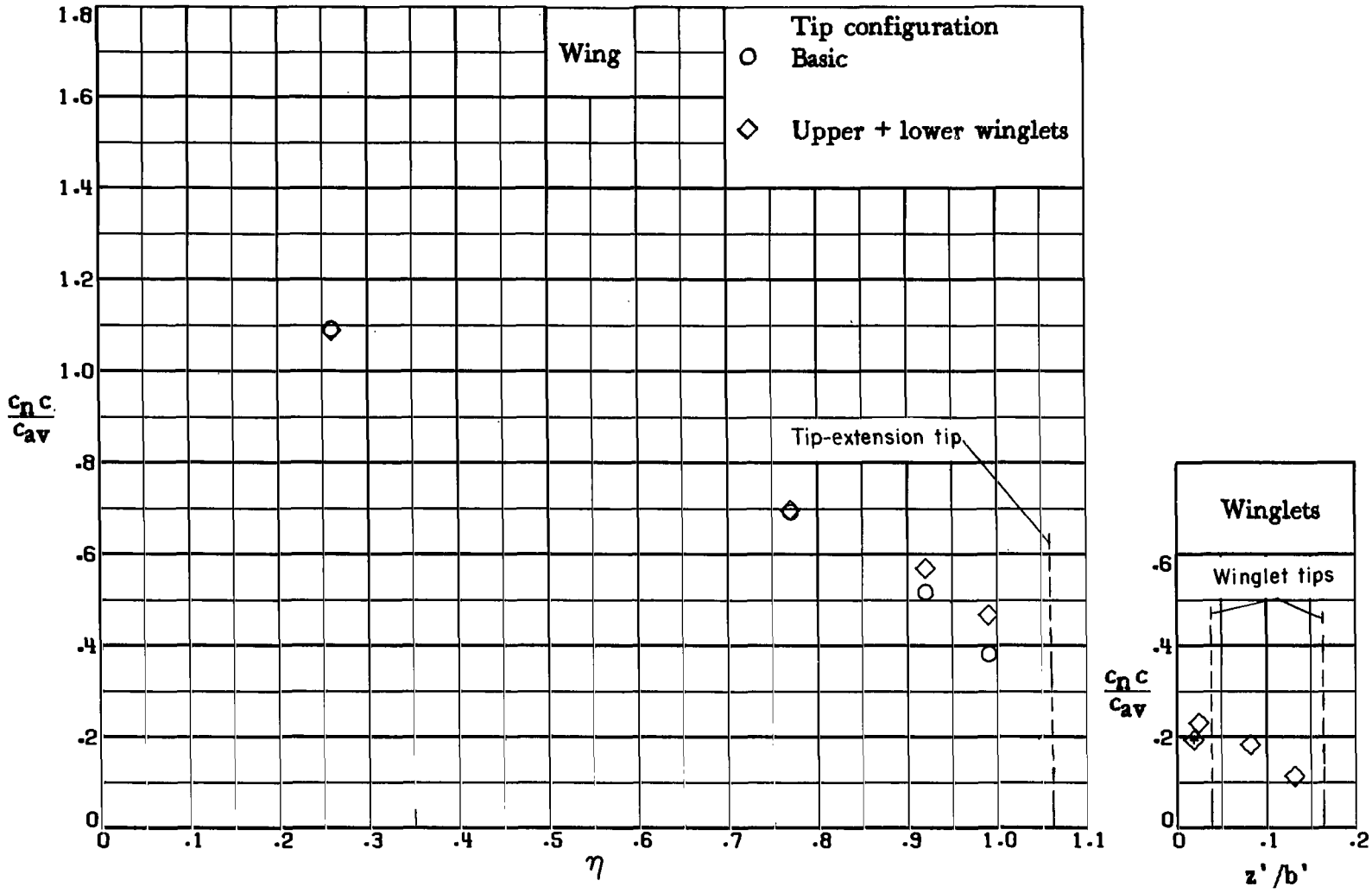

(c) $\alpha = 9.0^{\circ}$.

Figure 19.- Continued.

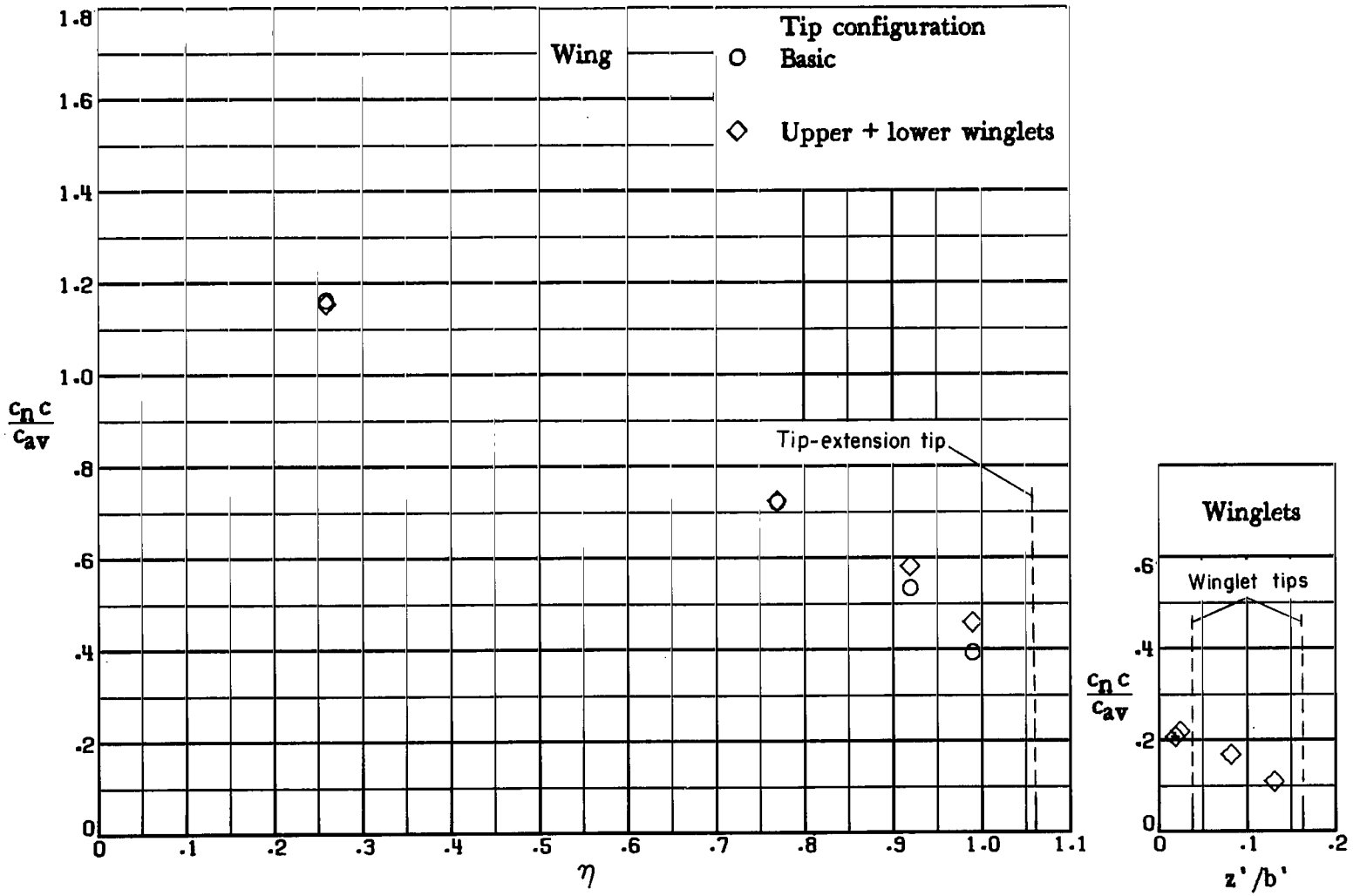

(d) $\alpha = 10.0^{\circ}$.

Figure 19.- Continued.

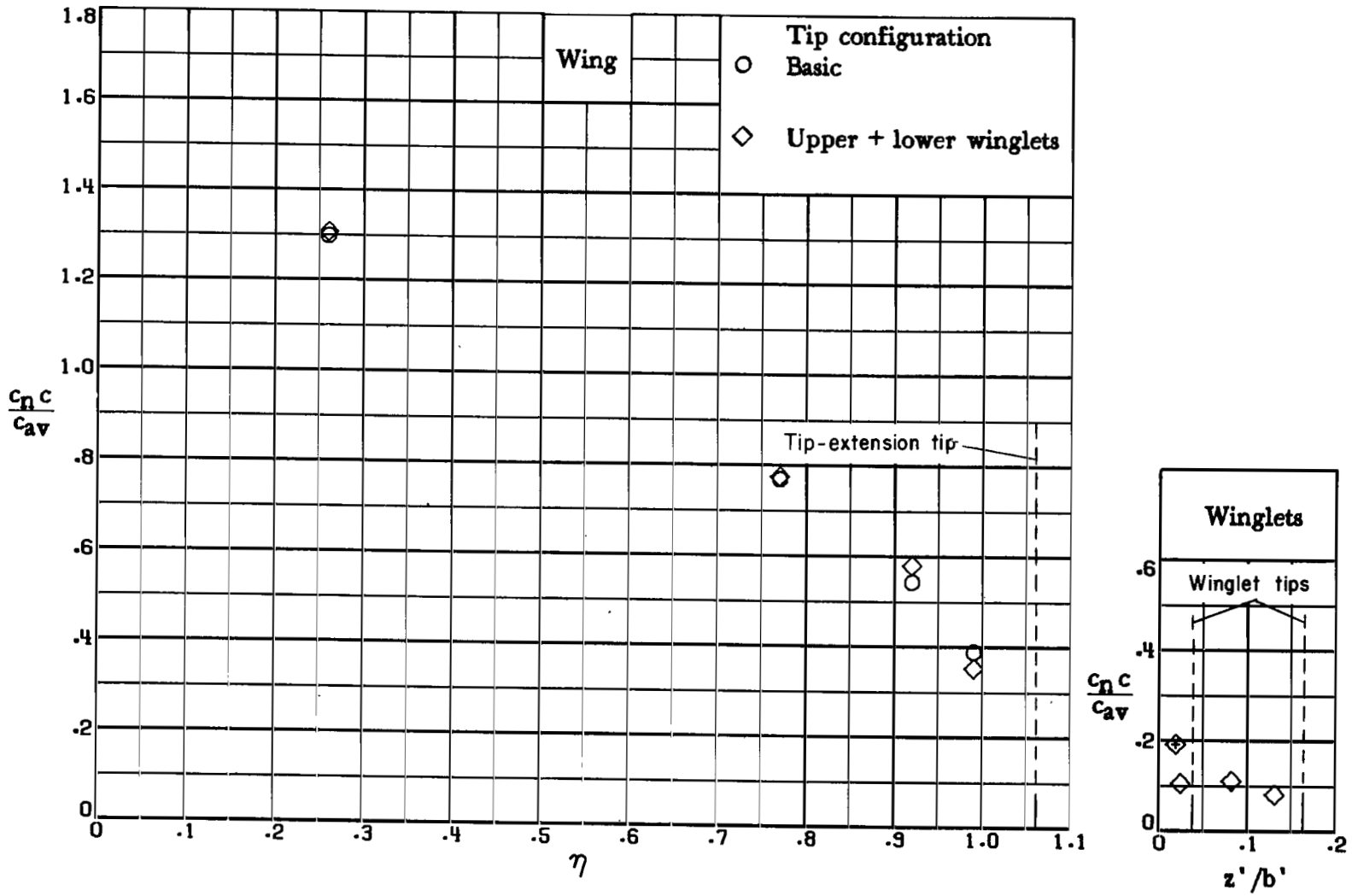

(e) $\alpha = 11.9^{\circ}$.

Figure 19.- Concluded.

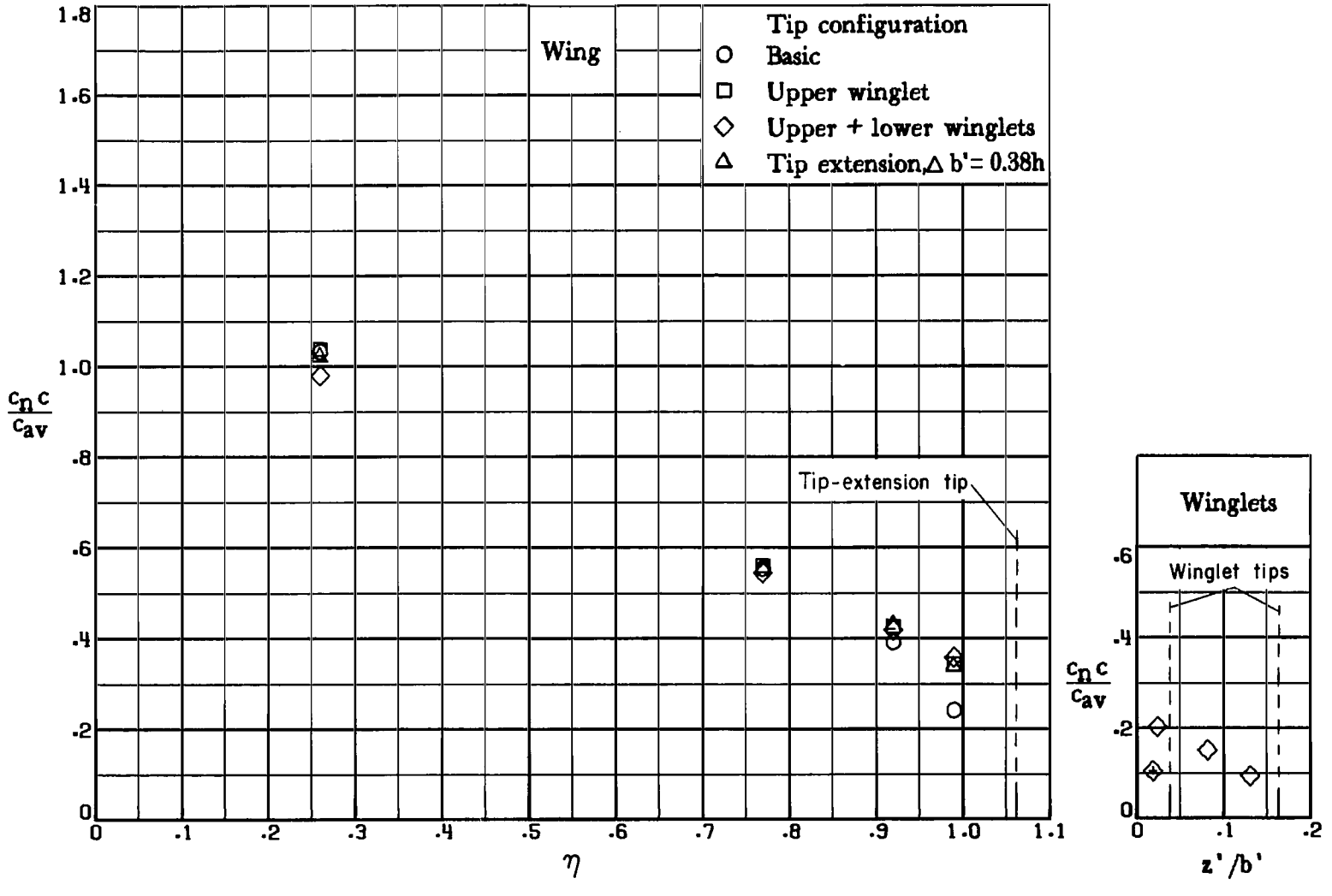

(a) $\alpha = 4.2^{\circ}$.

Figure 20.- Comparison of spanwise load distributions for several configurations with trailing-edge flaps. (⊕ indicates lower winglet data.)

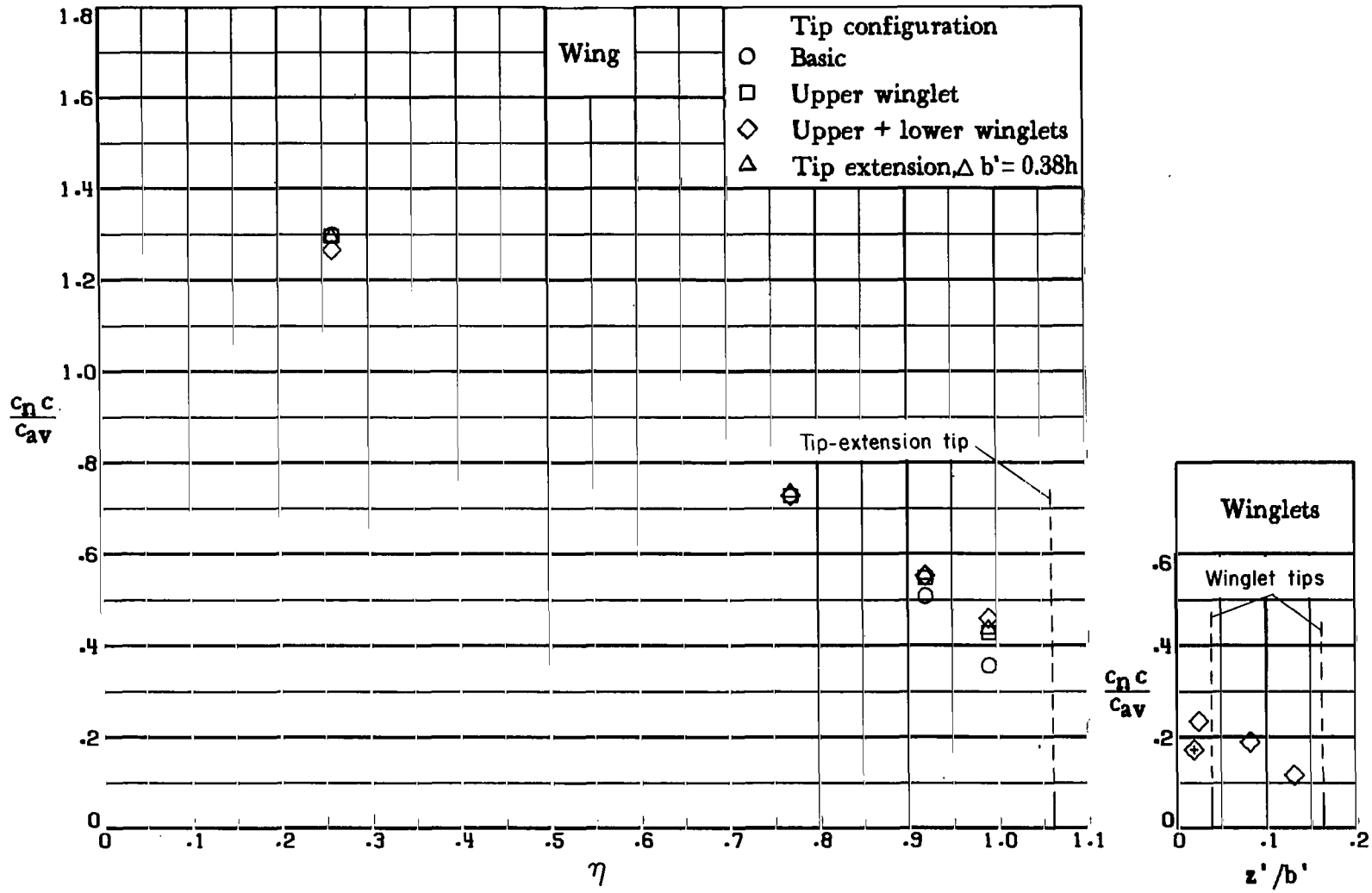

(b) $\alpha = 7.0^{\circ}$.

Figure 20.- Continued.

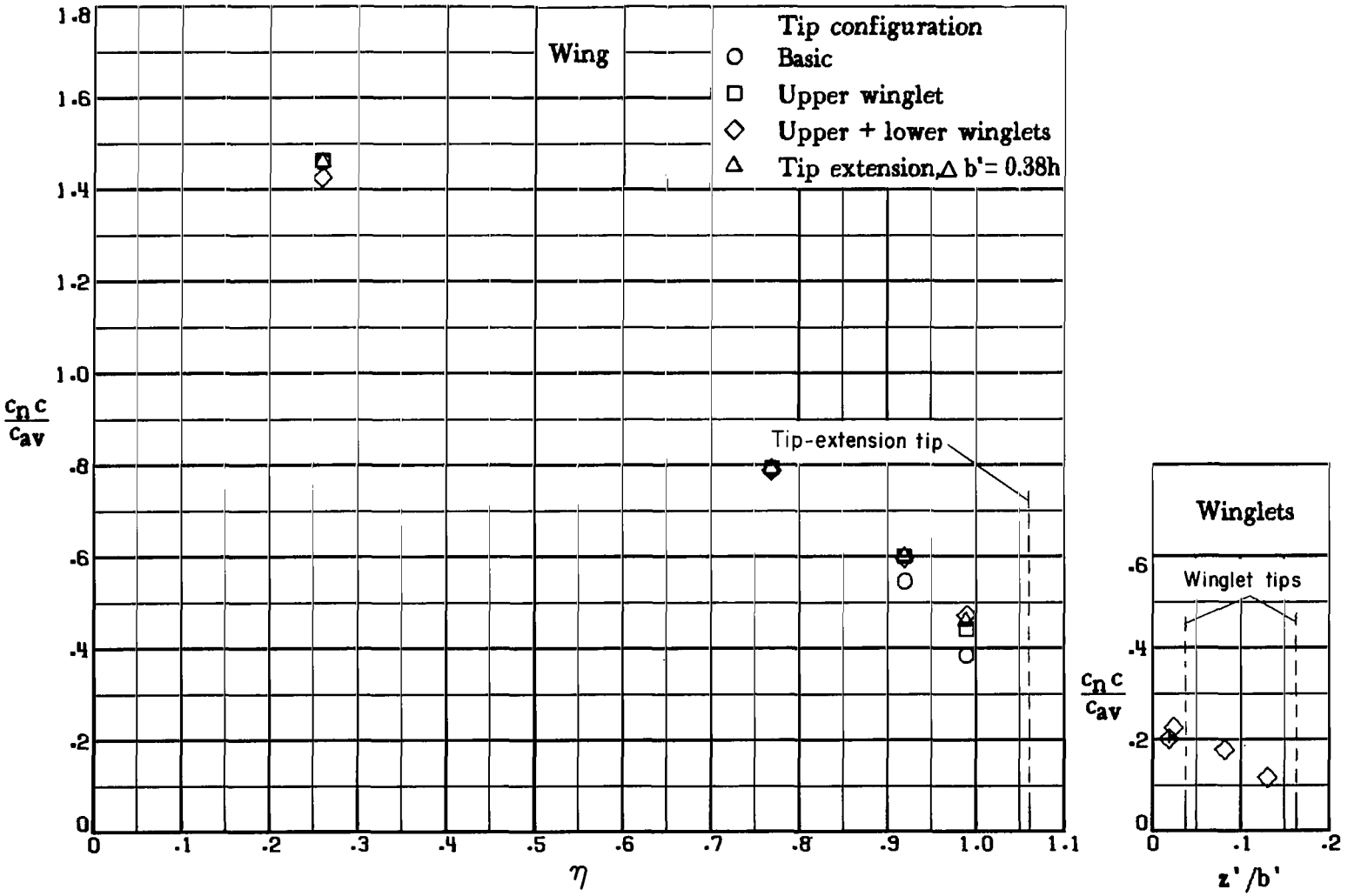

(c) $\alpha = 9.0^{\circ}$.

Figure 20.- Continued.

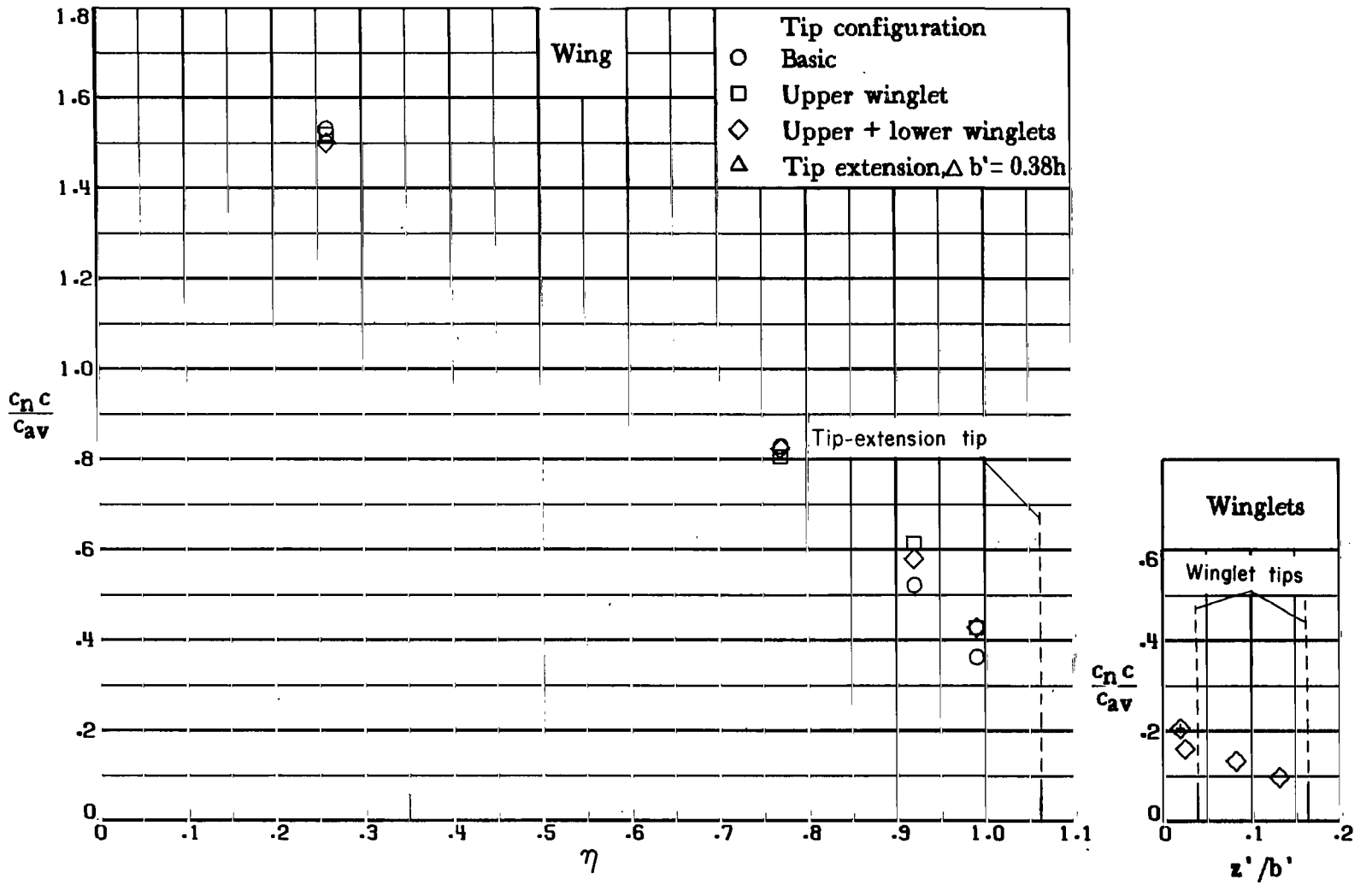

(d) α = 10.0°.

Figure 20.- Continued.

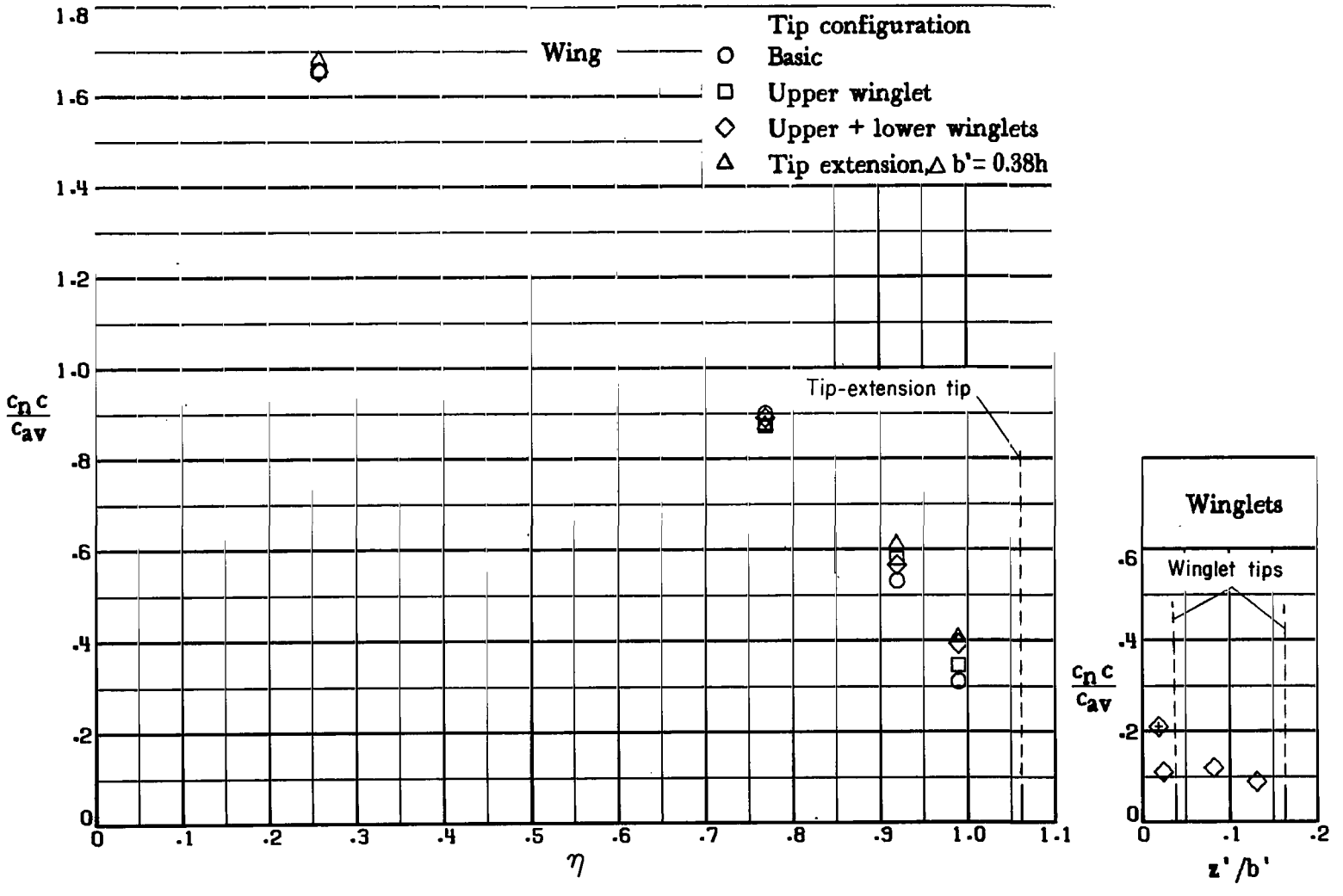

(e) $\alpha \approx 12.0^{\circ}$.

Figure 20.- Concluded.

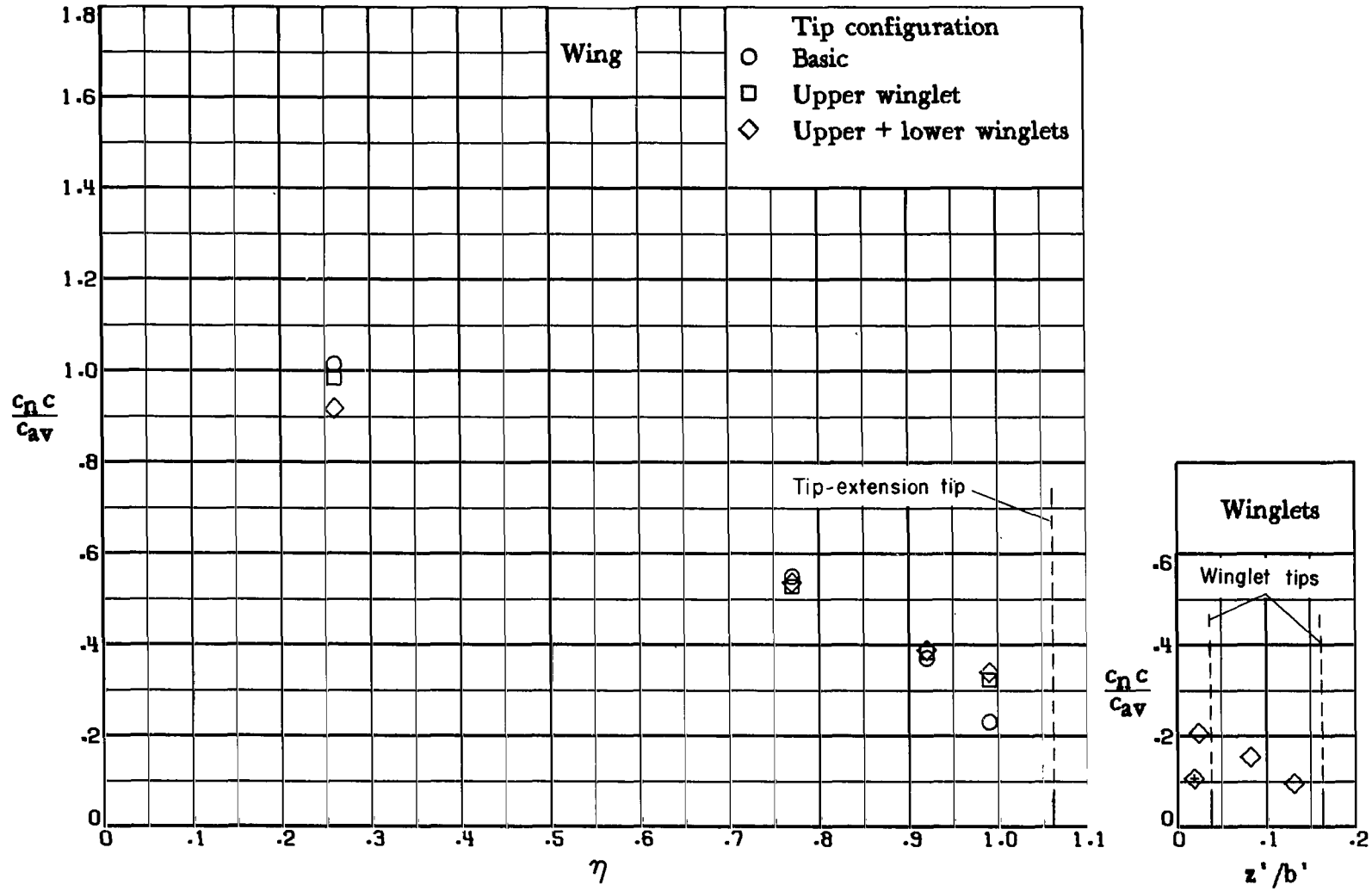

(a) $\alpha \approx 4.1^{\circ}$.

Figure 21.- Comparison of spanwise load distribution for several configurations with leading- and trailing-edge flaps. (⊕ indicates lower-winglet data.)

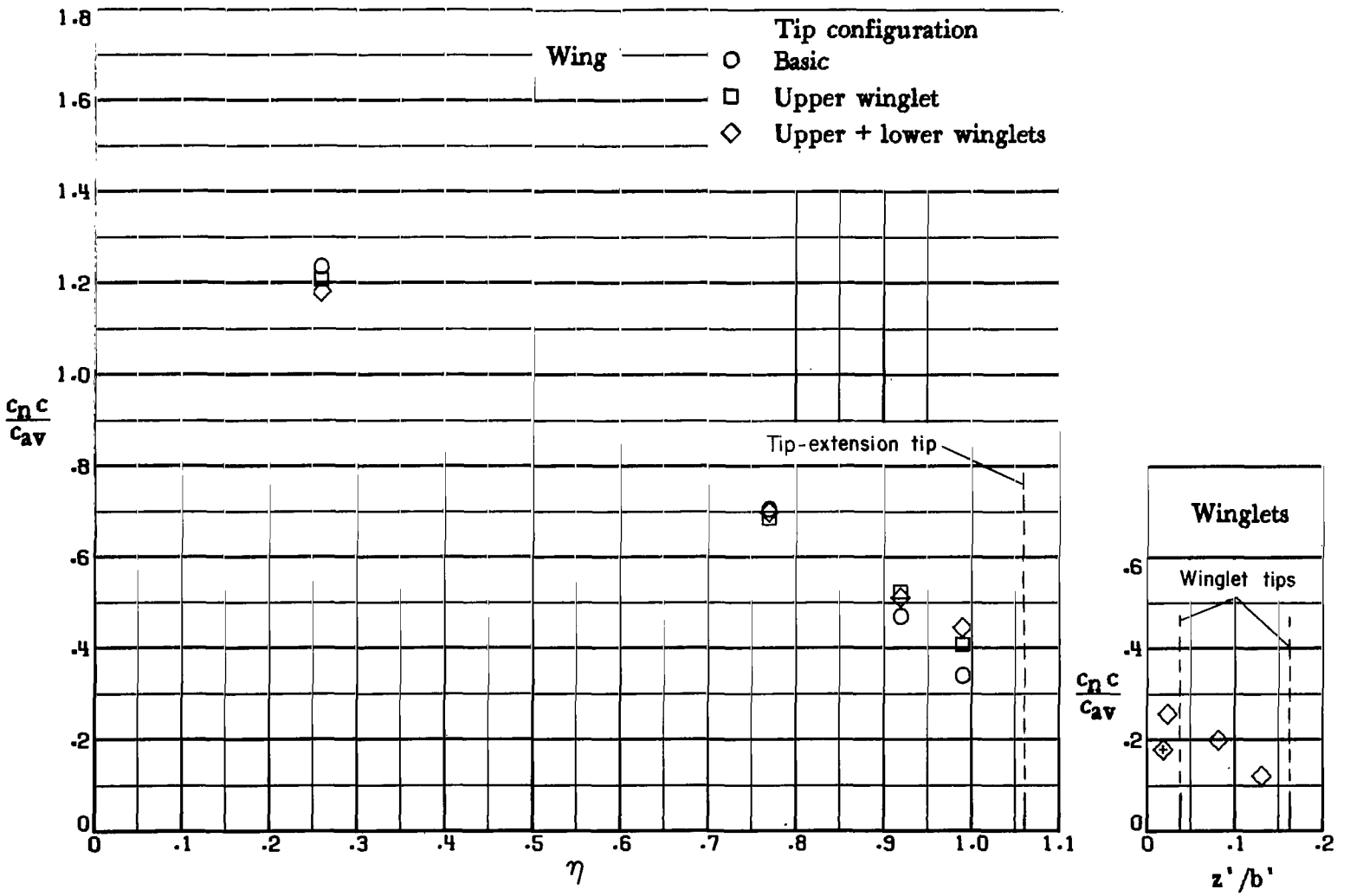

(b) $\alpha = 7.0^{\circ}$.

Figure 21.- Continued.

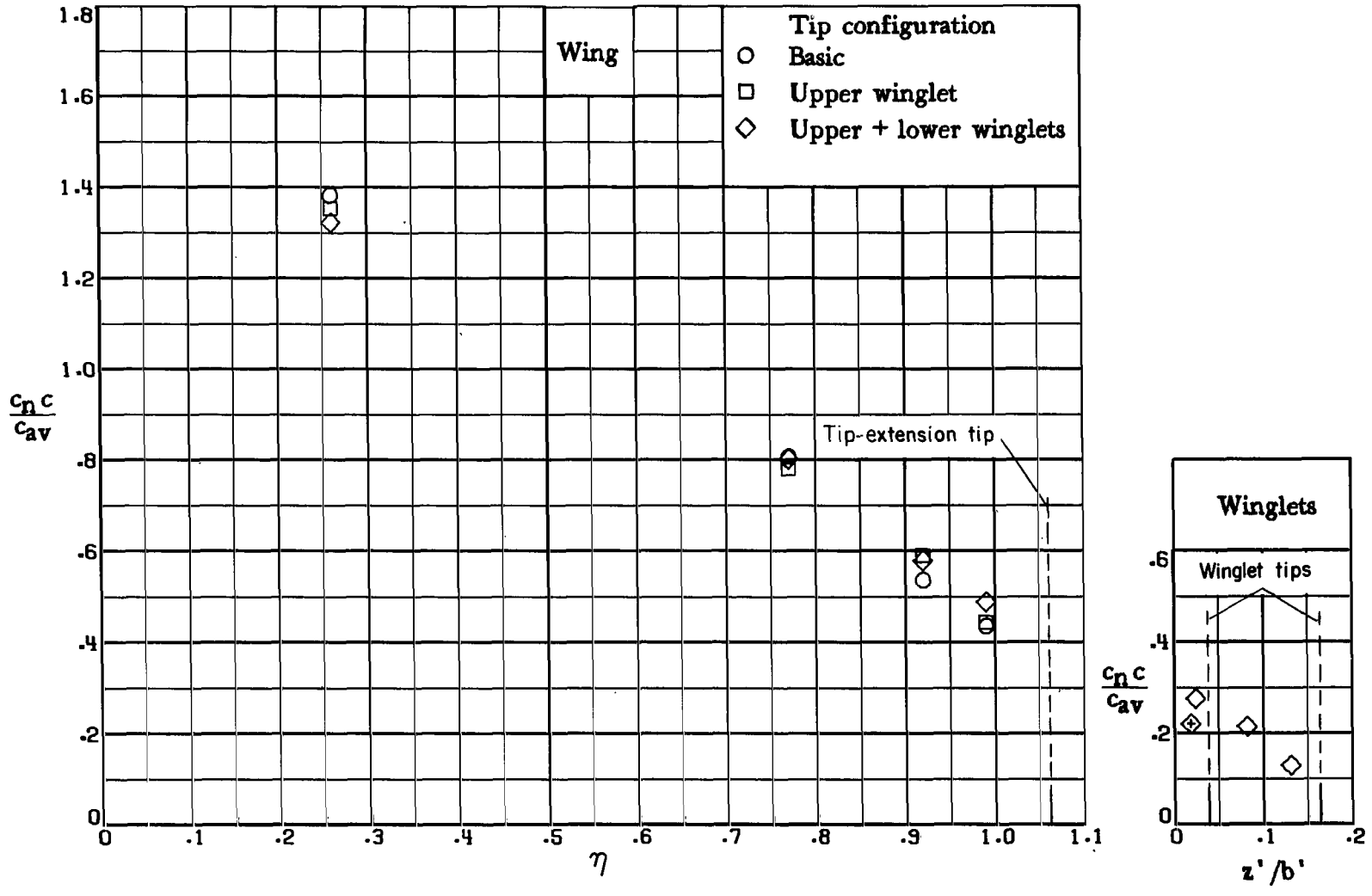

(c) $\alpha = 9.0^{\circ}$.

Figure 21.- Continued.

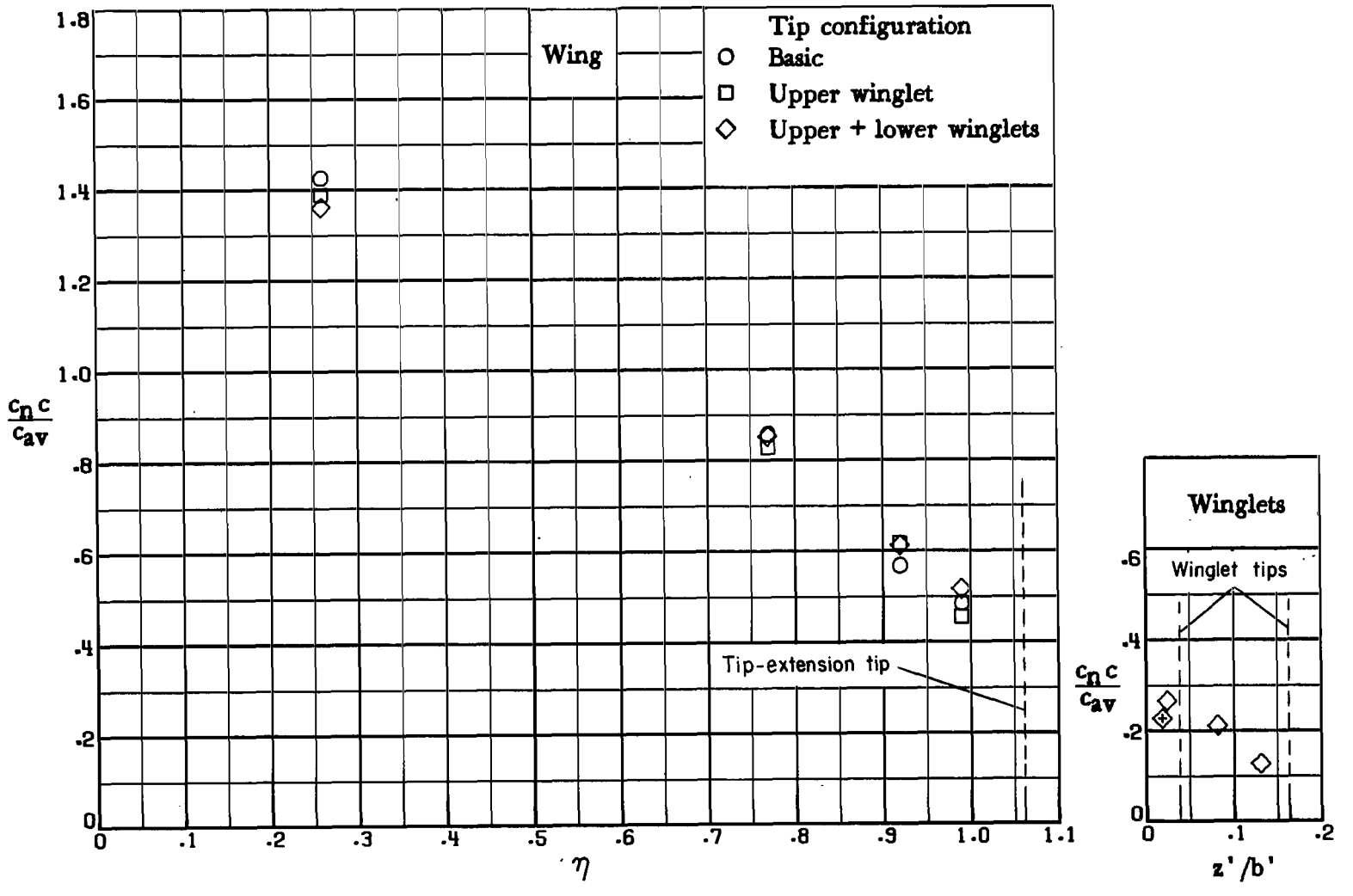

(d) $\alpha = 10.0^{\circ}$.

Figure 21.- Continued.

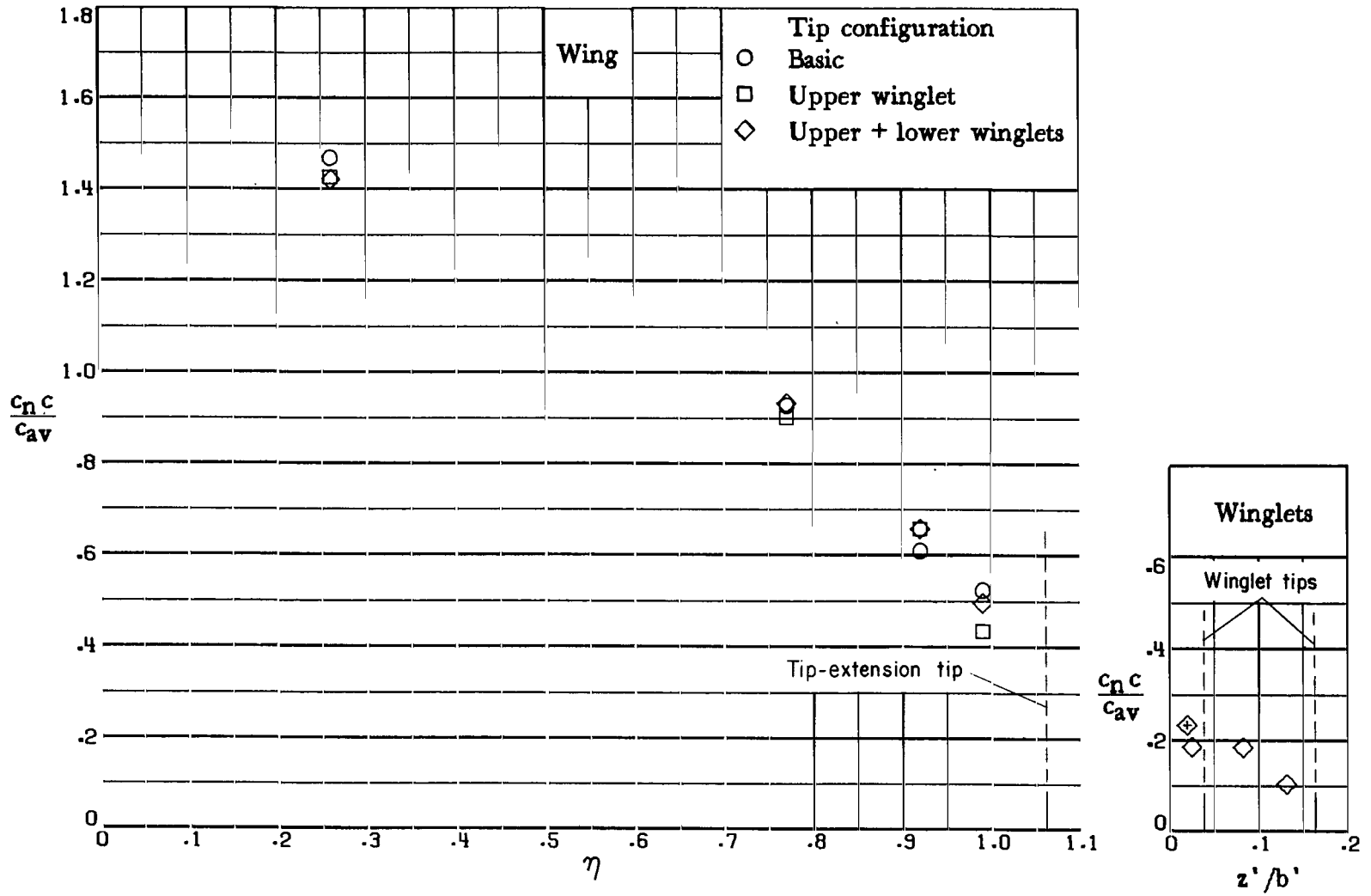

(e) $\alpha = 11.9^{\circ}$.

Figure 21.- Concluded.

"The aeronautical and space activities of the United States shall be conducted so as to contribute . . . to the expansion of human knowledge of phenomena in the atmosphere and space. The Administration shall provide for the widest practicable and appropriate dissemination of information concerning its activities and the results thereof."

—NATIONAL AERONAUTICS AND SPACE ACT OF 1958

NASA SCIENTIFIC AND TECHNICAL PUBLICATIONS

TECHNICAL REPORTS: Scientific and technical information considered important, complete, and a lasting contribution to existing knowledge.

TECHNICAL NOTES: Information less broad in scope but nevertheless of importance as a contribution to existing knowledge.

TECHNICAL MEMORANDUMS: Information receiving limited distribution because of preliminary data, security classification, or other reasons. Also includes conference proceedings with either limited or unlimited distribution.

CONTRACTOR REPORTS: Scientific and technical information generated under a NASA contract or grant and considered an important contribution to existing knowledge.

TECHNICAL TRANSLATIONS: Information published in a foreign language considered to merit NASA distribution in English.

SPECIAL PUBLICATIONS: Information derived from or of value to NASA activities. Publications include final reports of major projects, monographs, data compilations, handbooks, sourcebooks, and special bibliographies.

TECHNOLOGY UTILIZATION PUBLICATIONS: Information on technology used by NASA that may be of particular interest in commercial and other non-aerospace applications. Publications include Tech Briefs, Technology Utilization Reports and Technology Surveys.

Details on the availability of these publications may be obtained from:

SCIENTIFIC AND TECHNICAL INFORMATION OFFICE

NATIONAL AERONAUTICS AND SPACE ADMINISTRATION

Washington, D.C. 20546